

Testimony

U.S. House of Representative Committee on Science, Space, & Technology

Subcommittee on Environment

Thursday, June 21, 2018

By

Timothy Franquist, Air Quality Director

Mr. Chairman, members of the committee. My name is Timothy Franquist. I am the Air Quality Director at the Arizona Department of Environmental Quality and; I appreciate the opportunity to offer testimony today.

The Clean Air Act has done a remarkable job of reducing air pollution across our county for the past 48 years from industry and vehicles. Now, however, we face a new air quality challenge: global air pollution, specifically, air pollution that is transported to the U.S. in such quantities to cause areas of our country to exceed the National Ambient Air Quality Standards (NAAQS). Unfortunately, the Clean Air Act is ill equipped to address this new air quality problem in terms of protecting public health and our local economies.

The U.S. EPA has conducted ozone modeling for U.S. background, or what is more commonly referred to as international transport, several times over the past three years. The models continue to indicate that ozone concentrations are increasing from international sources and impacting the U.S. The most recent U.S. EPA model indicates that over 83% of ozone in Southern Arizona is attributed to international sources (Attachment A).

Arizona is not only impacted by Mexican emissions, 65 percent of the ozone in the Southwest is attributed to international transport from Asia, according to a surface ozone study conducted by a team of researchers from NOAA, Princeton University, Columbia University, and the U.S. EPA (Attachment B).

The surface ozone study further indicates that during summertime in the Western U.S., “increasing Asian emissions approximately offset the benefits of U.S. emissions reductions.”

Beginning in May 2017, the Arizona Department of Environmental Quality installed an ozone monitor in San Luis Rio Colorado, Mexico, to determine the impacts of international transport on Yuma, Arizona, a new ozone nonattainment area proposed by the U.S. EPA as of April 2018. Our preliminary analysis indicates that prevailing winds from the south and increasing high levels of ozone originating south of the U.S. border are causing Yuma to exceed the federal ozone standard (Attachment C).

Because Yuma exceeds the 2015 Ozone standard, the Clean Air Act will require the State of Arizona to develop a state implementation plan for the area. Yuma will be subject to emission offsets for new large businesses or major expansions to existing businesses and those sources will be required to install extremely expensive emission control equipment before operating. Yuma is not a heavy industrial or urban area and therefore, it does not generate the requisite emission offsets, which ultimately discourages new or expanding business in the area.

The only relief for Yuma under the Clean Air Act is for the State to pursue an international transport demonstration, but we can only submit that demonstration after three years of the area not meeting the standard. Yuma will remain in perpetual nonattainment until international emissions decrease to the extent that Yuma attains the ozone standard. The international transport demonstration does nothing to better protect Yuma residents from the health impacts of international pollution or lessen the burden on their local economy.

The negative health effects of ozone is well documented; as is poverty’s negative effect on public health. The impact of nonattainment on Yuma’s public health and economy creates an incredibly dire situation for a primarily agricultural community of 100,000 residents, 19 percent of which, live below the poverty

line¹. The World Bank states in a report entitled, “Poverty and Health”, that “Poverty is a major cause of ill health and a barrier to accessing health care when needed.” (Attachment E) According to a study, authored by Michael McCally, MD and his colleagues, people living in countries with a higher Gross National Product have a longer life expectancy (Attachment F). In short, public health is not just about clean air, it’s also about a healthy economy.

Finding state-level solutions for ozone nonattainment areas are made infinitely more complicated when the area is significantly impacted by international transport of air pollution, as we are in Arizona.

Therefore, we must look to our federal agencies and representatives for relief to the international air pollution transport problem so that the recipients of pollution are not punished, but protected.

The Clean Air Act has not been significantly revised since 1990. As Arizona and the U.S. confront the growing challenge of global air pollution impacts on the U.S., I urge congress to seriously consider meaningful revisions to the Clean Air Act to address international transport of air pollution. Senator Flake has introduced Senate Bill 2825, which helps remove some of the negative economic impacts to areas of the U.S. that do not meet the Ozone standard due to international transport, while maintaining adequate air quality control measures to ensure that public health and the environment are protected. Senate Bill 2825 would be a major step in protecting places like Yuma, Arizona, and the West from international air pollution.

Thank you and I am happy to take any questions at this time.

¹ Source: <https://www.census.gov/quickfacts/fact/table/yumacountyarizona/PST045217>

Attachment

A

U.S. EPA International Transport Modeling

Summary of Modeling Results for Yuma, AZ

Model	Average DV	AZ	CA	Mex/Can	Biogenics	Boundary	USB (three previous columns combined)
Jan 2015	70.7	6.8%	23.5%	6.8%	5.4%	56.8%	69%
Aug 2015	70.7	6.1%	19.5%	7.2%	3.8%	61.3%	72.3%
Sept 2016	71.5	6.0%	18.2%	7.6%	3.3%	62.8%	73.7%
Dec 2016	68.9	4.9%	8.1%	13.3%	2.8%	68.8%	84.9%
Mar 2018	70.4	5.5%	8.0%	14.1%	3.1%	66.3%	83.5%

Summary Modeling Results of Adjacent Locations to Yuma, AZ (March 2018)

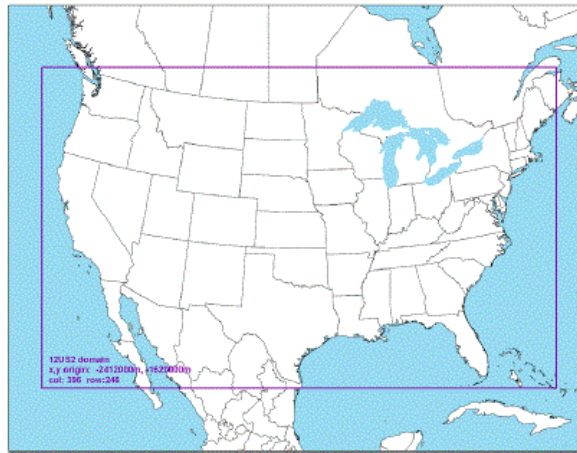
	Average DV	Mex/Can	Biogenics	Boundary	USB (three previous columns combined)
Imperial, CA	79.0	23.7%	2.6%	55.2%	81.5%
San Diego, CA	69.4	20.1%	2.3%	37.9%	60.3%
Dona Ana, NM	67.1	20.3%	4.5%	55.8%	80.6%
El Paso, TX	67.6	27.1%	4.4%	52.2%	83.7%
Brewster, TX	67.9	8.2%	3.6%	75.5%	87.3%

Summary of Modeling Results for Reference

	USB		USB
Maricopa, AZ	55.6%	Chicago, IL	38.6%
San Bernardino, CA	44.5%	Atlanta, GA	31.6%

Long Island, NY	34.2%	Orlando, FL	42.8%
Fairfield, CN	30.8%	Baltimore, MD	30.2%
Sheboygan, WI	35.3%	Denver, CO	52.9%

Modeling Boundary Map



Data Sources of U.S. EPA Modeling:

2008 NAAQS Ozone Transport Modeling

January 2015 – <https://www.epa.gov/airmarkets/january-2015-memo-and-information-0>

August/November 2015 – <https://www.epa.gov/airmarkets/proposed-cross-state-air-pollution-update-rule>

September 2016 – <https://www.epa.gov/airmarkets/final-cross-state-air-pollution-rule-update>

2015 NAAQS Ozone Transport Modeling

December 2016 – <https://www.epa.gov/airmarkets/notice-data-availability-preliminary-interstate-ozone-transport-modeling-data-2015-ozone>

March 2018 - <https://www.epa.gov/airmarkets/march-2018-memo-and-supplemental-information-regarding-interstate-transport-sips-2015>

Technical Notes:

- Mex/Can contribution is anthropogenic emissions from the portions of Mexico and Canada inside the boundary
- Boundary contribution is all (anthropogenic and natural sources) emissions for everything outside the boundary, a global model is used to determine this
- EPA's definition of U.S. Background (USB) as ozone formed from any sources other than US manmade emissions (which would include Mexico/Canada, Biogenics, and Boundary)

Attachment

B



US surface ozone trends and extremes from 1980 to 2014: quantifying the roles of rising Asian emissions, domestic controls, wildfires, and climate

Meiyun Lin^{1,2}, Larry W. Horowitz², Richard Payton³, Arlene M. Fiore⁴, and Gail Tonnesen³

¹Atmospheric and Oceanic Sciences, Princeton University, Princeton, NJ 08540, USA

²NOAA Geophysical Fluid Dynamics Laboratory, Princeton, NJ 08540, USA

³US Environmental Protection Agency, Region 8, Air Program, Denver, CO 80202, USA

⁴Lamont-Doherty Earth-Observatory and Department of Earth and Environmental Sciences, Columbia University, Palisades, NY 10964, USA

Correspondence to: Meiyun Lin (meiyun.lin@noaa.gov)

Received: 4 December 2016 – Discussion started: 7 December 2016

Revised: 2 February 2017 – Accepted: 6 February 2017 – Published: 1 March 2017

Abstract. US surface O₃ responds to varying global-to-regional precursor emissions, climate, and extreme weather, with implications for designing effective air quality control policies. We examine these conjoined processes with observations and global chemistry-climate model (GFDL-AM3) hindcasts over 1980–2014. The model captures the salient features of observed trends in daily maximum 8 h average O₃: (1) increases over East Asia (up to 2 ppb yr⁻¹), (2) springtime increases at western US (WUS) rural sites (0.2–0.5 ppb yr⁻¹) with a baseline sampling approach, and (3) summertime decreases, largest at the 95th percentile, and wintertime increases in the 50th to 5th percentiles over the eastern US (EUS). Asian NO_x emissions have tripled since 1990, contributing as much as 65 % to modeled springtime background O₃ increases (0.3–0.5 ppb yr⁻¹) over the WUS, outpacing O₃ decreases attained via 50 % US NO_x emission controls. Methane increases over this period contribute only 15 % of the WUS background O₃ increase. Springtime O₃ observed in Denver has increased at a rate similar to remote rural sites. During summer, increasing Asian emissions approximately offset the benefits of US emission reductions, leading to weak or insignificant observed O₃ trends at WUS rural sites. Mean springtime WUS O₃ is projected to increase by ~10 ppb from 2010 to 2030 under the RCP8.5 global change scenario. While historical wildfire emissions can enhance summertime monthly mean O₃ at individual sites by 2–8 ppb, high temperatures and the associated buildup of O₃ produced from regional anthropogenic emissions contribute

most to elevating observed summertime O₃ throughout the USA. GFDL-AM3 captures the observed interannual variability of summertime EUS O₃. However, O₃ deposition sink to vegetation must be reduced by 35 % for the model to accurately simulate observed high-O₃ anomalies during the severe drought of 1988. Regional NO_x reductions alleviated the O₃ buildup during the recent heat waves of 2011 and 2012 relative to earlier heat waves (e.g., 1988, 1999). The O₃ decreases driven by NO_x controls were more pronounced in the southeastern US, where the seasonal onset of biogenic isoprene emissions and NO_x-sensitive O₃ production occurs earlier than in the northeast. Without emission controls, the 95th percentile summertime O₃ in the EUS would have increased by 0.2–0.4 ppb yr⁻¹ over 1988–2014 due to more frequent hot extremes and rising biogenic isoprene emissions.

1 Introduction

Within the United States, ground-level O₃ has been recognized since the 1940s and 1950s as an air pollutant detrimental to public health. Decreases in summertime O₃ were observed in parts of California and throughout the EUS (e.g., Cooper et al., 2012; Simon et al., 2015), following regional NO_x controls after the lowering of the US National Ambient Air Quality Standard (NAAQS) for O₃ in 1997 to 84 ppb. On the basis of health evidence, the NAAQS level for O₃

has been further lowered to 75 ppb in 2008 and to 70 ppb in 2015 (Federal Register, 2015). There are concerns that rising Asian emissions and global methane (Jacob et al., 1999; Lin et al., 2015b), more frequent large wildfires in summer (e.g., Jaffe, 2011; Yang et al., 2015; Abatzoglou et al., 2016), and late spring deep stratospheric O₃ intrusions (Lin et al., 2012a, 2015a; Langford et al., 2014) may pose challenges in attaining more stringent O₃ standards in high-elevation WUS regions. A warming climate would also offset some of the air quality improvements gained from regional emission controls (e.g., Fiore et al., 2015). Quantitative understanding of sources of O₃ variability on daily to multi-decadal timescales can provide valuable information to air quality control managers as they develop O₃ abatement strategies under the NAAQS. Here we systemically investigate the response of US surface O₃ means and extremes to changes in Asian and North American anthropogenic emissions, global methane, regional heat waves, and wildfires over the course of 35 years from 1980 to 2014, using observations and chemistry-climate model (GFDL-AM3) hindcasts (Lin et al., 2014, 2015a, b).

Rapid economic growth has led to a tripling of O₃ precursor emissions from Asia in the past 25 years (e.g., Granier et al., 2011; Hilboll et al., 2013). Observed 1 h O₃ mixing ratios can frequently reach 200–400 ppb during regional pollution episodes in eastern China (Wang et al., 2006; Li et al., 2016), with a seasonal peak in the late spring to early summer (Wang et al., 2008; Lin et al., 2009). A synthesis of available observations from the mid-1990s to the 2000s indicates increases of 1–2 ppb yr⁻¹ in spring to summer O₃ in China (Ding et al., 2008; Ma et al., 2016; Sun et al., 2016). Long-range transport of Asian pollution plumes towards western North America has been identified by aircraft and satellite measurements and in chemical transport models (e.g., Jaffe et al., 1999; Fiore et al., 2009; Brown-Steiner and Hess, 2011; Lin et al., 2012b; Huang et al., 2013; Verstraeten et al., 2015). Systematic comparison of observed and modeled long-term O₃ trends over Asia is lacking in the published literature but is needed to establish confidence in models used to assess the global impacts of rising Asian emissions.

Model simulations indicate that import of Asian pollution enhances mean WUS surface O₃ in spring by ~5 ppb (Zhang et al., 2008; Lin et al., 2012b), and occasionally contributes 8–15 ppb during springtime pollution episodes observed at rural sites (Lin et al., 2012b) as supported by in situ aerosol composition analysis (VanCuren and Gustin, 2015). Stratospheric intrusions can episodically increase daily 8 h average surface O₃ by 20–40 ppb, contributing to the highest observed O₃ events at high-elevation WUS sites (Lin et al., 2012a, 2015a), in addition to pollution transport from California (e.g., Langford et al., 2010). In the densely populated EUS, both changes in regional anthropogenic emissions and air pollution meteorology have the greatest impacts on summer surface O₃ during pollution episodes (e.g., Jacob and Winner 2009; Rieder et al., 2015; Porter et al., 2015; Pusede et al., 2015). Discerning directly the effect of climate

change on air quality from long-term observation records of O₃ would be ideal, but concurrent trends in precursor emissions and large internal variability in regional climate impede such an effort. It is difficult to separate the impacts of changes in global-to-regional precursor emissions and different meteorological factors on O₃ at given locations without the benefit of multiple sensitivity experiments afforded by models.

On the other hand, process-oriented assessments of the models are needed to build confidence in their utility for assessing pollution control strategies, estimating tropospheric O₃ radiative forcing and projecting pollution extremes under future climate scenarios (e.g., Monks et al., 2015). A number of studies show that global models capture observed decreases in summertime O₃ over the EUS during 1990–2010, but have difficulty simulating O₃ increases measured at remote high-elevation sites that are believed to represent hemispheric-scale conditions with little influence from fresh local pollution (hereafter referred to as “baseline”) (e.g., Lamarque et al., 2010; Koumoutsaris and Bey, 2012; Parrish et al., 2014; Brown-Steiner et al., 2015; Strode et al., 2015). Recently, Lin et al. (2015b) examined the representativeness of O₃ trends derived from sparse measurements in the free troposphere over the WUS, originally reported by Cooper et al. (2010) and used in prior model evaluations. They found that discrepancies between observed and simulated O₃ trends reflect measurement sampling biases. Here we seek additional insights into the causes of the model–observation disagreement at the WUS rural sites with continuous, high-frequency measurements. Notably, we reconcile observed and simulated O₃ trends at these sites with a baseline sampling approach in the model.

Our goal in this paper is 2-fold: first, to systematically evaluate how well the GFDL-AM3 model represents trends and variability of surface O₃ observed at rural sites across the US; second, to examine changes in US surface O₃ means and extremes in a suite of multi-decadal hindcast simulations designed to isolate the response of O₃ to increases in Asian anthropogenic emissions, North American emission controls, rising global methane, wildfires, and interannual variability in meteorology. We examine trends across the entire probability distribution of O₃ concentration, which is crucial to assessing the ability of models to simulate the surface O₃ response under different temperature and chemical regimes depending on seasons, geographical location, and regional transport patterns. Specifically, we evaluate the trends separately for the 5th, 50th and 95th percentiles of the O₃ concentration distribution in spring (MAM), summer (JJA), autumn (SON), and winter (DJF).

Section 2 briefly describes the observational records, model experiments, and analysis approach. As a first step towards assessing our understanding of the impacts of rising Asian emissions, we briefly review Asian O₃ trends from observations in recent publications and evaluate modeled trends (Sect. 3). We then focus our analysis on the US, using both observations and models to assess the response of

US surface O₃ to changes in background O₃, regional anthropogenic emissions and meteorology (Sect. 4). In Sect. 5, we further separate the influence of background on WUS O₃ into components driven by rising Asian anthropogenic emissions, global methane, and wildfires. We quantify the contribution of these factors to surface O₃ in both rural areas such as national parks (Sect. 5.1 to 5.3) and in densely populated regions such as the Denver metropolitan area (Sect. 5.4). After evaluating historical trends, we additionally draw upon two simulations following the 21st century RCP4.5 versus RCP8.5 global change scenarios to project WUS O₃ through 2050 (Sect. 5.2). Section 6 examines how the EUS summertime O₃ probability distribution and pollution extremes respond to large-scale heat waves, droughts, and regional NO_x reductions over the past decade, and how well our model simulates the observed features. Finally, we summarize in Sect. 7 the key drivers of US surface O₃ trends and extremes and discuss the implications of this study.

2 Model and observations

2.1 Chemistry-climate model experiments

The GFDL-AM3 model includes interactive stratosphere–troposphere chemistry and aerosols on a cubed sphere grid with a resolution of approximately 200 × 200 km² (Donner et al., 2011). Table 1 summarizes the meteorology, radiative forcing agents, and emissions used in each experiment. The hindcast simulations (1979–2014) are nudged to the NCEP/NCAR reanalysis zonal and meridional winds using a height-dependent nudging technique (Lin et al., 2012b). Biogenic isoprene emissions and lightning NO_x are tied to model meteorology (Guenther et al., 2006; Rasmussen et al., 2012) and thus can respond to changes in climate, whereas soil NO_x and chemical dry deposition velocities are set to a monthly climatology (Naik et al., 2013), with a diurnal cycle applied for O₃ dry deposition. To investigate the possible influence of drought on O₃ removal (e.g., Emberson et al., 2013), we additionally conduct a sensitivity simulation for 1988 with reduced O₃ deposition velocity (see Sect. 6). Our BASE simulation and two additional simulations with modified emissions (FIXEMIS and IAVFIRE) were previously used to interpret the causes of increasing autumnal O₃ measured at Mauna Loa Observatory in Hawaii since 1974 (Lin et al., 2014), interannual variability of springtime O₃ (Lin et al., 2015a) and the representativeness of free tropospheric O₃ measurements over the WUS (Lin et al., 2015b).

With anthropogenic emissions and methane held constant (Table 1), the FIXEMIS and IAVFIRE simulations isolate the influence from meteorology and wildfire emissions, respectively. In IAVASIA, anthropogenic emissions from East Asia (15–50° N, 95–160° E) and South Asia (5–35° N, 50–95° E) are allowed to vary from year to year as in BASE, while anthropogenic emissions in the other regions of the

world, global methane and wildfire emissions are held constant as in FIXEMIS. In IAVCH₄, global methane is allowed to vary over time as in BASE, but with anthropogenic and wildfire emissions held constant as in FIXEMIS. The IAVASIA and IAVCH₄ simulations thus isolate the role of rising Asian anthropogenic emissions and global methane, respectively, by contrasting with the FIXEMIS simulation. Both BASE and IAVCH₄ simulations apply observed time-varying methane concentrations as a lower boundary condition for chemistry (Supplement Fig. S1). Thus, underestimates in historical methane emissions reported recently by Schwietzke et al. (2016) do not affect our results. We quantify the total contributions to surface O₃ from meteorological variability, stratosphere-to-troposphere transport, pollution from foreign continents and O₃ produced by global methane, lightning NO_x, wildfires and biogenic emissions with the Background simulation, in which North American anthropogenic emissions are zeroed out relative to BASE. We additionally draw upon two simulations with the GFDL Coupled Model CM3 following the 21st century RCP global change scenarios to project changes in WUS O₃ through 2050. Details of these CM3 simulations were described in John et al. (2012).

2.2 Anthropogenic and biomass burning emissions

We first examine how well the emission inventories in AM3 BASE represent changes in regional NO_x emissions over recent decades inferred from satellite measurements of tropospheric vertical column density (VCD_{trop}) of NO₂. The combined record of GOME and SCIAMACHY shows that VCD_{trop} NO₂ over the highly polluted region of eastern China almost tripled during 1996–2011 (Fig. 1a). In contrast, VCD_{trop} NO₂ over the EUS decreased by ~50% in the 2000s (Fig. 1b) due to NO_x State Implementation Plans (commonly known as the NO_x SIP Call) and many rules that tighten emission standards for mobile sources (McDonald et al., 2012). Similar decreases occurred in WUS cities, resulting from the NO_x control programs to achieve O₃ and regional haze planning goals. These trends are consistent with those reported by a few recent studies (e.g., Hilboll et al., 2013), including those using OMI NO₂ data (Russell et al., 2012; Duncan et al., 2016). For comparison with satellite data, we sample the model archived every 3 h closest to the time of satellite overpass for the SCIAMACHY and GOME products we use in Fig. 1 (10:00–10:30 local time). Trends in VCD_{trop} NO₂ are similar to those in NO_x emissions (orange lines versus red triangles in Fig. 1a–b), indicating that any changes in NO_x chemical lifetime or partitioning have negligible influence in our model, consistent with NO₂ loss against OH being minor during the morning overpasses of GOME and SCIAMACHY. The emission inventory used in BASE, from Lamarque et al. (2010) with annual interpolation after 2000 to RCP8.5 (Lamarque et al., 2012), mimics the opposing changes in NO_x emissions over eastern China versus the EUS during 1996–2011, consistent with

Table 1. Summary of forcings and emissions used in AM3 hindcasts and CM3 projections.

Experiment	Time periods	Meteorology	Radiative forcings	CH ₄ (chemistry)	Anthropogenic emissions	Fire emissions
BASE	1979–2014	Nudged to NCEP	Historical	Historical	Historical	Historical
Background	1979–2014	As BASE	Historical	Historical	Zeroed out in N. America; as in BASE elsewhere	Historical
FIXEMIS	1979–2014	As BASE	Historical	2000	Constant ¹	Constant ¹
IAVFIRE	1979–2014	As BASE	Historical	2000	Constant ¹	Historical
IAVASIA	1979–2012 ²	As BASE	Historical	2000	Varying in Asia as in BASE; as in FIXEMIS elsewhere	Constant ¹
IAVCH ₄	1979–2012 ²	As BASE	Historical	Historical	Constant ¹	Constant ¹
CM3_RCP4.5	2005–2050	Free running	RCP4.5	RCP4.5	RCP4.5	RCP4.5
CM3_RCP8.5	2005–2050	Free running	RCP8.5	RCP8.5	RCP8.5	RCP8.5

¹ Averaged over the whole 1970–2010 period. ² Note that the IAVASIA and IAVCH₄ simulations only extend to 2012.

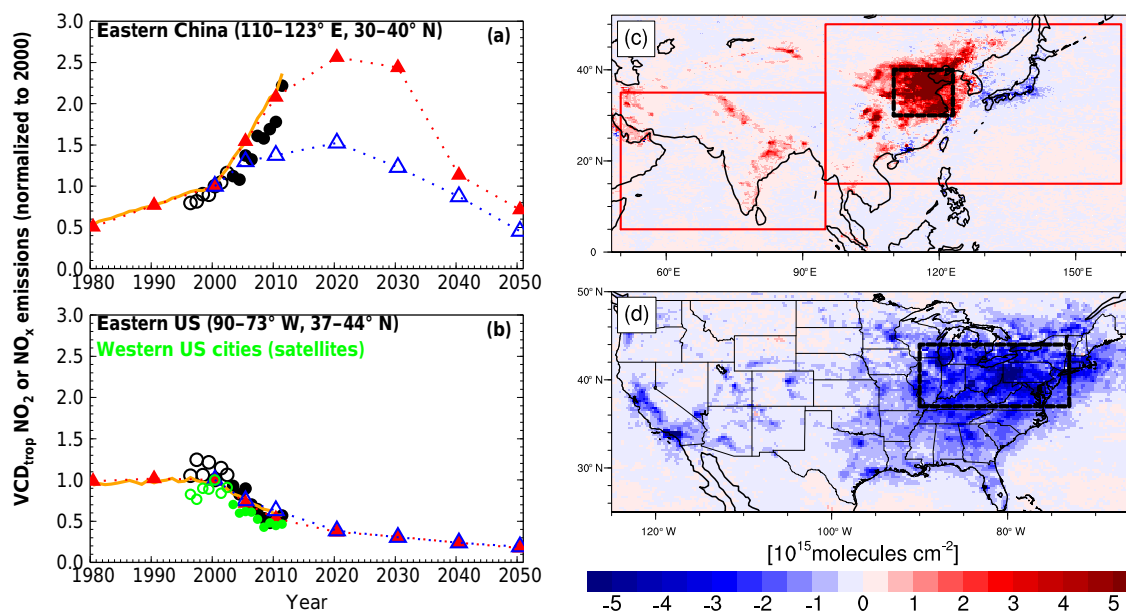


Figure 1. Changes in NO_x emissions. (a–b) Mean annual vertical column densities of tropospheric (VCD_{trop}) NO₂ normalized to the year 2000 for the eastern China and eastern US domains (black boxes on map) from GOME (1996–2002, open circles) and SCIAMACHY (2003–2011, closed circles) measurements and AM3 BASE simulations (orange lines). Triangles indicate trends in NO_x emissions (normalized to 2000) from Lamarque et al. (2010) with annual interpolation after 2000 to RCP8.5 (red) versus RCP4.5 (blue). (c–d) Differences in annual mean SCIAMACHY VCD_{trop} NO₂ from 2003–2005 to 2009–2011. The red boxes denote the regions where emissions vary over time in the IAVASIA simulation (Table 1). Satellite NO₂ data are from www.temis.nl, with the retrieval technique described in Boersma et al. (2004).

changes in VCD_{trop} NO₂ retrieved from the satellite instruments. For comparison, the RCP4.5 interpolation for 2001–2010 in CMIP5 historical simulations analyzed by Parrish et al. (2014) underestimates the increase in Chinese NO_x emissions by a factor of 2 (Fig. 1a). Recent reductions in Chinese NO_x emissions after 2011 (Duncan et al., 2016) are not represented in the inventories used in AM3.

Our BASE model applies interannually varying monthly mean emissions from biomass burning based on the RETRO inventory (Schultz et al., 2008) for 1970 to 1996 and GFEDv3 (van der Werf et al., 2010) for 1997 onwards, distributed vertically as recommended by Dentener et al. (2006).

Figure S2 illustrates the interannual variability of biomass burning CO emissions from the main source regions of the Northern Hemisphere over the period 1980–2014. Boreal fire emissions in Eurasia almost doubled from 1980–1995 to 1996–2014, with large fires occurring more frequently in the recent decade, as found for the WUS (Dennison et al., 2014; Yang et al., 2015).

2.3 Ozone observation records and uncertainties

Long-term surface O₃ observation records were obtained at 70 selected rural monitoring sites with 20 (1995–2014) to 27 (1988–2014) years of continuous hourly measurements

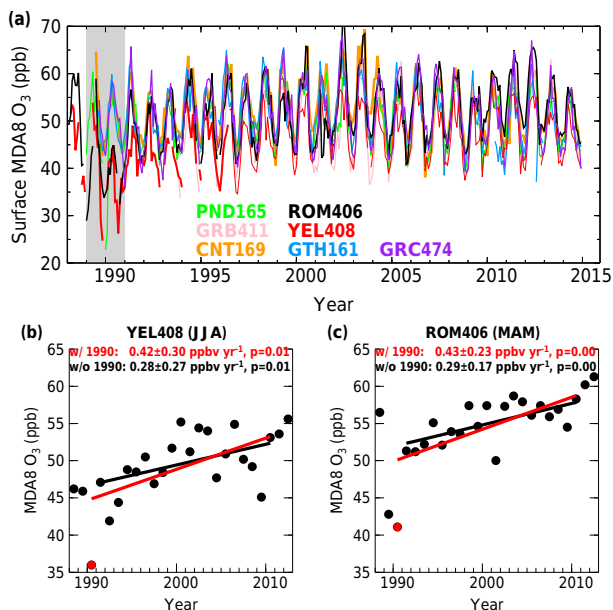


Figure 2. Measurement uncertainties. (a) Comparison of observed monthly mean MDA8 O₃ at WUS CASTNet sites. All sites have more than 90 % data availability in every month shown. The gray shading denotes the period when data at Yellowstone (red) and Rocky Mountain (black) were inconsistent with the other sites. (b–c) The 1990–2010 trends of median JJA MDA8 O₃ at Yellowstone and median MAM MDA8 O₃ at Rocky Mountain with and without data in 1990.

from the US National Park Services, the US Clean Air Status and Trends Network (CASTNet), and the US EPA Air Quality System. Cooper et al. (2012) reported trends in daytime (11:00–16:00) O₃ over 1990–2010 at 53 rural sites. We investigate trends in daily maximum 8 h averaged (MDA8) O₃ and expand the analysis of Cooper et al. (2012) using additional data to 2014 and including 17 additional sites with measurements begun in 1991–1995. All sites have at least 20 years of data. If a site has less than 50 % data availability in any season, then that particular season is discarded. The trend is calculated separately for the 5th, 50th and 95th percentiles of daily MDA8 O₃ for each season through ordinary linear least-square regression. Statistics are derived for the slope of the linear regression in units of ppb yr⁻¹, the range of the slope with a 95 % confidence limit (not adjusted for sample autocorrelation), and the *p* value indicating the statistical significance of the trend based on a two-tailed *t* test.

A cross-site consistency analysis was performed to determine robust changes in the time evolution of O₃ over the WUS during 1988–2014 (Fig. 2). The monitor at Yellowstone National Park was moved 1.5 km from the Lake Yellowstone site to the Water Tank site in 1996. While the local transport patterns are slightly different for the two sites, using MDA8 data from the well-mixed midday period minimizes the differences (Jaffe and Ray, 2007). Observed O₃ interannual variations show large-scale similarity across sites over

the Intermountain West except for the earlier period 1989–1990. During this period, observations at Yellowstone and Rocky Mountain national parks show low-O₃ anomalies that do not appear at other sites, but there is no change in measurement technique. Jaffe and Ray (2007) suggest this represents large-scale variations in background O₃ that are seen in common at these two parks. However, analysis of meteorological fields and model diagnostics does not reveal any obvious transport anomaly influencing O₃ variations at these sites in 1990 (Lin et al., 2015a). Observations at Pinedale in January–February 1990 are also anomalously low relative to Grand Canyon (GRC474), Centennial (CNT169), and Gothic (GTH161). These anomalous data at the beginning of measurement records can substantially influence trends calculated from short records. For example, Cooper et al. (2012) found a summer O₃ increase of 0.42 ± 0.30 ppb yr⁻¹ at Yellowstone over 1990–2010. Removing 1990, we find a weaker increase of 0.28 ± 0.27 ppb yr⁻¹ (Fig. 2b). Removing 1990 at Rocky Mountain resulted in a weaker springtime O₃ increase of 0.29 ± 0.17 ppb yr⁻¹ compared to 0.43 ± 0.23 ppb yr⁻¹ over 1990–2010 (Fig. 2c). To assess robust O₃ changes, we thus remove these apparently uncertain measurements in 1990 from the subsequent analysis.

2.4 Model baseline sampling approach

Springtime O₃ observations at WUS high-elevation sites (≥ 1.5 km a.s.l.) typically represent baseline conditions with little influence from fresh local pollution. In a global model with $\sim 200 \times 200$ km² horizontal resolution, however, these remote sites can reside in the same grid cell that contains urban cities where NO_x emissions decreased over the analysis period. For example, Rocky Mountain National Park (2.7 km a.s.l.) is less than 100 km from the Denver metropolitan area in Colorado. This limitation of large-scale models in resolving urban-to-rural gradients and sharp topography results in an artificial offset of increased baseline O₃ at remote sites by decreased urban pollution within the same model grid cell. Thus, coarse-resolution models are often unable to reproduce observed O₃ increases at the high-elevation sites representative of remote baseline conditions (Fig. 3a versus b), as found in many prior modeling analyses (e.g., Parrish et al., 2014; Strode et al., 2015, and references therein). This limitation can be addressed by using a baseline selection procedure to identify conditions for sampling the model to avoid model artifacts caused by poor spatial resolution, as described below.

All measurements presented in this study are unfiltered. We implement a set of regional CO-like tracers (CO_t), with a 50-day exponential decay lifetime and surface emissions constant in time from each of four northern mid-latitude source regions (Lin et al., 2014). We use these CO_t tracers to bin modeled O₃ according to the dominant influence of different continental air regimes. To represent observed baseline conditions at WUS sites, we sample AM3

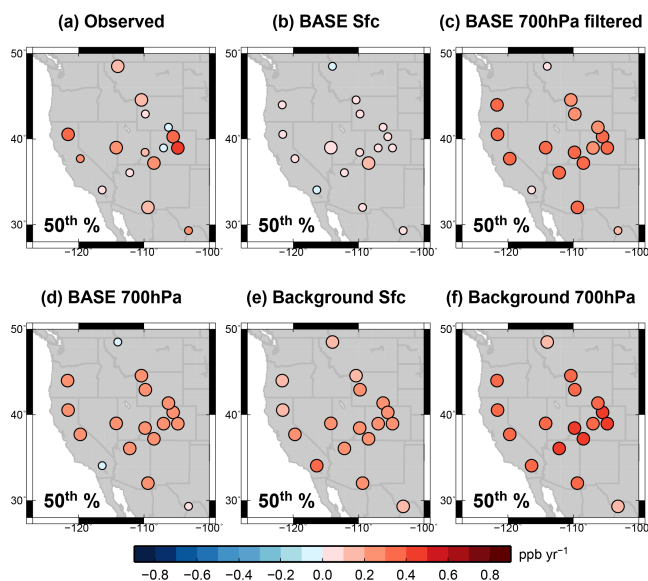


Figure 3. Influence of baseline sampling. Median spring MDA8 O₃ trends over 1988–2014 at WUS sites from (a) observations, (b) BASE model sampled at the surface, (c) BASE sampled at 700 hPa and filtered to remove the influence from fresh local pollution (see Sect. 2.4), (d) BASE sampled at 700 hPa without filtering, and (e–f) Background (with North American anthropogenic emissions shut off) sampled at the surface versus at 700 hPa. Note that three low-elevation (< 1.5 km) sites, Joshua Tree, Big Bend and Glacier national parks, are always sampled at the surface. Larger circles indicate sites with statistically significant trends ($p < 0.05$).

at 700 hPa (~ 3 km a.s.l.) and filter the O₃ data in the BASE simulation to remove the influence from fresh local pollution. Specifically, our filter excludes days when North American CO_t (NACo_t) exceeds the 67th percentile for each season. This procedure yields higher calculated baseline O₃ increases (Fig. 3c), bringing it closer to observations (Fig. 3a). When sampled at 700 hPa without filtering (Fig. 3d), BASE gives statistically significant O₃ increases, but the rate of increase is ~ 0.1 ppb yr⁻¹ weaker than with filtering. With North American anthropogenic emissions shut off, the model simulates significant O₃ increases that are similar at the surface (Fig. 3e) and at 700 hPa (Fig. 3f). This finding indicates that the underestimate of O₃ increases in BASE, when sampled at the surface (Fig. 3b), reflects an excessive offset from domestic pollution decreases in the model relative to observed conditions, as opposed to the insufficient mixing of free tropospheric O₃ to the surface. As individual sites display observed trends falling in between the filtered model, and those sampled at the surface versus aloft, we can use the model to interpret which sites most frequently sample baseline versus being influenced by North American anthropogenic emissions. For consistency, in the subsequent analysis we apply model baseline filtering to all WUS sites with elevations greater than 1.5 km altitude. In the EUS, where the terrain and monitor elevations are much lower than in

the west and observed O₃ trends are largely controlled by regional emission changes, we always sample the model at the surface without filtering.

3 Global distribution of lower tropospheric O₃ trends

3.1 Global O₃ burden and distribution of trends

We begin by examining the global distribution of lower tropospheric O₃ trends over 1988–2014 from the BASE simulation (Fig. 4) and focus on the differences between the surface and free troposphere (~ 700 hPa), with implications for understanding the impact of trends in hemispheric baseline O₃ on surface air quality. The model indicates that surface MDA8 O₃ levels in Asia have increased significantly by 1.5–2.5 ppb yr⁻¹ in the 95th percentile (Fig. 4a–b) and by 1–2 ppb yr⁻¹ in the median values (Fig. 4c–d), with the largest increases occurring in southern Asia during spring and over eastern China during summer. In contrast, there is a marked decrease in surface MDA8 O₃ in WUS cities, throughout the EUS and in central Europe, particularly at the high percentiles and during summer. The increase in surface O₃ over Asia and decreases over the US and Europe are consistent with changes in regional emissions of O₃ precursors over this period (Fig. 1).

Over Southeast Asia (south of 30° N) during spring, earlier springtime O₃ photochemical production at lower latitudes coupled with active frontal transport (Liu et al., 2002; Carmichael et al., 2003; Lin et al., 2010) leads to a comparable or even greater increase in O₃ in the free troposphere than at the surface (Fig. 4c versus e). In contrast, over central eastern China during summer the simulated trends of O₃ in the free troposphere are at least a factor of 3 weaker than in surface air (Fig. 4d versus f), consistent with the analysis of MOZAIC aircraft data over Beijing in 1995–1999 versus 2003–2005 (Ding et al., 2008). Mean O₃ at 700 hPa above parts of North America and Europe show little change in summer or even increase during spring in the model, similar to the trends at 500 hPa (Fig. S3), despite the significant decreases in surface air. The global tropospheric O₃ burden in the BASE simulation increases by approximately 30 Tg over the past 35 years (Fig. 5a), attributed mainly to changes in anthropogenic emissions. Over the 2004–2015 OMI/MLS satellite era, however, meteorological variability contributes approximately half to the total simulated decadal trends of O₃ burden (Fig. 5a), indicating that attribution of the satellite-derived decadal trends of global tropospheric O₃ burden requires consideration of internal climate variability.

3.2 Comparison of observed and simulated O₃ trends in Asia

Long-term O₃ observations are very sparse in Asia, making it difficult to evaluate modeled O₃ trends. We compile available measurements from the published literature, includ-

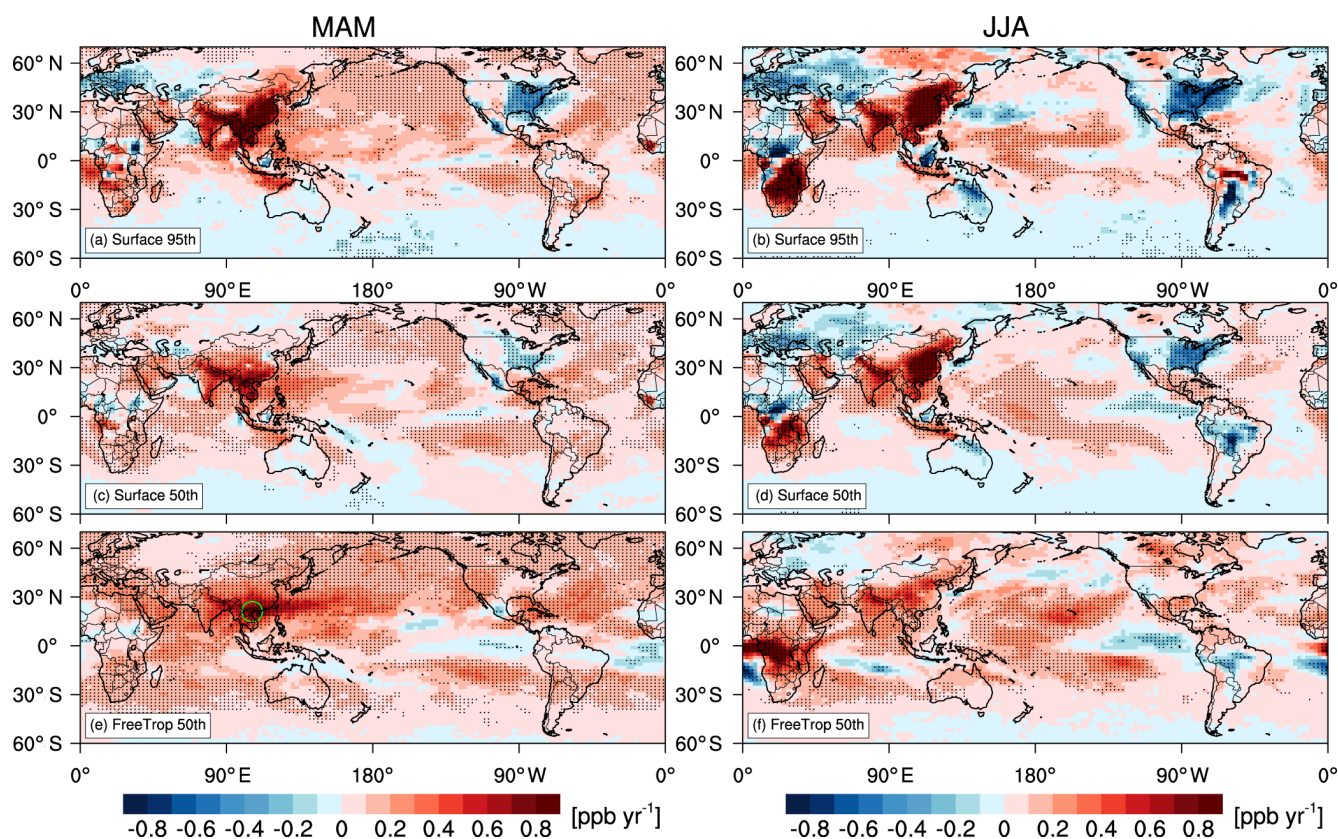


Figure 4. Global distribution of MDA8 O₃ trends from AM3 BASE over 1988–2014 for boreal spring (left) and summer (right) for the 95th percentile at the surface (a–b), median at the surface (c–d), and median in the free troposphere (700 hPa; e–f). Stippling indicates areas where the trend is statistically significant ($p < 0.05$). The color scale is designed to resolve regional features rather than extreme values and saturates. The range of the trends is -1 to $+2.5$ ppb yr⁻¹.

ing ozonesonde profiles at Hong Kong (2000–2014; www.woudc.org) and Hanoi (2005–2015; SHADOZ, Thompson et al., 2007), MOZAIC aircraft profiles collected on summer afternoons in the boundary layer (below 1250 m altitude) over Beijing for 1995–2005 (Ding et al., 2008), ground-based measurements at Mt. Tai (1.5 km a.s.l.) in central eastern China for July–August 2003–2015 (Sun et al., 2016), at the GAW stations, Shangdianzi north of Beijing for 2004–2014 (Ma et al., 2016) and Mt. Waliguan (3.8 km a.s.l.) on the Tibetan Plateau for 1994–2013 (Xu et al., 2016), at Taiwan for 1994–2007 (Lin et al., 2010), South Korea for 1990–2010 (Lee et al., 2014), Mt. Happo (1.9 km a.s.l.) in Japan for 1991–2011 (Tanimoto, 2009; Parrish et al., 2014), and a coastal site at Hong Kong in southern China for 1994–2007 (Wang et al., 2009).

Recently, Zhang et al. (2016) compiled sparse O₃ profiles above Southeast Asia from IAGOS commercial aircraft and ozonesondes from Hanoi for 1994–2004 versus 2005–2014 and found a total springtime O₃ increase of 20–25 ppb between the two periods (~ 2 ppb yr⁻¹). However, our model indicates an increase of up to 1 ppb yr⁻¹ for free tropospheric O₃ over Southeast Asia in spring (Fig. 4e). We illus-

trate the possible influence of sampling deficiencies on the O₃ trends inferred from sparse observations (Fig. 5). The ozonesonde frequency is four profiles per month at Hong Kong and only one to two profiles per month at Hanoi. To determine the representativeness of O₃ trends derived from these sparse measurements, we compare observations and model results co-sampled on sonde launch days, with the “true average” determined from O₃ fields archived every 3 h from the model, as in our prior work for WUS sites (Lin et al., 2015a, b). Figure 5b and c show the comparisons for the annual trends of O₃ over 900–600 hPa. The trends are generally consistent across the sonde data, model co-sampled and “true average” results for Hong Kong, with an increase of 0.5 ± 0.1 ppb yr⁻¹ over 2000–2014. Observations at Hanoi show an apparently rapid O₃ increase of 1.1 ± 0.2 ppb yr⁻¹ over 2005–2014. AM3 BASE, when sampled sparsely as in the ozonesondes, captures the observed variability ($r^2 = 0.7$), whereas the “true average” over this period indicates the trend (0.7 ± 0.1 ppb yr⁻¹) is only 63 % of that inferred from observations. Moreover, interannual variability of O₃ resulting from wildfire emissions and meteorology in IAVFIRE is as large as the total O₃ change in

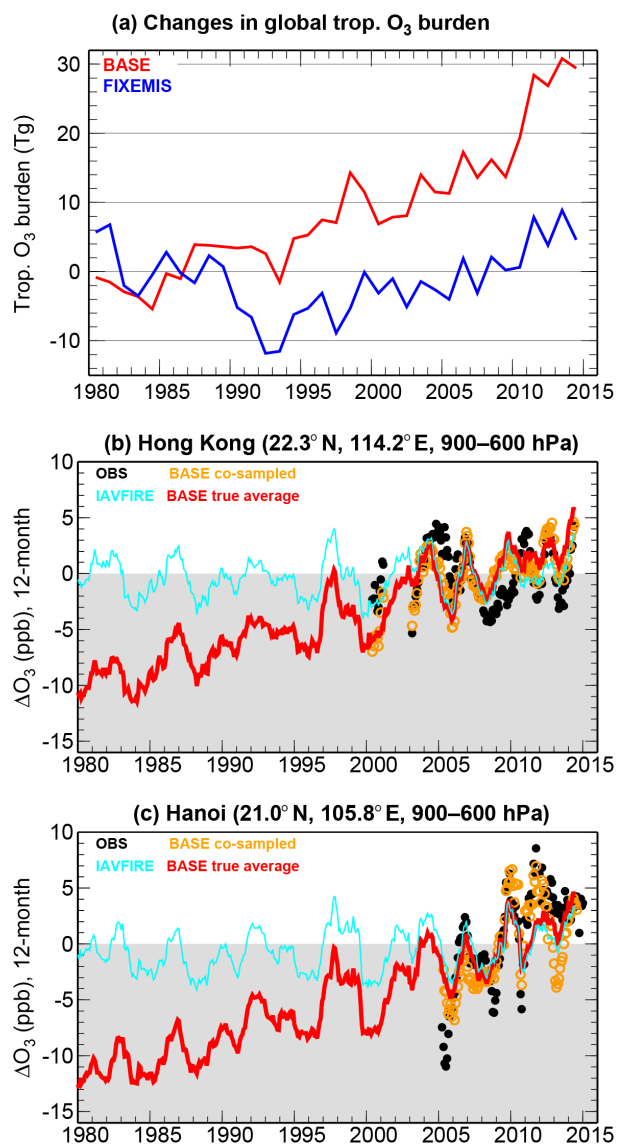


Figure 5. (a) Time series of changes in global tropospheric O_3 burden relative to the 1981–1990 mean from BASE and FIXEMIS simulations (Table 1). (b) Time series of 12-month running mean anomalies (relative to the 2005–2014 mean) of O_3 averaged over 900–600 hPa at Hong Kong from the averages of ozonesonde samples (black circles) and the BASE model co-sampled on sonde launch days (orange circles) versus the true average from BASE and IAVFIRE with continuous daily sampling (solid lines). (c) Same as (b), but for Hanoi.

BASE over the short period 2005–2014. We conclude that measurement sampling artifacts influence the O_3 trends reported by Zhang et al. (2016).

Expanding the comparison to a suite of sites across East Asia (Fig. 6), we find that AM3 captures the key features of observed O_3 trends in Asia, including their seasonal to regional variations, summertime increases ($1\text{--}2\text{ ppb yr}^{-1}$) in central eastern China where NO_x emissions have approxi-

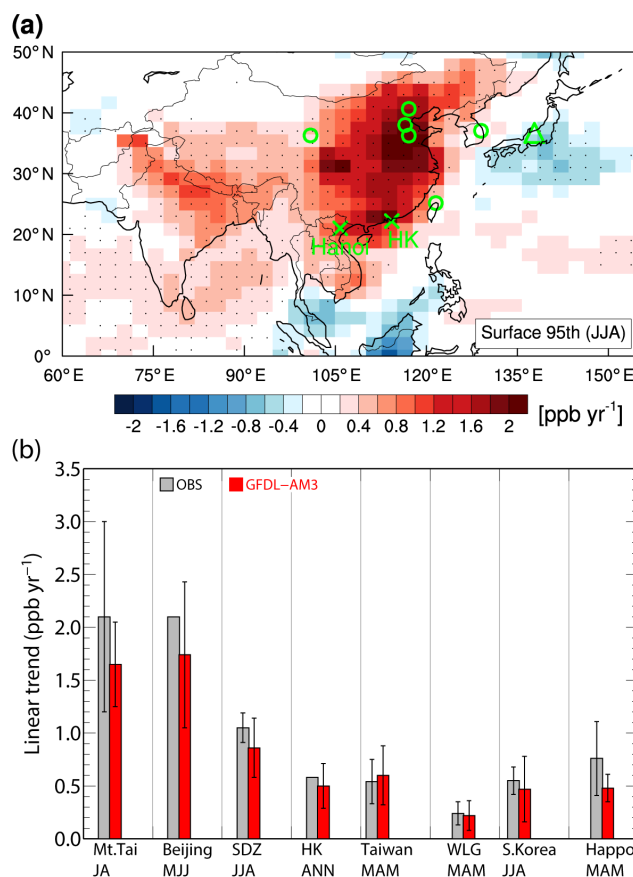


Figure 6. Surface O_3 trends in Asia. (a) Observation sites superimposed on a map of the 95th percentile summer MDA8 O_3 trends over 1995–2014 from AM3 BASE. (b) Comparison of median O_3 trends from AM3 (1995–2014) with observations (see text for periods): in central eastern China at Mt. Tai (July–August, Sun et al., 2016), Beijing (May–June–July, Ding et al., 2008) and Shangdianzi (SDZ) (JJA, Ma et al., 2016); in South China at Hong Kong (HK) (annual average, Wang et al., 2009) and Taiwan (MAM, Lin et al., 2010); at Mt. Waliguan (WLG) in western China (MAM, Xu et al., 2016); in South Korea (JJA, Lee et al., 2014) and Mt. Happo Japan (MAM, Tanimoto, 2009). For Mt. Happo (triangle on map) AM3 is sampled at 700 hPa and filtered for the influence from Asian continental air – more representative of observed baseline conditions in spring.

mately tripled since 1990 (Fig. 1a), and springtime increases (0.5 ppb yr^{-1}) at Taiwan and Mt. Happo that are driven by pollution outflow from the Asian continent. Note that to place the trends derived from the short observational records into a broader context, we show the 20-year trends over 1995–2014 from the model, except for South Korea (1990–2010) and Happo, Japan (1991–2011). We match the time period in the model with observations at these two sites because AM3 shows weaker O_3 increases when data for the recent years are included, which likely reflects the offsetting effects of regional emission reductions in South Korea and Japan.

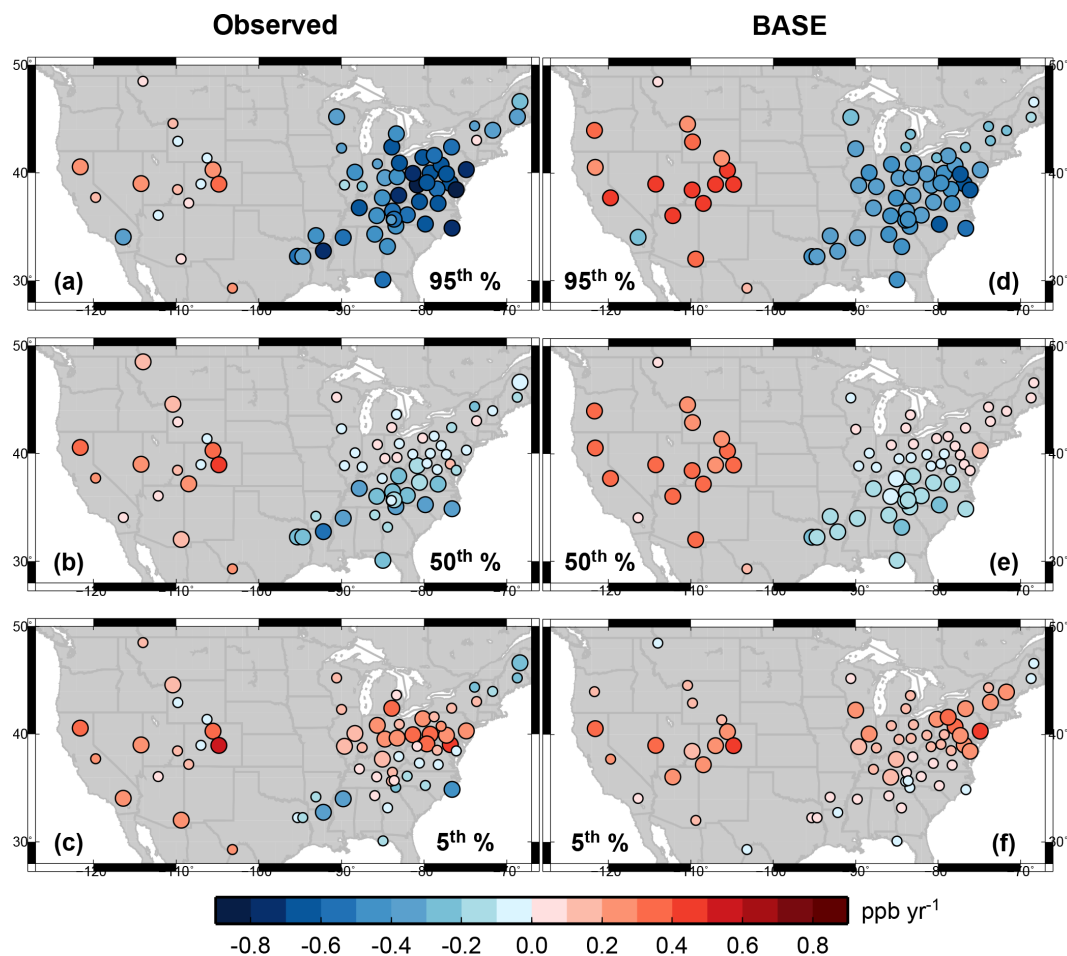


Figure 7. Linear trends in spring (MAM) MDA8 O₃ over 1988–2014 at US rural sites for the 95th, 50th, and 5th percentiles as observed (left) and simulated (right) in AM3 BASE. Larger circles indicate sites with statistically significant trends ($p < 0.05$). For WUS high-elevation sites, the model is sampled at 700 hPa and filtered to remove local influence (see text in Sect. 2.4).

Parrish et al. (2014) show that three CMIP5-like models underestimate the observed springtime O₃ increase at Mt. Happon by a factor of 4. This discrepancy may reflect a combination of factors: (1) underestimates of Asian emission growth in the RCP4.5 interpolation after 2000 used in CMIP5 historical simulations (Fig. 1a); (2) trends driven by inter-annual meteorological variability that free-running CMIP5 models are not expected to reproduce exactly; (3) an excessive offset from Japanese pollution decreases in the models owing to their coarse resolution and limitation in resolving observed baseline conditions at Mt. Happon. Sampling our BASE model at 700 hPa above Happon, we find an O₃ increase of 0.35 ± 0.13 ppb yr⁻¹. When focusing on days strongly influenced by outflow from the East Asian continent (Chinese CO_t ≥ 67 th), the model O₃ trend increases to 0.48 ± 0.13 ppb yr⁻¹, approximating the observed increase of 0.76 ± 0.35 ppb yr⁻¹ at Mt. Happon (Fig. 6b). The observed and simulated trends are not statistically different given the overlapping confidence limits. The larger confidence limit

(uncertainty) derived from the Happon observations reflects the measurement inconsistency before 1998 and instrumental problems after 2007 (Tanimoto et al., 2016). We conclude that GFDL-AM3 captures 65–90 % of the observed O₃ increases in Asia, lending confidence in its application to assess the global impacts of rising Asian emissions.

4 Regional and seasonal variability of US surface O₃ trends

We next focus our analysis on the US, where dense, high-frequency, long-term, reliable measurements of surface O₃ facilitate process-oriented model evaluation. Comparisons of surface O₃ trends over 1988–2014 at 70 rural monitoring sites across the US as observed and simulated in AM3 BASE are shown in Fig. 7 for spring, Fig. 8 for summer, Fig. 9 for winter, and in Fig. S4 for autumn. The trends are calculated separately for the 5th, 50th and 95th percentiles of the daily MDA8 O₃ concentration distribution, with larger circles on

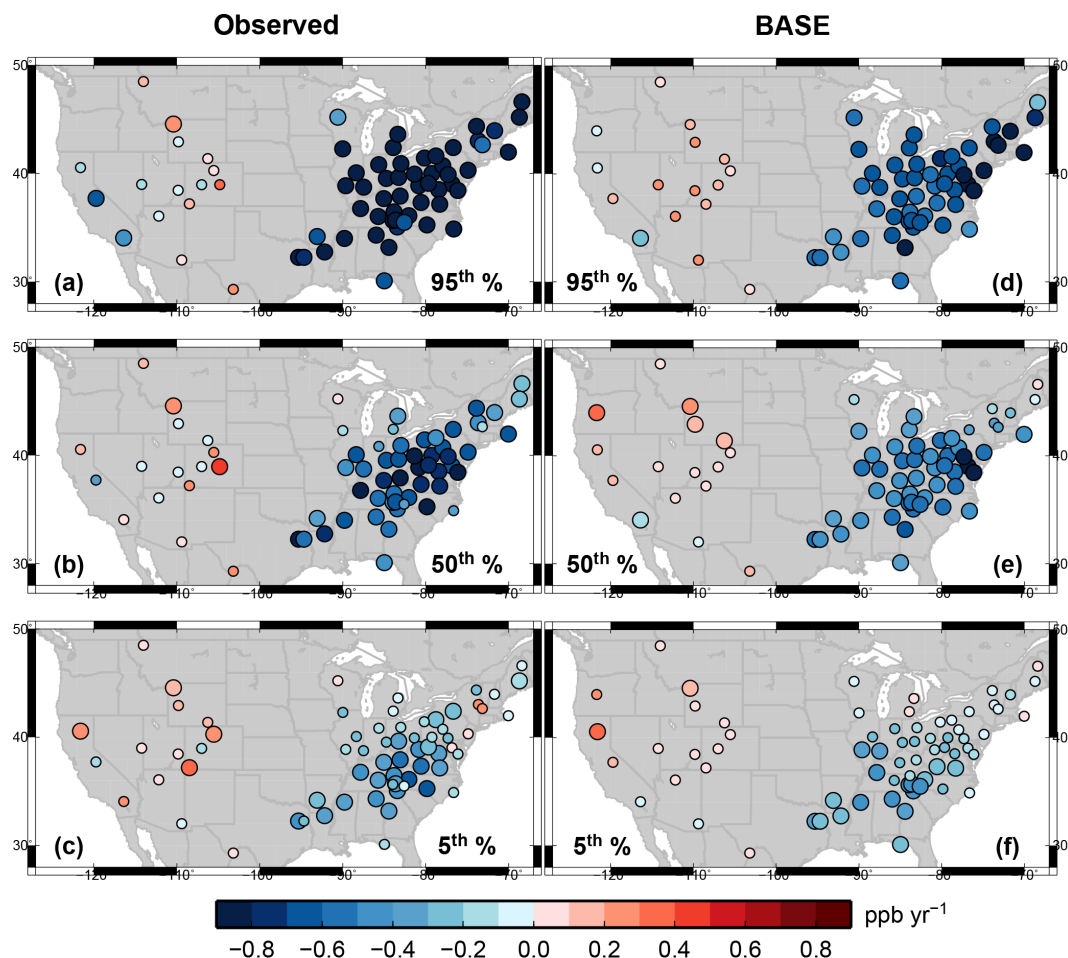


Figure 8. As in Fig. 7, but for summer (JJA). Note that the color scale saturates at ± 0.8 .

the maps indicating sites with statistically significant trends ($p < 0.05$). We first discuss observations (Sect. 4.1), followed by model evaluation and trend attribution (Sect. 4.2).

4.1 Observations

In spring (Fig. 7), observations indicate spatial heterogeneity in O_3 trends across the Intermountain West and the northeastern (north of $38^\circ N$) and southeastern US. At the 95th percentile (Fig. 7a) the pattern of observed trends is homogeneous across the northeastern and southeastern US, with approximately 85 % of the sites having statistically significant O_3 decreases of $0.4\text{--}0.8\text{ ppb yr}^{-1}$ and no sites showing a significant increase. In contrast, significant increases occur at 25 % of the sites in the Intermountain West. Only Joshua Tree National Park located downwind of the Los Angeles Basin shows a significant decrease at the 95th percentile. At the 50th percentile (Fig. 7b) there are significant O_3 decreases of $0.2\text{--}0.4\text{ ppb yr}^{-1}$ in the southeast and little overall change in the northeast, while significant increases of $0.2\text{--}0.5\text{ ppb yr}^{-1}$ occur at 50 % of the sites in the Intermountain West. Significant springtime O_3 increases occur at all observed per-

centiles at Lassen Volcanic National Park in California, Great Basin National Park in Nevada, Rocky Mountain National Park and US Air Force Academy in Colorado. At the 5th percentile (Fig. 7c) significant O_3 increases occur at most sites in the northeast, while little change and some negative trends are found in the southeast. The occurrence of the greatest observed O_3 decreases for the highest percentiles is consistent with high-temperature O_3 production being more NO_x -limited (Pusede et al., 2015) and thus more responsive to decreases in NO_x emissions.

The north-to-south gradient in springtime O_3 trends over the EUS reflects the earlier seasonal transition from NO_x -saturated to NO_x -sensitive O_3 production regimes in the southeast, where plentiful radiation in spring enhances HO_x supply and biogenic isoprene emissions begin earlier than in the northeast. The different response of springtime O_3 to NO_x controls in the southeast versus northeast noticed in this work is not present in prior analyses for shorter time periods (1990–2010 in Cooper et al., 2012, and 1998–2013 in Simon et al., 2015). We find 72 % of the southeastern sites experiencing significant median O_3 decreases in spring over

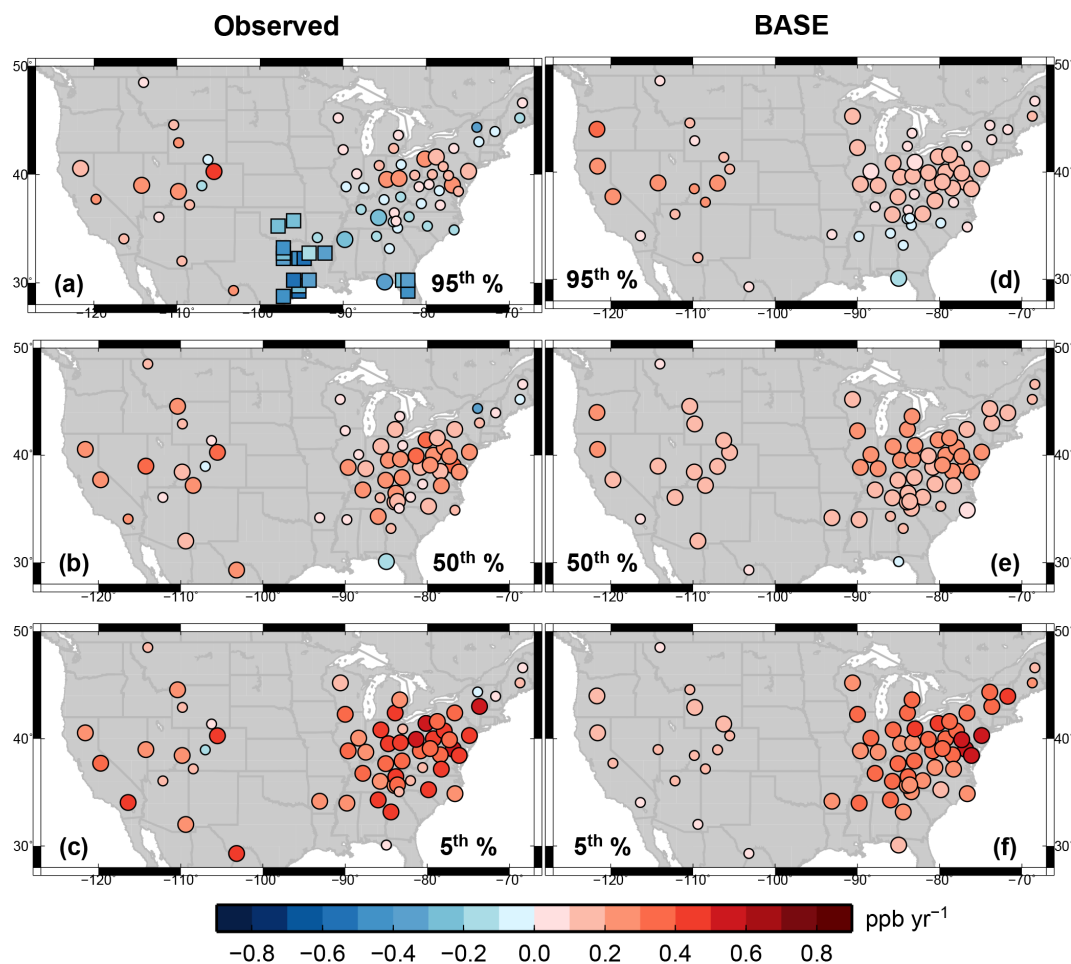


Figure 9. As in Fig. 7, but for winter (DJF). Large squares in (a) denote AQS sites with significant O₃ decreases in the 95th percentile.

1988–2014, while Cooper et al. (2012) found only 8 %. Sites with significant 95th percentile springtime O₃ decreases in the EUS are also much more common in our study (85 % versus 43 % in Cooper et al. (2012)). In the 5th percentile, 45 % of the northeastern sites in our analysis have significant spring O₃ increases, with only 15 % in Cooper et al. (2012). Stronger O₃ reductions in the southeast than the northeast also occur during autumn (Fig. S4), reflecting an extension of biogenic isoprene emissions and NO_x-sensitive O₃ production in the southeast to autumn.

In summer (Fig. 8), as radiation intensifies and isoprene emissions peak seasonally, the O₃ production becomes more NO_x-limited across both the southeastern and northeastern US, where NO_x emission controls have led to significant O₃ decreases of 0.8–1.8 ppb yr⁻¹ in the 95th percentile and 0.4–0.8 ppb yr⁻¹ in the median value (Fig. 8a–b). In the southeast, significant decreases have also occurred at the lowest percentiles during summer (Fig. 8c), in contrast to the weak response during spring (Fig. 7c). Many northeastern states in the late 1990s and early 2000s did not turn on power plant NO_x emission controls until the O₃ season

(May–September), which may contribute to observed differences between spring and summer O₃ trends. Compared to the 1990–2010 trends reported in Cooper et al. (2012), the EUS summer O₃ decreases reported here with additional data to 2014 are 33 % stronger. Despite reductions in precursor emissions in the WUS cities (Fig. 1d), there are no significant summer O₃ decreases at the intermountain sites, except in Yosemite and Joshua Tree national parks for the 95th percentile. Instead, a significant summer increase of ~0.3 ppb yr⁻¹ occurs across the entire O₃ distribution at Yellowstone. Significant summer increases are found in the 5th percentile for Lassen, Mesa Verde, and Rocky Mountain national parks.

In winter (Fig. 9), observed O₃ increases are more common than in spring and summer across the US. The wintertime O₃ increases are strongest in the lowest percentiles over the EUS, indicating the influence from weakened NO_x titration as a result of regional NO_x emission controls (see also Gao et al., 2013; Clifton et al., 2014; Simon et al., 2015). Even during winter, some decreasing O₃ trends are found in the highest percentiles over the southeast (Fig. 9a),

most prominently in Texas (Dallas and Houston), where tropical climate and year-round active photochemistry makes O₃ most responsive to regional NO_x emission controls. Despite the greatest NO_x emission reductions over the past decade in the central and northeastern US regions, observed O₃ reductions have been most pronounced in the southeast, particularly in spring and autumn.

4.2 Model evaluation and attribution of observed O₃ trends

The BASE simulation with GFDL-AM3 captures the salient features of observed O₃ trends over 1988–2014 at rural sites across the US: (1) the overall springtime increases and the lack of significant trends in summer over the Intermountain West; (2) the north-to-south gradients in O₃ trends during spring and the largest decreases in the 95th percentile during summer over the EUS; (3) wintertime increases in the 5th and 50th percentiles (left versus right panels in Figs. 7 to 9). AM3 also simulates a median springtime O₃ increase of 0.32 ± 0.11 ppb yr⁻¹ over 1988–2014 (0.64 ± 0.50 ppb yr⁻¹ over 2004–2014) at Mount Bachelor Observatory in Oregon, consistent with the positive trend (0.63 ± 0.41 ppb yr⁻¹) observed over the shorter 2004–2015 period (Gratz et al., 2014). These analyses imply that GFDL-AM3 represents the underlying chemical and physical processes controlling the response of US surface O₃ means and extremes to changes in global-to-regional precursor emissions and climate, despite mean state biases (Figs. S5–S6).

The filtered model shows greater 95th percentile O₃ increases than observed at some WUS sites (e.g., Yosemite; Grand Canyon; Canyonlands) for both spring and summer (Figs. 7a, d and 8a, d), reflecting that observations at these sites sometimes can be influenced by transport of photochemically aged plumes from nearby urban areas and from southern California during late spring and summer. When sampled at the surface, AM3 simulates small summertime O₃ decreases in the 95th and 50th percentiles over the Intermountain West (Fig. 4b, d), consistent with observations at Yosemite, Grand Canyon, and Canyonlands (Fig. 8a, b). As illustrated in Fig. 3 for spring and discussed in Sect. 2.4, individual sites in the west display observed trends falling in between the filtered model and those sampled at the surface versus aloft.

We examine how US surface O₃ responds to changes in regional anthropogenic emissions, hemispheric background, and meteorology by comparing O₃ trends in the BASE, Background, and FIXEMIS experiments (Figs. 10–11). With North American anthropogenic emissions shut off in the Background simulation, little difference is discernable from the BASE simulation for WUS O₃ trends during spring (first versus second rows in Fig. 10), indicating the key role of hemispheric background driving increases in springtime O₃ over the WUS. With anthropogenic emissions held constant in time, FIXEMIS still shows statistically significant

spring O₃ increases in the 95th percentile (Fig. 10c), approximately half of the trends simulated in BASE, for Grand Canyon, Canyonlands, Mesa Verde and Rocky Mountain national parks. Prior work shows that deep stratospheric intrusions contribute to the highest observed and simulated surface O₃ events at these sites (Langford et al., 2009; Lin et al., 2012a). Strong year-to-year variability of such intrusion events (Lin et al., 2015a) can confound the attribution of springtime O₃ changes over the WUS to anthropogenic emission trends, particularly in the highest percentile and over a short record length. Summer avoids this confounding influence when stratospheric intrusions are at their seasonal minimum, as evidenced by little O₃ change in FIXEMIS over the WUS (Fig. 11c, f). In contrast to spring, the model shows larger differences in WUS O₃ trends between BASE and Background for summer when North American pollution peaks seasonally (Fig. 10a, d versus b, e compared to Fig. 11a, d versus b, e). There are significant increases of 0.2–0.5 ppb yr⁻¹ in the 95th and 50th percentile summer background O₃ at more than 50 % of the western sites (Fig. 11b, e), offsetting the O₃ decreases resulting from US NO_x reductions and leading to little overall change in total observed and simulated O₃ at WUS rural sites during summer (Fig. 8).

Over the EUS, AM3 also simulates background O₃ increases, occurring in both the 95th and 50th percentiles, with a rate of 0.1–0.3 ppb yr⁻¹ during spring (Fig. 10b, e) and 0.2–0.5 ppb yr⁻¹ during summer (Fig. 11b, e). Based on prior model estimates that springtime background O₃ is greater in the northeast than the southeast (Lin et al., 2012a, b; Fiore et al., 2014), one might assume that the springtime O₃ increases in the 5th percentile observed over the northeast (Fig. 7c) have been influenced by a rising background. However, AM3 simulates homogeneous background O₃ trends across the entire EUS (Fig. 10b, e), indicating that the observed north-to-south gradient in O₃ trends reflects an earlier seasonal onset of NO_x-sensitive photochemistry in the southeast, as opposed to the background influence.

A warming climate is most likely to worsen the highest O₃ events in polluted regions (e.g., Schnell et al., 2016; Shen et al., 2016). With anthropogenic emissions held constant in time over 1988–2014, FIXEMIS suggests significant increases of 0.2–0.4 ppb yr⁻¹ in the 95th percentile summertime O₃ over the EUS (Fig. 11c). Using self-organizing map cluster analysis, Horton et al. (2015) identified robust increases in the occurrence of summer anticyclonic circulations over eastern North America since 1990. We find that biogenic isoprene emissions over this period increased significantly by 1–2 % yr⁻¹ (10 to 20 mg C m⁻² summer⁻¹) throughout the EUS in the model, consistent with simulated increases in the 90th percentile JJA daily maximum temperature (Fig. 12a–b). Increases in isoprene emissions contribute to raising EUS background O₃ in summer (Fig. 11b, e). Using the Global Land-Based Datasets for Monitoring Climate Extremes (GHCNDEX; Donat et al., 2013), we find increases in the number of warm days above the 90th percentile and

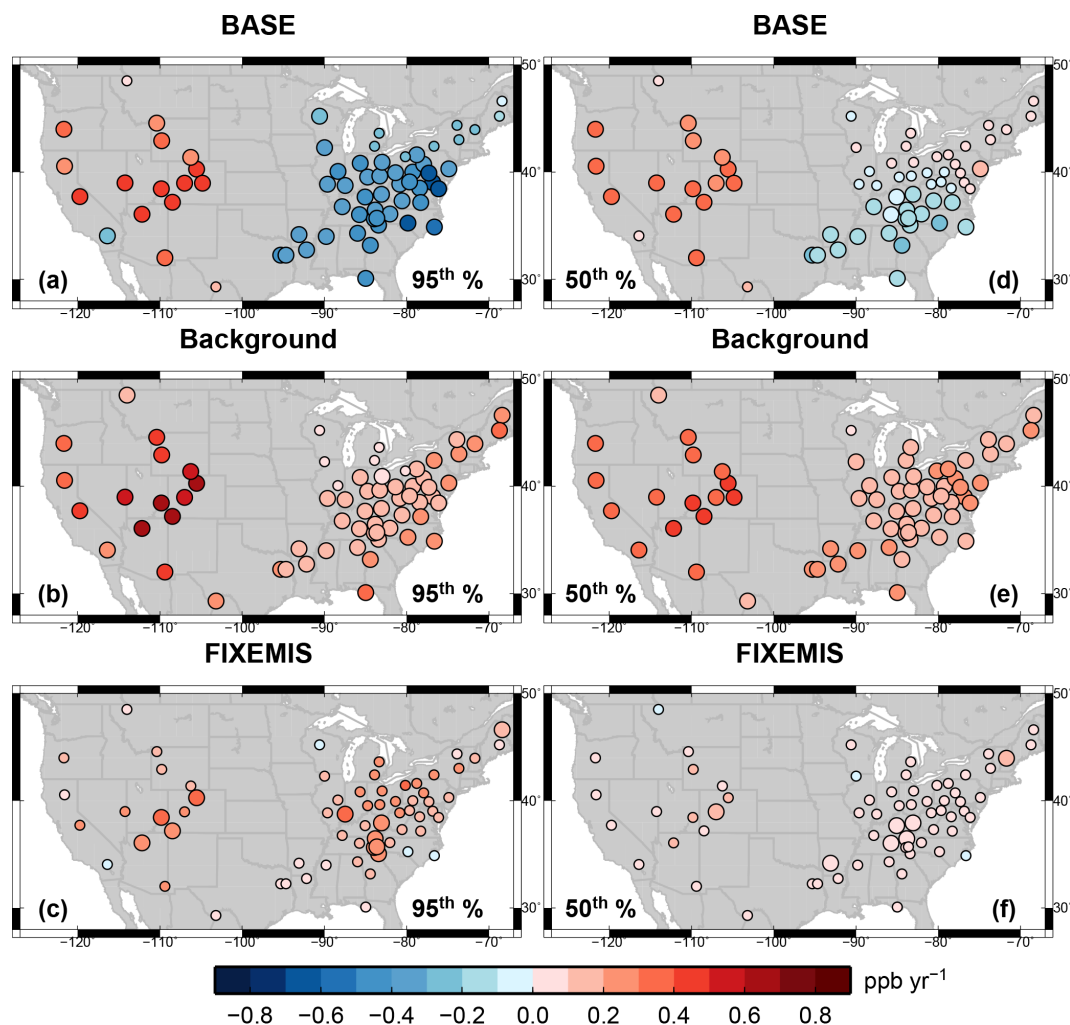


Figure 10. Linear trends in the 95th (left) and 50th (right) percentile springtime MDA8 O₃ over 1988–2014 at US rural sites from BASE (top), Background (middle) and FIXEMIS simulations (bottom). Larger circles indicate sites with statistically significant trends ($p < 0.05$). Top panels are repeated from Fig. 7d, e. Note that the 95th (50th) percentile is sampled separately from the Background and FIXEMIS simulations without depending on the times when the BASE simulation is experiencing the 95th (50th) percentile days.

maximum temperature over the southeastern US in August (Fig. 12c–d). The trends in temperature extremes are similar between June and August, but there is no significant trend in July (not shown). While changes in regional temperature extremes on 20- to 30-year time series may reflect internal climate variability (Shepherd, 2015), we suggest that increasing hot extremes and biogenic isoprene emissions over the last 2 decades may have offset some of the benefits of regional NO_x reductions in the EUS.

5 Impacts of rising Asian emissions, methane and wildfires on western US O₃

5.1 Historical western US O₃ trends in spring

Further indications of the factors driving baseline O₃ changes over the WUS can be inferred by examining the time series at several high-elevation sites, which most frequently sample baseline O₃ in the free troposphere during spring (Sect. 2.4). Figure 13 shows the results, both observed and simulated, for six such monitoring sites: Great Basin National Park in Nevada (2.1 km a.s.l.), Rocky Mountain National Park (2.7 km a.s.l.) in Colorado, US Air Force Academy (1.9 km a.s.l.) in Colorado Springs, Yellowstone National Park (2.4 km a.s.l.) and Pinedale (2.4 km a.s.l.) in Wyoming, and Mesa Verde National Park (2.2 km a.s.l.) in the Colorado–New Mexico–Arizona–Utah four-corner

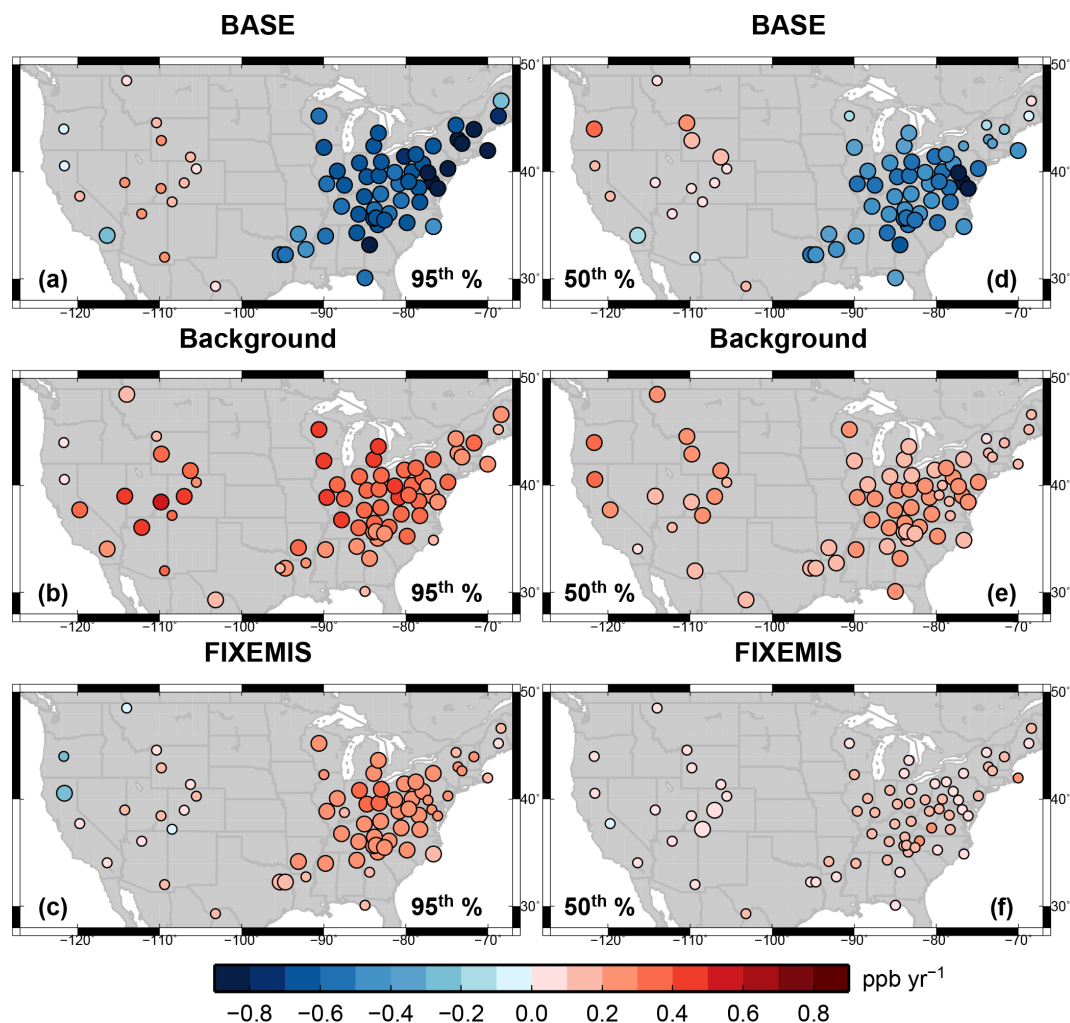


Figure 11. As in Fig. 10, but for summer. Top panels are repeated from Fig. 8d, e.

region. The observed median values of springtime MDA8 O_3 have increased significantly at a rate of $0.2\text{--}0.5\text{ ppb yr}^{-1}$ over the past 20–27 years at these sites, except Pinedale, where the increase in background O_3 is likely offset by the O_3 decrease due to recent emission control for the large oil and gas production fields in this area (<http://deq.wyoming.gov/aqd/winter-ozone/resources/technical-documents/>). When filtered to remove the influence from fresh local pollution (Sect. 2.4), AM3 BASE captures the long-term trends of O_3 observed at these sites.

Correlating AM3 Background with observed O_3 indicates that most of the observed variability reflects changes in the background, with fluctuations in stratospheric influence contributing to anomalies on interannual timescales (e.g., the 1999 anomaly, Lin et al., 2015a), whereas Asian influence dominates the decadal trends as discussed below. The O_3 reduction resulting from US anthropogenic emission controls is less than 0.1 ppb yr^{-1} (BASE minus Background) at these baseline sites. We show model results for the entire 1980–

2014 period for Great Basin, Rocky Mountain, and the US Air Force Academy to provide context for observed trends in the 2 most recent decades (Fig. 13a). In the 1980s when Chinese NO_x emissions ($\sim 4\text{ Tg yr}^{-1}\text{ NO}$) were much lower than US NO_x emissions ($\sim 15\text{ Tg yr}^{-1}\text{ NO}$) (Granier et al., 2011), there was little overall O_3 change over the WUS in the model. From the mid-1990s onwards, with NO_x emissions in China rising steeply (Fig. 1a) and surpassing US emissions in the 2000s, the O_3 trends at remote WUS sites appear to be dominated by trends of background, reflecting rising emissions outside the US. The largest spring O_3 increases from 1981–1990 to 2003–2012 at 700 hPa extend from Southeast Asia to the subtropical North Pacific Ocean to the southwestern US (Fig. S7a), consistent with the influence of rising Asian precursor emissions.

Table 2 contains a summary of the drivers of O_3 trends in the model at seven CASTNet sites that exhibit a significant spring O_3 increase observed over 1988–2012. Here we focus our attribution analysis on the period 1988–2012 (in-

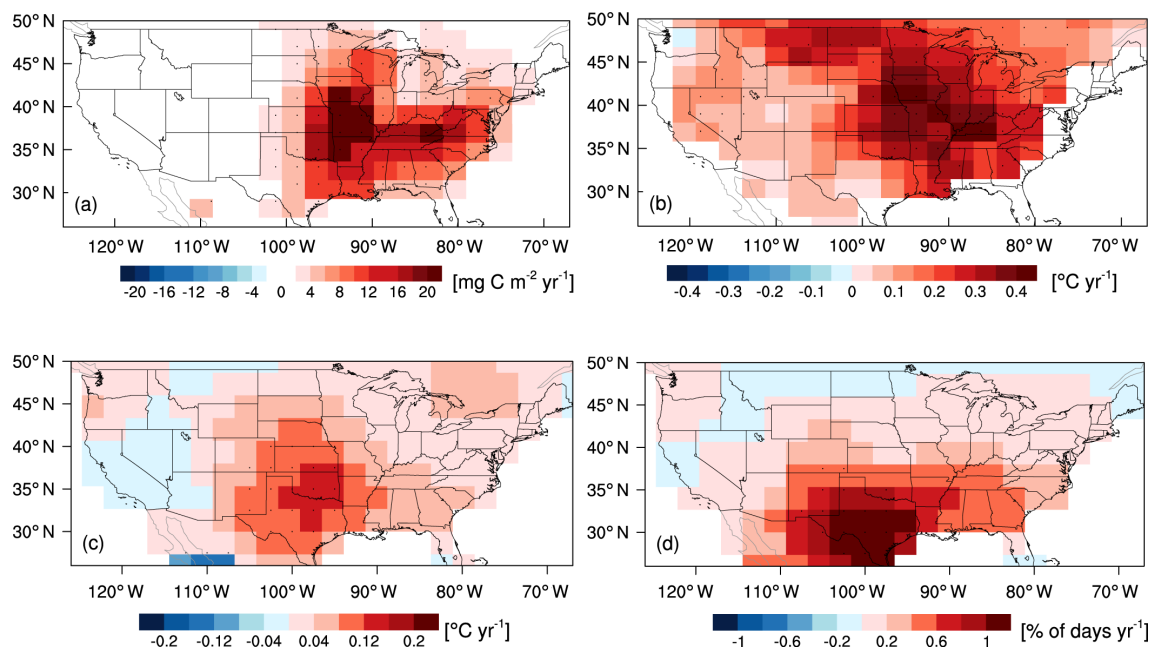


Figure 12. The 1990–2012 trends in (a) model JJA total biogenic isoprene emissions, (b) model 90th percentile JJA daily maximum temperature, (c) the warmest daily maximum temperature and (d) the frequency of warm days (i.e., those above the 90th percentile for the base period 1961–1990) for August obtained from the GHCNDEX dataset (Donat et al., 2013; available at <http://www.climdex.org/viewdownload.html>). Stippling denotes areas where the change is statistically significant ($p < 0.05$). Note that the trends are calculated for the 1990–2012 period, instead of 1988–2014, to avoid the influence from hot extremes in 1988 and cold conditions in 2014 (Sect. 6). When these years are included, the trends in (c) and (d) are swamped by the anomalies. The trends in (a) and (b) are similar between 1990–2012 and 1988–2014.

Table 2. Summary of springtime median MDA8 O₃ trends (in ppb yr⁻¹) over 1988–2012 at WUS sites from observations and AM3 simulations. Trends with the 95 % confidence intervals and levels of significance (bold: < 1 %; italic: 1–5 %; plain: ≥ 5 %) were estimated by the two-tailed t test.

Experiment	Lassen	Great Basin	Rocky Mountain	Mesa Verde	Yellowstone	Yosemite	Chiricahua
Observed	0.38 ± 0.14	0.38 ± 0.26	0.37 ± 0.18	0.30 ± 0.18	<i>0.21 ± 0.19</i>	<i>0.37 ± 0.32</i>	0.17 ± 0.10
BASE*	0.33 ± 0.11	0.34 ± 0.12	0.32 ± 0.13	0.37 ± 0.14	0.21 ± 0.11	0.35 ± 0.17	<i>0.25 ± 0.19</i>
Background	0.31 ± 0.12	0.40 ± 0.13	0.45 ± 0.13	0.43 ± 0.17	0.30 ± 0.11	0.41 ± 0.16	0.32 ± 0.21
Background _{EA}	0.41 ± 0.12	0.39 ± 0.18	0.50 ± 0.15	0.52 ± 0.20	0.40 ± 0.16	0.47 ± 0.17	0.47 ± 0.21
IAVASIA*	0.29 ± 0.13	0.31 ± 0.11	0.25 ± 0.11	0.27 ± 0.11	0.19 ± 0.11	0.24 ± 0.14	0.15 ± 0.15
IAVASIA _{EA}	0.26 ± 0.16	0.26 ± 0.16	0.35 ± 0.13	0.32 ± 0.13	0.27 ± 0.16	0.31 ± 0.18	0.25 ± 0.15
IAVCH ₄ *	<i>0.18 ± 0.12</i>	0.20 ± 0.11	<i>0.12 ± 0.09</i>	<i>0.16 ± 0.12</i>	0.09 ± 0.12	0.15 ± 0.16	0.04 ± 0.15
IAVFIRE	0.10 ± 0.12	<i>0.14 ± 0.12</i>	<i>0.17 ± 0.14</i>	<i>0.16 ± 0.14</i>	0.11 ± 0.13	0.15 ± 0.16	0.08 ± 0.17
FIXEMIS	0.08 ± 0.12	<i>0.12 ± 0.12</i>	<i>0.16 ± 0.12</i>	<i>0.13 ± 0.12</i>	0.09 ± 0.13	0.12 ± 0.16	0.04 ± 0.16
O ₃ Strat	0.18 ± 0.18	0.20 ± 0.25	0.18 ± 0.18	0.25 ± 0.23	0.15 ± 0.18	0.27 ± 0.30	0.07 ± 0.24

The * mask indicates data filtered to represent baseline conditions (NACOT ≤ 67th). The EA subscript indicates that data were filtered to represent transport conditions favoring the import of Asian pollution (EACOT ≥ 67th).

stead of 1988–2014) because the IAVASIA and IAVCH₄ simulations only extend to 2012. Meteorology varies from year to year in all experiments. Thus, we quantify the contributions of rising Asian emissions in IAVASIA, global methane in IAVCH₄, and wildfire emissions in IAVFIRE by subtracting out the slope of the linear regression of seasonal O₃ means in FIXEMIS. Simulated O₃ with anthropogenic emissions varying in both South and East Asia but held constant

elsewhere shows statistically significant increases of 0.1–0.2 ppb yr⁻¹ ($p \leq 0.01$; IAVASIA minus FIXEMIS in Table 2), consistent with trends of 0.2 ppb yr⁻¹ estimated by scaling results from HTAP phase 1 multi-model sensitivity experiments with Asian emissions reduced by 20 % (Reidmiller et al., 2009). This Asian influence can explain 50–65 % of the modeled background O₃ increase in spring (Table 2).

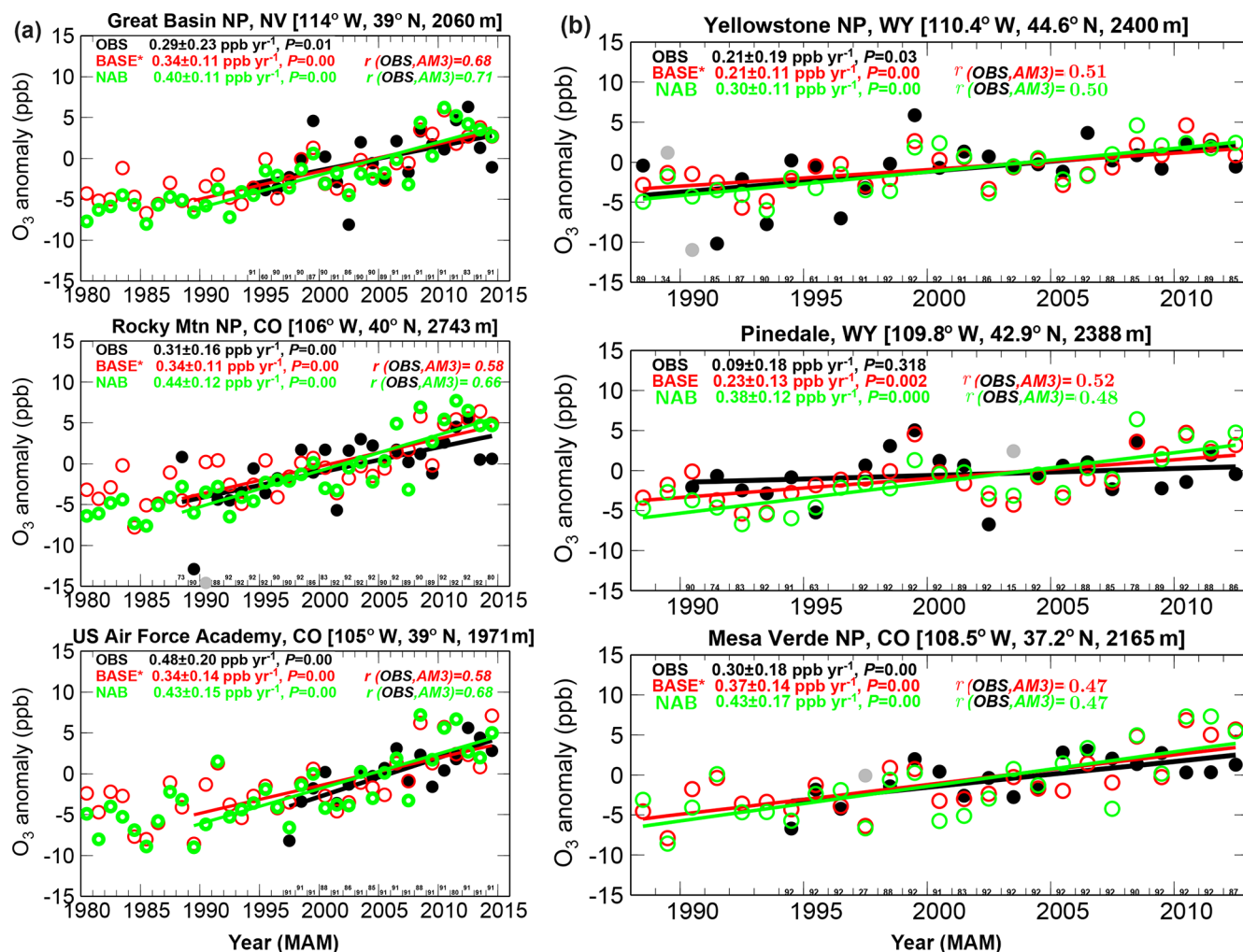


Figure 13. (a) Time series of median spring MDA8 O₃ anomalies (relative to the 1995–2014 mean) at Great Basin, Rocky Mountain, and US Air Force Academy as observed (black) and simulated in AM3 BASE filtered for baseline conditions (red; see Sect. 2.4) and in Background with North American anthropogenic emissions zeroed out (NAB; green). Presented at the top of the graph are statistics from the linear fit and correlations between observations and simulations. Numbers at the bottom of the graph denote the sample size of observations for each year. Gray dots indicate uncertain observations that are removed from the linear fit (see Sect. 2.3). (b) Same as Fig. 13a, but for Yellowstone, Pinedale, and Mesa Verde over the period 1988–2012.

With only methane varying, the model trends are less than 0.1 ppb yr⁻¹ (IAVCH₄ minus FIXEMIS), accounting for an average of 15% of the background increase. The contribution from wildfire emissions during spring is of minor importance (IAVFIRE minus FIXEMIS, Table 2). A stratospheric O₃ tracer (O₃Strat) in AM3 (Lin et al., 2012a, 2015a) demonstrates a positive but insignificant trend in stratospheric O₃ transport to the sites. We examine the trends of lower tropospheric O₃ at these sites when transport conditions favor the import of Asian pollution into western North America, as diagnosed by the East Asian CO tracer (EACoT) exceeding the 67th percentile for each spring. Similar to the conclusion of Lin et al. (2015b), we find that the rate of O₃ increase in the Background simulation is greater by 0.05 – 0.1 ppb yr⁻¹ under strong transport from Asia than without filtering. Filter-

ing the IAVASIA simulation for Asian influence also results in greater O₃ increases than filtering for baseline conditions (Table 2).

Rising Asian emissions even influence trends of O₃ downwind of the Los Angeles Basin during spring. O₃ measured in Joshua Tree National Park shows an increase of 0.31 ± 0.25 ppb yr⁻¹ in spring over 1990–2010 (Cooper et al., 2012), despite significant improvements in O₃ air quality in the Los Angeles Basin (Warneke et al., 2012). The O₃ record extended to 2014 shows a decline in the 95th percentile O₃ in Joshua Tree National Park for both spring and summer (Figs. 7–8), whereas the 5th percentile continues to increase in spring and there is no significant trend in the median. Sampling the AM3 Background simulation at this site indicates a rising background (0.31 ± 0.14 ppb yr⁻¹). Air-

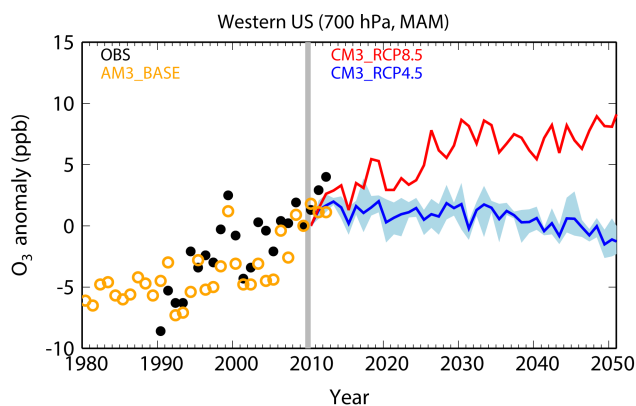


Figure 14. Future projections. Time series of median springtime O₃ changes relative to 2010 in GFDL AM3 hindcast (orange circles) and CM3 future simulations for RCP8.5 (red) versus RCP4.5 (blue; shading represents the range of three ensemble members), sampled at 700 hPa over the WUS (35–45° N, 120–105° W). Black circles indicate observed changes averaged from the Lassen, Great Basin, and Rocky Mountain national parks.

craft measurements in May–June 2010 indicate the presence of Asian pollution layers 2 km above southern California with distinct sulfate enhancements coincident with low organic mass (Lin et al., 2012b), supporting the conclusion that rising Asian emissions can contribute to trends of O₃ observed in this region. Yosemite National Park (1.6 km a.s.l.) and Chiricahua National Monument (1.5 km a.s.l.) are also influenced by increases in Asian emissions and concurrent decreases in local pollution in California. O₃ observed at Yosemite shows an increase from 1995 to around 2012 (0.37 ± 0.32 ppb yr⁻¹; Fig. S8), which the model attributes primarily to rising Asian emissions (Table 2), but observations have remained constant since then, reflecting an offset by O₃ decreases in California (Fig. 4).

5.2 Projecting western US springtime O₃ for the 21st Century

Under the RCP8.5 scenario, Chinese NO_x emissions are projected to peak in 2020–2030, reflecting an increase of ~50% from 2010 (Fig. 1a), followed by a sharp decrease, reaching 1990 levels by 2050. Global methane increases by ~60% from 2010 to 2050 under RCP8.5 (Fig. S1). Under the RCP4.5 scenario, in contrast, NO_x emissions in China change little over 2010–2030 and global methane remains almost constant from 2010 to 2050. NO_x emissions in the US decrease through 2050 under both scenarios, by ~40% from 2010. A number of studies have examined future US O₃ changes under the RCPs (e.g., Gao et al., 2013; Clifton et al., 2014; Pfister et al., 2014; Fiore et al., 2015; Barnes et al., 2016). However, as discussed earlier, the trends of O₃ in the model when sampled near the surface are overwhelmingly dominated by US anthropogenic emission trends. Thus,

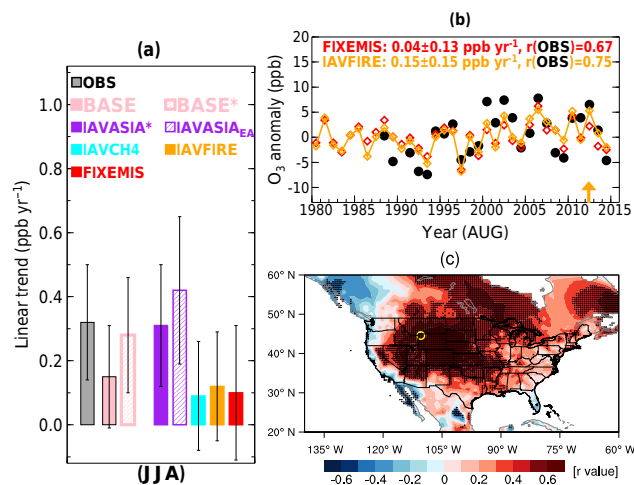


Figure 15. Summertime O₃ in Yellowstone National Park. (a) Median JJA MDA8 O₃ trends over 1988–2012 at Yellowstone from observations (black) and simulations sampled at 700 hPa for BASE without filtering (pink), BASE filtered for baseline conditions (hatched pink), IAVASIA (solid purple, baseline), IAVASIA filtered for Asian influence (EACOT \geq 67th, hatched purple), IAVCH4 (cyan), IAVFIRE (orange) and FIXEMIS (red). (b) Time series of anomalies in August median MDA8 O₃ at Yellowstone as observed (black) and simulated by the model sampled at the surface, with constant (red) and time-varying wildfire emissions (orange). Trends over 1988–2014 are reported. (c) Interannual correlations of JJA mean MDA8 O₃ observed at Yellowstone with JJA mean daily maximum temperature from observations (Harris et al., 2014).

the future O₃ changes estimated by these prior studies do not represent baseline conditions, particularly the response to rising Asian emissions. In Fig. 14 we show changes in WUS free tropospheric (700 hPa) O₃ relative to 2010 in the CM3 future simulations under RCP8.5 versus RCP4.5. Historical hindcasts and observations are also shown for context. Under RCP4.5, springtime O₃ over the WUS shows little overall change over 2010–2050. Under RCP8.5, in contrast, springtime WUS O₃ increases by ~10 ppb from 2010 to 2030 and remains almost constant from 2030 to 2050, consistent with the projected trends in Asian emissions and global methane.

5.3 Trends and variability of western US O₃ in summer

Yellowstone National Park is the only site with statistically significant summer O₃ increases observed across all percentiles (Fig. 8a–c). The 1988–2012 trends for the median observed and simulated O₃ are summarized in Fig. 15a. Observations show an increase of 0.32 ± 0.18 ppb yr⁻¹ for JJA, with a greater rate of increase in June (0.38 ± 0.25 ppb yr⁻¹) than in July–August (0.26 ± 0.18 ppb yr⁻¹). AM3 BASE sampled at 700 hPa and filtered for baseline conditions (hatched pink bar in Fig. 15a) captures the observed increase. Without baseline filtering (solid pink bar), North American emission reductions offset almost 50% of the simulated

O₃ increase at Yellowstone, causing the model to underestimate the observed O₃ trend. The model attributes much of the observed summer O₃ increase at Yellowstone to rising Asian emissions, with IAVASIA simulating an O₃ increase of 0.31 ± 0.19 ppb yr⁻¹ under baseline conditions, increasing to 0.42 ± 0.23 ppb yr⁻¹ under conditions of Asian influence (EACOt \geq 67th percentile). The stronger increase measured in June than in July–August is consistent with the influence of the Asian summer monsoon producing a surface O₃ minimum in July–August in East Asia (e.g., Lin et al., 2009), as well as the seasonality of intercontinental pollution transport. Changes in methane, wildfires, and meteorology over this period are of minor importance for the JJA O₃ trends at Yellowstone.

Enhanced wildfire activity in hot and dry weather is thought to be a key driver of interannual variability of surface O₃ in the Intermountain West in summer (Jaffe et al., 2008; Jaffe, 2011). However, hot and dry conditions also facilitate the buildup of O₃ produced from regional anthropogenic emissions, which can complicate the unambiguous attribution of observed O₃ enhancements. Using August data at Yellowstone as an example, we isolate the relative contribution of these two processes to observed O₃ with the IAVFIRE versus FIXEMIS experiments (Fig. 15b). Here we sample AM3 at the surface to account for any influence of varying boundary layer mixing depths. Even without interannual variations of wildfire emissions, FIXEMIS captures much of the observed year-to-year variability of August mean O₃ at Yellowstone ($r = 0.67$). IAVFIRE with interannually varying fire emissions only moderately improves the correlations ($r = 0.75$). FIXEMIS also captures the observed O₃ increase from the early 1990s to around 2002, likely reflecting warmer temperatures and deeper mixing depths allowing more baseline O₃ to mix down to the surface. Over the entire 1988–2014 (or 1980–2014) period, IAVFIRE gives ~ 0.1 ppb yr⁻¹ greater O₃ increases in August than FIXEMIS, consistent with an overall increase in boreal wildfire activity (Figs. S2 and S7b).

Figure 16 shows year-to-year variability in surface MDA8 O₃ enhancements from wildfires during summer, as diagnosed by the differences between IAVFIRE and FIXEMIS. The results are shown for individual months since fires are highly episodic. During the summers of 1998, 2002, and 2003, biomass fires burned a large area of Siberia and parts of the North American boreal forests, raising carbon monoxide across the Northern Hemisphere as detected from space (Yurganov et al., 2005; van der Werf et al., 2010). Long-range transport of Siberian fire plumes resulted in 2–6 ppb enhancements in surface MDA8 O₃ at the US western coast and in parts of the Intermountain West in AM3. The model calculates enhancements in monthly mean MDA8 O₃ of up to 8 ppb from the intense wildfire events in northern California during July 2008 (Huang et al., 2013; Pfister et al., 2013), over Texas–Mexico during June 2011 (Wang et al., 2015), and in Wyoming–Utah during August 2012 (Jaffe et

al., 2013). The AM3 estimates are roughly consistent with a previous analysis of boundary layer aircraft data with and without fire influences (as diagnosed by CH₃CN) during June 2008 over California (Pfister et al., 2013).

While fires during hot and dry summers clearly result in enhanced O₃ at individual sites for some summers, the ability of AM3 with constant fire emissions to simulate variability of O₃ for a high (e.g., 1988, 2002, 2006) versus low (e.g., 1997, 2009) fire year (Fig. 15b) indicates that biomass burning is not the primary driver of observed O₃ interannual variability. Year-to-year variability of JJA mean MDA8 O₃ observed at Yellowstone is strongly correlated ($r > 0.6$) with observed large-scale variations in JJA mean daily maximum temperature across the Intermountain West (Fig. 15c). Correlations for other ground stations show a similar large-scale feature. Similar to the conclusion from Zhang et al. (2014), our analysis indicates that the correlation between O₃ and biomass burning reported by Jaffe et al. (2008) and Jaffe (2011) at rural sites reflects common underlying correlations with temperature rather than a causal relationship of fire with O₃. At remote mountain sites (e.g., Yellowstone), warmer surface temperatures lead to deeper mixed layers that facilitate mixing of free tropospheric O₃-rich air down to the surface. At sites near sources of air pollution, hot conditions enhance regional O₃ production and orographic lifting of urban pollution to mountaintop sites during daytime, as occurs at Rocky Mountain National Park located downwind of the Denver metropolitan area during summer (Sect. 5.4). Reactive volatile organic compound (VOC) emissions from fires may enhance O₃ production in NO_x-rich urban areas (Baker et al., 2016), although evaluating these impacts needs high-resolution models and better treatment of sub-grid-scale fire plumes.

5.4 Ozone trends in the Denver metropolitan area

Efforts to improve air quality have led to a marked decrease in high-O₃ events in the Los Angeles Basin as illustrated by the annual 4th highest MDA8 O₃ at Crestline – a regionally representative monitor operated continuously from 1980 to the present (Fig. 17a). In striking contrast, the 4th highest MDA8 O₃ in the Denver metropolitan area shows little change over the past decades, despite significant reductions in NO_x (Fig. 1) and CO emissions ($\sim 80\%$ from 1990 to 2010; Cooper et al., 2012). Recent field measurements indicate that increased VOC emissions from oil and natural gas operations are an important source of O₃ precursors in the Denver–Julesberg Basin (Gilman et al., 2013; Halliday et al., 2016; McDuffie et al., 2016). However, total VOC emissions in Denver may not be increasing over time due to the marked reductions in VOC emissions from vehicles (Bishop and Stedman, 2008, 2015). We seek insights into the causes of the lack of significant O₃ responses to emission controls in Denver by separately analyzing trends in spring and summer (Fig. 17b–c).

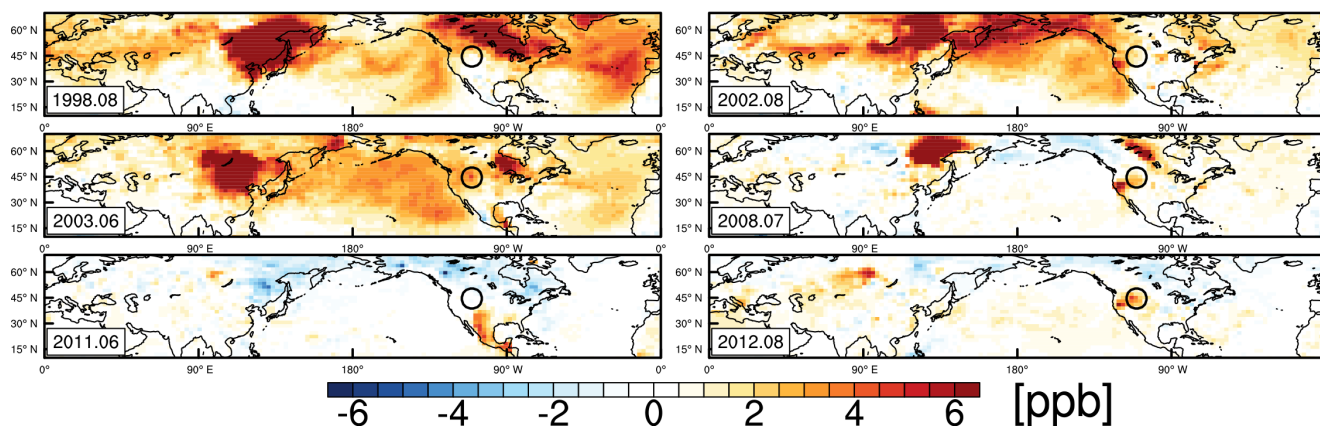
IAVFIRE - FIXEMIS: surface MDA8 O₃ anomaly

Figure 16. Surface MDA8 O₃ enhancements from wildfire emissions for individual months in the years with large biomass burning in boreal regions (1998, 2002, 2003) and over the WUS (2008, 2011, 2012), as diagnosed by the differences between IAVFIRE and FIXEMIS. The black circle denotes the location of Yellowstone National Park.

The $\sim 200 \times 200 \text{ km}^2$ AM3 model is not expected to resolve the urban-to-rural differences between Rocky Mountain National Park and the Denver metropolitan area. However, if observed O₃ variability in Denver correlates with that at remote sites in the Intermountain West, then model attribution for the remote sites can be used to infer sources of observed O₃ in Denver. This is demonstrated in Fig. 17b for spring using data at three representative sites in Denver, Rocky Flats North, National Renewable Energy Lab (NREL), and Welby, with continuous measurements since the early 1990s. Year-to-year variability of median MDA8 O₃ at these sites during spring correlates strongly with that in Great Basin National Park ($r = 0.7$), a fairly remote site in Nevada not influenced by urban emissions from Denver. Median spring O₃ observations in Denver increased significantly by $\sim 0.3 \text{ ppb yr}^{-1}$, similar to the rate of increase in Great Basin National Park, which the model attributes to rising background (Fig. 13a), implying that the tripling of Asian emissions since 1990 also raised mean springtime O₃ in the Denver metropolitan area. Trends in the 95th percentile are statistically insignificant.

During summer, changes in regional emissions and temperature have the greatest impacts on the highest observed O₃ concentrations in polluted environments. Figure 17c shows times series of July–August 95th percentile MDA8 O₃ in Denver, together with the distribution of daily maximum temperature. In every year since 1993, the highest summer MDA8 O₃ observed at these sites exceeds the 70 ppb NAAQS level. There is a small negative trend that is swamped by large interannual variability. The summers with the highest observed O₃ coincide with those with the highest observed temperatures, such as 1998, 2003, 2007, 2011 and 2012. During these summers, enhancements of MDA8 O₃ were also recorded in Rocky Mountain National Park, reflect-

ing enhanced lifting of pollution from Denver under warmer conditions (Brodin et al., 2010). Applying quantile regression (e.g., Porter et al., 2015) to daily observations at Rocky Flats North over 1993–2015, we find a $2 \text{ ppb } ^\circ\text{C}^{-1}$ sensitivity of 95th percentile July–August O₃ to changes in maximum daily temperature. We suggest that the substantial increases in extreme heat occurrence over central North America over the last 2 decades, as found by Horton et al. (2015), contribute to raising summer O₃ in Denver, which offsets O₃ reductions that otherwise would have occurred due to emission controls in Denver. Potential shifts in the O₃ photochemistry regime can also contribute to trends of summer O₃ in Denver, although advancing this knowledge would require a high-resolution air quality model.

6 Impacts of heat waves and droughts on eastern US summer O₃

We discuss in this section interannual variability and long-term changes in summer O₃ over the EUS, where air stagnation and high temperatures typically yield the highest O₃ observed in surface air (e.g., Jacob and Winner, 2009). Evaluating the ability of models to simulate the high-O₃ anomalies during historical heat waves and droughts is crucial to establishing confidence in the model projection of pollution extremes under a warming climate. Figure 18a shows comparisons of July mean MDA8 O₃ at one regionally representative site, the Pennsylvania State University (PSU) CAST-Net site, from observations and model simulations. With time-varying emissions, the BASE model simulates an O₃ decrease ($-0.45 \pm 0.32 \text{ ppb yr}^{-1}$) consistent with observations ($-0.67 \pm 0.33 \text{ ppb yr}^{-1}$) and captures the observed July mean O₃ interannual variability ($r = 0.82$) that is correlated with large-scale variations in daily maximum temperature

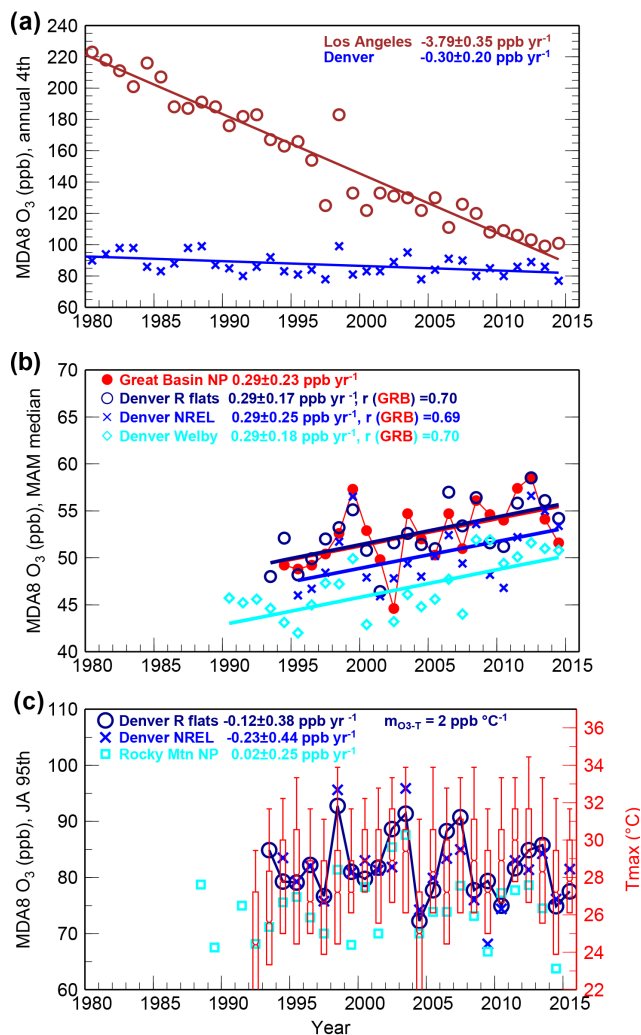


Figure 17. Surface O₃ trends in Denver. (a) Comparison of observed trends in annual fourth highest MDA8 O₃ at Crestline Los Angeles (brown) and in Denver (blue, computed from all monitors available in Denver non-attainment counties). (b) Time series of observed median MAM MDA8 O₃ at Great Basin National Park (red), in comparison with three monitors in Denver. (c) Time series of observed 95th percentile July–August MDA8 O₃ in Denver, together with statistics (25th, 50th, 75th, 95th) of observed July–August daily maximum temperature at Rocky Flats (red, right axis).

($r = 0.57$). In particular, O₃ pollution extremes are successfully simulated during the EUS summer heat waves of 1988, 1995, 1999, 2002, 2011 and 2012 (Leibensperger et al., 2008; Fiore et al., 2015; Jia et al., 2016). Year-to-year variations in meteorology can explain 30% of the total observed O₃ variability ($r = 0.55$), as inferred by FIXEMIS with constant anthropogenic emissions. If US anthropogenic emissions remained at 1990s levels (as in FIXEMIS), then anomalies in July mean MDA8 O₃ would have been 10 ppb greater during the 2011 and 2012 heat waves. Loughner et al. (2014) found that half of the days in July 2011 would have been classified

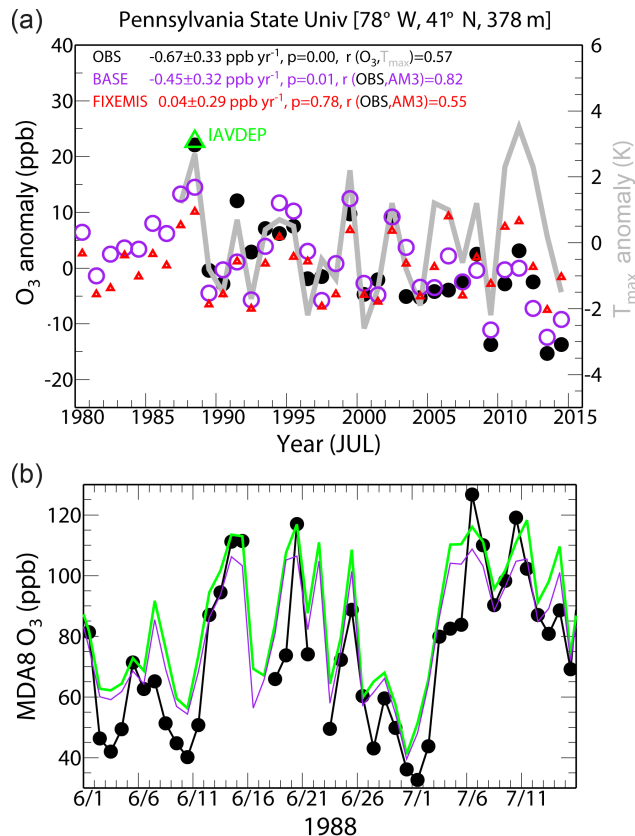


Figure 18. (a) Time series of July mean MDA8 O₃ anomalies (relative to 1988–2014) at the Pennsylvania State University (PSU) CASTNET site as observed (black) and simulated by the GFDL-AM3 model with time-varying (purple) and constant anthropogenic emissions (red), along with observed anomalies in July mean daily maximum temperature (gray lines; right axis). The green triangle denotes the 1988 O₃ anomaly from a sensitivity simulation using BASE emissions but with 35% decreases in V_{d, O_3} (IAVDEP). (b) Time series of daily MDA8 O₃ at PSU from 1 June to 16 July in 1988 from observations (black), BASE (purple), and IAVDEP simulations (green).

as O₃ exceedance days for much of the mid-Atlantic region if emissions had not declined.

Figure 19a compares the probability density functions of MDA8 O₃ at 40 EUS surface sites for JJA in the pre-NO_x SIP Call (1988–2002) versus post-NO_x SIP Call (2003–2014) periods and during the extreme heat waves of 1988 versus 2012. Following the NO_x SIP Call, the probability distribution of observed JJA MDA8 O₃ over the EUS shifted downward (solid black versus dotted gray lines in Fig. 19a). The median value declined by 9 ppb and the largest decreases occurred in the upper tails, leading to weaker day-to-day O₃ variability and a narrower O₃ range (standard deviation σ decreased from 16.4 to 12.9 ppb). These observed O₃ changes driven by regional NO_x reductions are even more prominent when comparing the heat waves of 1988 versus 2012 (solid

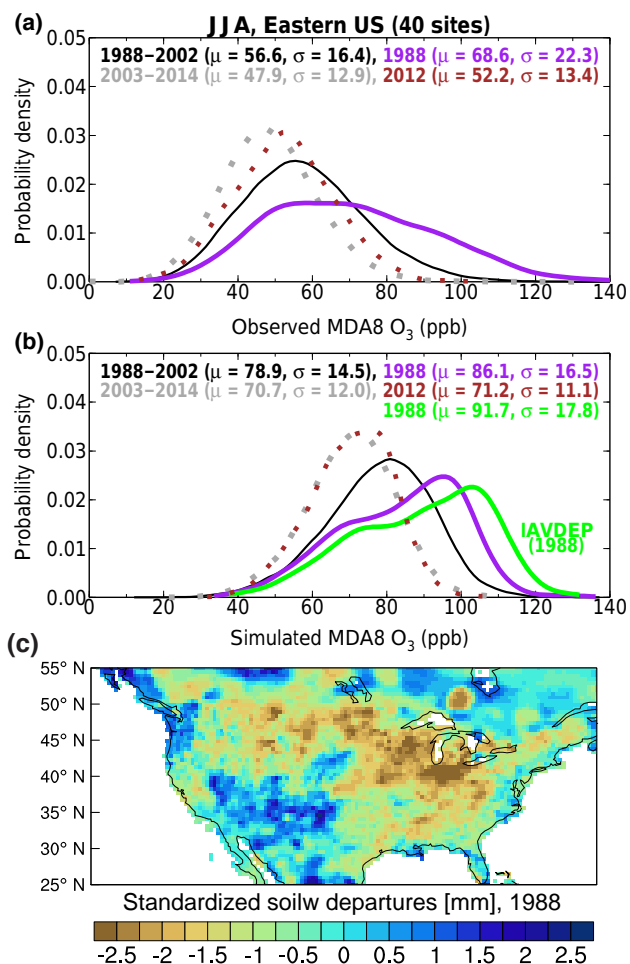


Figure 19. (a) Comparisons of probability distributions of summertime MDA8 O₃ from 40 EUS CASTNet sites for the pre-NO_x SIP Call (1988–2002; solid black) versus post-NO_x SIP Call (2003–2014; dashed gray) periods and during the extreme heat waves of 1988 (solid purple) versus 2012 (dashed brown). The median (μ) and standard deviation (σ) are shown (ppb). (b) Same as (a), but from AM3 BASE. Also shown is the O₃ distribution in 1988 from a sensitivity simulation with 35 % decreases in V_{d,O_3} in drought areas (green). (c) Standardized soil moisture departures for JJA 1988 (calculated by dividing anomalies by the 1979–2010 climatological standard deviation, using data from the NOAA Climate Prediction Center).

purple versus dotted brown lines in Fig. 19a): $\sigma = 22.3$ versus 13.4 ppb and median value $\mu = 68.6$ versus 52.2 ppb.

Figure 19b shows the corresponding comparisons using the results from AM3 BASE. Despite the high mean model bias (~ 20 ppb), AM3 captures the overall structure of the changes in the surface O₃ distributions and thus the response of surface O₃ to the NO_x SIP Call, including the reductions of high-O₃ events during the heat wave of 2012 compared to 1988. Nevertheless, there is a noticeable difference between the observations and simulations in the shape of MDA8 O₃ probability distributions for summer 1988, particularly in the

upper tail of the distribution above 110 ppb (purple lines in Fig. 19a versus b). The BASE model also underestimates the observed July mean O₃ anomaly at PSU in 1988 by ~ 10 ppb (purple versus black dots in Fig. 18a). One possible explanation for these biases is that drought stress can effectively reduce the O₃ deposition sink to vegetation, leading to an increase in surface O₃ concentrations as found during the 2003 European heat wave (Solberg et al., 2008), whereas AM3 does not include interannually varying dry deposition velocities.

The North American drought of 1988 ranks among the worst episodes of drought in the US (e.g., Seager and Hoerling, 2014), with JJA soil moisture deficits occurring over the northern Great Plains–Midwest region with magnitudes of 1–2.5 mm standardized departures from the 1979–2010 climatology (Fig. 19c). Huang et al. (2016) found that monthly mean O₃ dry deposition velocities (V_{d,O_3}) for forests decreased by 33 % over Texas during the dry summer of 2011. Based on this estimate, we conduct a sensitivity simulation for 1988 using BASE emissions but decreasing monthly mean V_{d,O_3} from May to August by 35 % in the areas over North America (20–60° N) where soil moisture deficits in 1988 exceed -1.0σ mm (Fig. 19c). This experiment (hereafter referred to as IAVDEP) simulates ~ 10 ppb higher July mean MDA8 O₃ at the PSU CASTNet site than the BASE model and matches the observed O₃ anomaly in 1988 relative to the record mean (green symbol in Fig. 18a). The impact is largest (up to 15 ppb) on days when observed MDA8 O₃ exceeds 100 ppb (Fig. 18b; $T_{\max} \geq 30^\circ\text{C}$). Simulated JJA MDA8 O₃ at EUS sites in IAVDEP shows an upward shift in the probability distribution, particularly in the upper tail above 110 ppb (green versus purple lines in Fig. 19b), bringing it closer to observations in 1988 (Fig. 19a). The O₃ standard deviation in IAVDEP ($\sigma = 18$ ppb) shifts towards that in observations ($\sigma = 22$ ppb) relative to the BASE model ($\sigma = 16$ ppb).

Quantile mapping can be applied to correct systematic distributional biases in surface O₃ compared to observations (Rieder et al., 2015), but this approach has limitations if there are structural biases in the O₃ distribution due to missing physical processes in the model (e.g., variations of V_{d,O_3} with droughts). Travis et al. (2016) suggest that the National Emission Inventory (NEI) for NO_x from the US EPA is too high nationally by 50 %. Decreasing US NO_x emissions by this amount corrects their model bias for boundary layer O₃ by 12 ppb in the southeast for summer 2013, while surface MDA8 O₃ in their model is still biased high by 6 ± 14 ppb, which the authors attribute to excessive boundary layer mixing. US NO_x emissions in the emission inventory used in AM3 (Sect. 2.2) are approximately 15 % lower than those from the NEI. The 35 % decrease in NO_x emissions from the pre-NO_x SIP Call to the post-NO_x SIP Call in the model reduces mean O₃ by 8 ppb in the EUS, implying that the NO_x emission bias could correct 40 % of our model mean bias of ~ 20 ppb. These estimates support the idea that the common

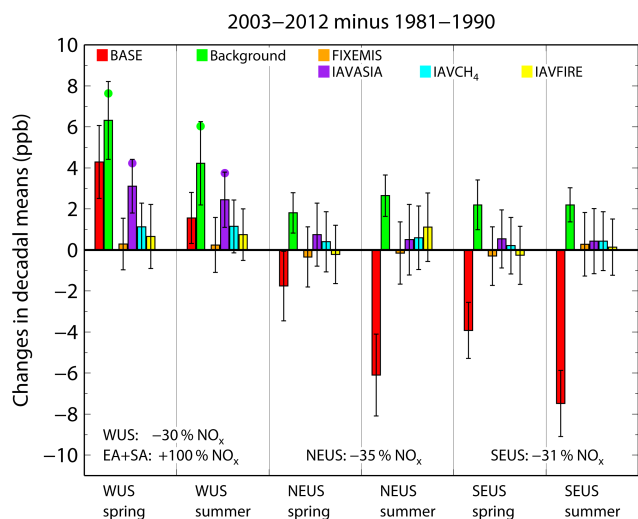


Figure 20. Summary of US surface O₃ trends and drivers. Changes in decadal mean MDA8 O₃ from 1981–1990 to 2003–2012 simulated in a suite of GFDL-AM3 experiments for spring and summer for the western (32–46° N and 123–102° W), northeastern (37–45° N and 90–65° W) and southeastern (30–36° N and 95–77° W) US domains. Observations are not shown because limited data are available during 1981–1990. Experiments are color-coded, with the error bars indicating the range of the mean change at the 95 % confidence level. Filled circles represent the changes under Background (green) and IAVASIA (purple) when filtered for Asian influence (EACot \geq 67th), while other results are from the unfiltered models. The text near the bottom of the plot provides the change in NO_x emissions over the same period for each region.

model biases in simulating surface O₃ over the southeastern US (e.g., Fiore et al., 2009) may partly reflect excessive NO_x emissions. Some of the positive O₃ biases could be also due to the averaging over a deep vertical box in the model surface layer (\sim 60 m in AM3) that can not resolve near-surface gradients (Travis et al., 2016).

7 Conclusions and recommendations

Through an observational and modeling analysis of interannual variability and long-term trends in sources of O₃ over the past 35 years, we have identified the key drivers of O₃ pollution over the US. We initially evaluated the trends of O₃ in Asia resulting from rising Asian precursor emissions (Figs. 4–6). Our synthesis of available observations and simulations indicates that surface O₃ over East Asia has increased by 1–2 ppb yr⁻¹ since 1990 (i.e., 25–50 ppb over 25 years), with significant implications for regional air quality and global tropospheric O₃ burden. Shifting next to the US, we find 0.2–0.5 ppb yr⁻¹ increases in median springtime MDA8 O₃ measured at 50 % of 16 WUS rural sites, with 25 % of the sites showing increases across the entire O₃ concentration distribution, despite stringent US domestic

emission controls (Fig. 7). While many prior studies show that global models have difficulty simulating O₃ increases observed at rural baseline sites (e.g., Parrish et al., 2014; Strode et al., 2015), we reconcile observed and simulated O₃ trends in GFDL-AM3 with a novel baseline sampling approach (Figs. 3 and 13). We suggest that the common model–observation disagreement in baseline O₃ trends reflects limitations of coarse-resolution global models in resolving observed baseline conditions. This representativeness problem can be addressed by filtering model O₃ for hemispheric-scale baseline conditions using the easy-to-implement, low-cost regional CO-like tracers. This approach allows trends of O₃ measured at baseline sites to be compared directly with multi-decadal global model hindcasts, such as those being conducted for the Chemistry-Climate Model Initiative (CCMI; Morgenstern et al., 2017).

The ability of the GFDL-AM3 model to reproduce observed US surface O₃ trends lends confidence in its application to attribute these observed trends to specific processes (Figs. 7 to 11). We summarize the overall statistics in Fig. 20, drawing upon the decadal mean O₃ changes from 1981–1990 to 2003–2012 in the BASE and sensitivity simulations. The changes in BASE are over the WUS 4.3 ± 1.8 ppb for spring and 1.6 ± 1.2 ppb for summer; over the northeast, -1.8 ± 1.7 ppb for spring and -6.0 ± 2.0 ppb for summer; and over the southeast, -3.9 ± 1.4 ppb for spring and -7.5 ± 1.6 ppb for summer. Increasing O₃ in the WUS under BASE coincides with an increase in background O₃ by 6.3 ± 1.9 ppb for spring and 4.2 ± 2.0 ppb for summer. Under conditions of strong transport from Asia (East Asian COt \geq 67th), the background trend rose to 7.6 ± 2.2 ppb for spring and 6.0 ± 2.1 ppb for summer (green dots in Fig. 20). The WUS background O₃ increase reflects contributions from increases in Asian anthropogenic emissions (accounting for 50 % of background increase in spring; 52 % in summer), rising global methane (13 % in spring; 23 % in summer), and variability in biomass burning (6 % in spring; 12 % in summer; excluding the meteorological influence).

We conclude that the increase in Asian anthropogenic emissions is the major driver of rising background O₃ over the WUS for both spring and summer in the past decades, with a lesser contribution from methane increases over this period. The tripling of Asian NO_x emissions since 1990 contributes up to 65 % of modeled springtime background O₃ increases (0.3 – 0.5 ppb yr⁻¹) over the WUS, outpacing O₃ decreases resulting from 50 % US NO_x emission controls (≤ 0.1 ppb yr⁻¹; Table 2 and Fig. 10). Springtime O₃ observed in the Denver metropolitan area has increased at a rate similar to remote rural sites (Fig. 17b). Mean springtime O₃ above the WUS is projected to increase by ~ 10 ppb from 2010 to 2030 under the RCP8.5 global change scenario but to remain constant throughout 2010 to 2050 under the RCP4.5 scenario (Fig. 14). As NO_x emissions in China continue to decline in response to efforts to improve air quality (Krotkov et al., 2016; Liu et al., 2016), rising global methane

and NO_x emissions in the tropical countries (e.g., India) in Asia, where O_3 production is more efficient, may become more important in the coming decades. A global perspective is necessary when designing a strategy to meet US O_3 air quality objectives.

During summer, a tripling of Asian anthropogenic emissions from 1988 to 2014 approximately offsets the benefits of 50 % reductions in US domestic emissions, leading to weak or insignificant O_3 trends observed at most WUS rural sites (Figs. 8 and 11). Rising Asian emissions contribute to observed summertime O_3 increases (0.3 ppb yr^{-1}) at Yellowstone National Park. Our findings confirm the earliest projection of Jacob et al. (1999) with a tripling of Asian emissions. While wildfire emissions can result in 2–8 ppb enhancements to monthly mean O_3 at individual sites in some summers, they are not the primary driver of observed O_3 interannual variability over the Intermountain West (Figs. 15 and 16). Instead, boundary layer depth, high temperatures and the associated buildup of O_3 produced from regional anthropogenic emissions contribute most to the observed interannual variability of O_3 in summer. Summertime O_3 measured in Denver during pollution episodes frequently exceeds the 70 ppb NAAQS level, with little overall trend despite stringent precursor emission controls (Fig. 17c), likely due to the effects of more frequent occurrences of hot extremes in the last decade.

In the eastern US, if emissions had not declined, the 95th percentile summertime O_3 would have increased by $0.2\text{--}0.4 \text{ ppb yr}^{-1}$ over 1988–2014 (Fig. 11c), due to more frequent hot summer extremes and increases in biogenic isoprene emissions ($1\text{--}2 \text{ \% yr}^{-1}$) over this period (Fig. 12). Regional NO_x reductions alleviated the O_3 buildup during the recent heat waves of 2011 and 2012 relative to earlier heat waves (e.g., 1988, 1995, 1999). GFDL-AM3 captures year-to-year variability in monthly mean O_3 enhancements associated with large-scale variations in temperatures (Figs. 18 and 19). However, there is a need to improve the model representation of O_3 deposition sink to vegetation, in particular its reduced efficiency under drought stress, as we demonstrated for the severe North American drought of 1988. Such land–biosphere couplings are poorly represented in current models and further work is needed to examine their impacts on O_3 pollution extremes in a warming climate.

Following the NO_x SIP Call, surface O_3 in the eastern US declined throughout its probability distribution, with the largest decreases occurring in the highest percentiles during summer (-0.8 to -1.8 ppb yr^{-1} ; Fig. 8). Spatially, historical O_3 decreases during non-summer seasons were more pronounced in the southeast, where the seasonal onset of biogenic isoprene emissions and NO_x -sensitive O_3 production occurs earlier than in the northeast (Figs. 7, 9 and S4). The 95th percentile O_3 concentration in the southeast has even decreased during winter. Despite high mean-state biases, GFDL-AM3 captures the salient features of observed O_3 trends over the eastern US, including wintertime increases in

the 5th and 50th percentiles in the northeast, greater springtime decreases in the southeast than the northeast, and summertime decreases throughout the O_3 concentration distribution. These results suggest that NO_x emission controls will continue to provide long-term O_3 air quality benefits in the southeastern US during all seasons.

8 Data availability

All data derived from observations and model simulations used in this study are archived at NOAA GFDL and are available to the public upon request to Meiyun Lin.

The Supplement related to this article is available online at doi:10.5194/acp-17-2943-2017-supplement.

Competing interests. The authors declare that they have no conflict of interest.

Acknowledgements. This work was supported by funding from NASA grants NNH13ZDA001N-AURAST and NNX14AR47G to Meiyun Lin. We thank O. Cooper, S. Fan and J. Schnell for helpful comments on the manuscript. We acknowledge the free use of ozonesonde data at Hong Kong available on www.woudc.org and GOME-SCIAMACHY tropospheric NO_2 column data available on www.temis.nl. Arlene M. Fiore acknowledges support under EPA Assistance Agreement no. 83587801. The views expressed in this document are solely those of the authors and do not necessarily reflect those of the agency. Meiyun Lin devotes this article to her father Tianci Lin, who is the motivation of her life and research career.

Edited by: B. N. Duncan

Reviewed by: two anonymous referees

References

- Abatzoglou, J. T. and Williams, A. P.: Impact of anthropogenic climate change on wildfire across western US forests, *P. Natl. Acad. Sci. USA*, 113, 11770–11775, doi:10.1073/pnas.1607171113, 2016.
- Baker, K. R., Woody, M. C., Tonnesen, G. S., Hutzell, W., Pye, H. O. T., Beaver, M. R., Pouliot, G., and Pierce, T.: Contribution of regional-scale fire events to ozone and $\text{PM}_{2.5}$ air quality estimated by photochemical modeling approaches, *Atmos. Environ.*, 140, 539–554, doi:10.1016/j.atmosenv.2016.06.032, 2016.
- Barnes, E. A., Fiore, A. M., and Horowitz, L. W.: Detection of trends in surface ozone in the presence of climate variability, *J. Geophys. Res.*, 121, 6112–6129, doi:10.1002/2015jd024397, 2016.
- Bishop, G. A. and Stedman, D. H.: A decade of on-road emissions measurements, *Environ. Sci. Technol.*, 42, 1651–1656, doi:10.1021/es702413b, 2008.

- Bishop, G. A. and Stedman, D. H.: Reactive Nitrogen Species Emission Trends in Three Light-/Medium-Duty United States Fleets, *Environ. Sci. Technol.*, 49, 11234–11240, doi:10.1021/acs.est.5b02392, 2015.
- Boersma, K. F., Eskes, H. J., and Brinkma, E. J.: Error analysis for tropospheric NO₂ retrieval from space, *J. Geophys. Res.*, 109, D04311, doi:10.1029/2003jd003962, 2004.
- Brodin, M., Helmig, D., and Oltmans, S.: Seasonal ozone behavior along an elevation gradient in the Colorado Front Range Mountains, *Atmos. Environ.*, 44, 5305–5315, doi:10.1016/j.atmosenv.2010.06.033, 2010.
- Brown-Steiner, B. and Hess, P.: Asian influence on surface ozone in the United States: A comparison of chemistry, seasonality, and transport mechanisms, *J. Geophys. Res.*, 116, D17309, doi:10.1029/2011jd015846, 2011.
- Brown-Steiner, B., Hess, P. G., and Lin, M. Y.: On the capabilities and limitations of GCM simulations of summertime regional air quality: A diagnostic analysis of ozone and temperature simulations in the US using CESM CAM-Chem, *Atmos. Environ.*, 101, 134–148, doi:10.1016/j.atmosenv.2014.11.001, 2015.
- Carmichael, G. R., Tang, Y., Kurata, G., Uno, I., Streets, D., Woo, J. H., Huang, H., Yienger, J., Lefler, B., Shetter, R., Blake, D., Atlas, E., Fried, A., Apel, E., Eisele, F., Cantrell, C., Avery, M., Barrick, J., Sachse, G., Brune, W., Sandholm, S., Kondo, Y., Singh, H., Talbot, R., Bandy, A., Thornton, D., Clarke, A., and Heikes, B.: Regional-scale chemical transport modeling in support of the analysis of observations obtained during the TRACE-P experiment, *J. Geophys. Res.*, 108, 8823, doi:10.1029/2002jd003117, 2003.
- Clifton, O. E., Fiore, A. M., Correa, G., Horowitz, L. W., and Naik, V.: Twenty-first century reversal of the surface ozone seasonal cycle over the northeastern United States, *Geophys. Res. Lett.*, 41, 7343–7350, doi:10.1002/2014gl061378, 2014.
- Cooper, O. R., Parrish, D. D., Stohl, A., Trainer, M., Nedelec, P., Thouret, V., Cammas, J. P., Oltmans, S. J., Johnson, B. J., Tarasick, D., Leblanc, T., McDermid, I. S., Jaffe, D., Gao, R., Stith, J., Ryerson, T., Aikin, K., Campos, T., Weinheimer, A., and Avery, M. A.: Increasing springtime ozone mixing ratios in the free troposphere over western North America, *Nature*, 463, 344–348, doi:10.1038/nature08708, 2010.
- Cooper, O. R., Gao, R.-S., Tarasick, D., Leblanc, T., and Sweeney, C.: Long-term ozone trends at rural ozone monitoring sites across the United States, 1990–2010, *J. Geophys. Res.*, 117, D22307, doi:10.1029/2012JD018261, 2012.
- Dennison, P. E., Brewer, S. C., Arnold, J. D., and Moritz, M. A.: Large wildfire trends in the western United States, 1984–2011, *Geophys. Res. Lett.*, 41, 2928–2933, doi:10.1002/2014gl059576, 2014.
- Dentener, F., Kinne, S., Bond, T., Boucher, O., Cofala, J., Generoso, S., Ginoux, P., Gong, S., Hoelzemann, J. J., Ito, A., Marelli, L., Penner, J. E., Putaud, J.-P., Textor, C., Schulz, M., van der Werf, G. R., and Wilson, J.: Emissions of primary aerosol and precursor gases in the years 2000 and 1750 prescribed data-sets for AeroCom, *Atmos. Chem. Phys.*, 6, 4321–4344, doi:10.5194/acp-6-4321-2006, 2006.
- Ding, A. J., Wang, T., Thouret, V., Cammas, J.-P., and Nédélec, P.: Tropospheric ozone climatology over Beijing: analysis of aircraft data from the MOZAIC program, *Atmos. Chem. Phys.*, 8, 1–13, doi:10.5194/acp-8-1-2008, 2008.
- Donat, M., Alexander, L., Yang, H., Durre, I., Vose, R., and Caesar, J.: Global Land-Based Datasets for Monitoring Climatic Extremes, *B. Am. Meteorol. Soc.*, 94, 997–1006, doi:10.1175/Bams-D-12-00109.1, 2013.
- Donner, L. J., Wyman, B. L., Hemler, R. S., et al.: The Dynamical Core, Physical Parameterizations, and Basic Simulation Characteristics of the Atmospheric Component AM3 of the GFDL Global Coupled Model CM3, *J. Climate*, 24, 3484–3519, doi:10.1175/2011jcli3955.1, 2011.
- Duncan, B. N., Lamsal, L. N., Thompson, A. M., Yoshida, Y., Lu, Z. F., Streets, D. G., Hurwitz, M. M., and Pickering, K. E.: A space-based, high-resolution view of notable changes in urban NO_x pollution around the world (2005–2014), *J. Geophys. Res.*, 121, 976–996, doi:10.1002/2015jd024121, 2016.
- Emberson, L. D., Kitwiroon, N., Beevers, S., Büker, P., and Cinderby, S.: Scorched Earth: how will changes in the strength of the vegetation sink to ozone deposition affect human health and ecosystems?, *Atmos. Chem. Phys.*, 13, 6741–6755, doi:10.5194/acp-13-6741-2013, 2013.
- Federal Register: US Environmental Protection Agency, National Ambient Air Quality Standards for Ozone – Final Rule, Federal Register 80, available at: <http://www.gpo.gov/fdsys/pkg/FR-2015-10-26/pdf/2015-26594.pdf>, 65292–65468, 2015.
- Fiore, A. M., Dentener, F. J., Wild, O., et al.: Multimodel estimates of intercontinental source-receptor relationships for ozone pollution, *J. Geophys. Res.*, 114, D04301, doi:10.1029/2008jd010816, 2009.
- Fiore, A. M., Oberman, J. T., Lin, M. Y., Zhang, L., Clifton, O. E., Jacob, D. J., Naik, V., Horowitz, L. W., and Pinto, J. P.: Estimating North American background ozone in U.S. surface air with two independent global models: Variability, uncertainties, and recommendations *Atmos. Environ.*, 96, 284–300, doi:10.1016/j.atmosenv.2014.07.045, 2014.
- Fiore, A. M., Naik, V., and Leibensperger, E. M.: Air Quality and Climate Connections, *J. Air Waste Manage.*, 65, 645–685, doi:10.1080/10962247.2015.1040526, 2015.
- Gao, Y., Fu, J. S., Drake, J. B., Lamarque, J.-F., and Liu, Y.: The impact of emission and climate change on ozone in the United States under representative concentration pathways (RCPs), *Atmos. Chem. Phys.*, 13, 9607–9621, doi:10.5194/acp-13-9607-2013, 2013.
- Gilman, J. B., Lerner, B. M., Kuster, W. C., and de Gouw, J. A.: Source Signature of Volatile Organic Compounds from Oil and Natural Gas Operations in Northeastern Colorado, *Environ. Sci. Technol.*, 47, 1297–1305, doi:10.1021/es304119a, 2013.
- Granier, C., Bessagnet, B., Bond, T., D'Angiola, A., van der Gon, H. D., Frost, G. J., Heil, A., Kaiser, J. W., Kinne, S., Klimont, Z., Kloster, S., Lamarque, J.-F., Liousse, C., Masui, T., Meleux, F., Mieville, A., Ohara, T., Raut, J.-C., Riahi, K., Schultz, M. G., Smith, S. J., Thompson, A., van Aardenne, J., van der Werf, G. R., and van Vuuren, D. P.: Evolution of anthropogenic and biomass burning emissions of air pollutants at global and regional scales during the 1980–2010 period, *Climatic Change*, 109, 163–190, doi:10.1007/s10584-011-0154-1, 2011.
- Gratz, L. E., Jaffe, D. A., and Hee, J. R.: Causes of increasing ozone and decreasing carbon monoxide in springtime at the Mt. Bachelor Observatory from 2004 to 2013, *Atmos. Environ.*, 109, 323–330, doi:10.1016/j.atmosenv.2014.05.076, 2014.

- Guenther, A., Karl, T., Harley, P., Wiedinmyer, C., Palmer, P. I., and Geron, C.: Estimates of global terrestrial isoprene emissions using MEGAN (Model of Emissions of Gases and Aerosols from Nature), *Atmos. Chem. Phys.*, 6, 3181–3210, doi:10.5194/acp-6-3181-2006, 2006.
- Halliday, H. S., Thompson, A. M., Wisthaler, A., Blake, D. R., Hornbrook, R. S., Mikoviny, T., Müller, M., Eichler, P., Apel, E. C., and Hills, A. J.: Atmospheric benzene observations from oil and gas production in the Denver-Julesburg Basin in July and August 2014, *J. Geophys. Res.-Atmos.*, 121, 11055–11074, doi:10.1002/2016jd025327, 2016.
- Harris, I., Jones, P. D., Osborn, T. J., and Lister, D. H.: Updated high-resolution grids of monthly climatic observations – the CRU TS3.10 Dataset, *Int. J. Climatol.*, 34, 623–642, doi:10.1002/joc.3711, 2014.
- Hilboll, A., Richter, A., and Burrows, J. P.: Long-term changes of tropospheric NO₂ over megacities derived from multiple satellite instruments, *Atmos. Chem. Phys.*, 13, 4145–4169, doi:10.5194/acp-13-4145-2013, 2013.
- Horton, D. E., Johnson, N. C., Singh, D., Swain, D. L., Rajaratnam, B., and Diffenbaugh, N. S.: Contribution of changes in atmospheric circulation patterns to extreme temperature trends, *Nature*, 522, 465–469, doi:10.1038/nature14550, 2015.
- Huang, L., McDonald-Buller, E. C., McGaughey, G., Kimura, Y., and Allen, D. T.: The impact of drought on ozone dry deposition over eastern Texas, *Atmos. Environ.*, 127, 176–186, doi:10.1016/j.atmosenv.2015.12.022, 2016.
- Huang, M., Carmichael, G. R., Chai, T., Pierce, R. B., Oltmans, S. J., Jaffe, D. A., Bowman, K. W., Kaduwela, A., Cai, C., Spak, S. N., Weinheimer, A. J., Huey, L. G., and Diskin, G. S.: Impacts of transported background pollutants on summertime western US air quality: model evaluation, sensitivity analysis and data assimilation, *Atmos. Chem. Phys.*, 13, 359–391, doi:10.5194/acp-13-359-2013, 2013.
- Jacob, D. J. and Winner, D. A.: Effect of climate change on air quality, *Atmos. Environ.*, 43, 51–63, doi:10.1016/j.atmosenv.2008.09.051, 2009.
- Jacob, D. J., Logan, J. A., and Murti, P. P.: Effect of rising Asian emissions on surface ozone in the United States, *Geophys. Res. Lett.*, 26, 2175–2178, doi:10.1029/1999gl1900450, 1999.
- Jaffe, D.: Relationship between Surface and Free Tropospheric Ozone in the Western U.S, *Environ. Sci. Technol.*, 45, 432–438, doi:10.1021/es1028102, 2011.
- Jaffe, D. and Ray, J.: Increase in surface ozone at rural sites in the western US, *Atmos. Environ.*, 41, 5452–5463, doi:10.1016/j.atmosenv.2007.02.034, 2007.
- Jaffe, D., Chand, D., Hafner, W., Westerling, A., and Spracklen, D.: Influence of fires on ozone concentrations in the western US, *Environ. Sci. Technol.*, 42, 5885–5891, doi:10.1021/es800084k, 2008.
- Jaffe, D., Wigder, N., Downey, N., Pfister, G., Boynard, A., and Reid, S. B.: Impact of Wildfires on Ozone Exceptional Events in the Western US, *Environ. Sci. Technol.*, 47, 11065–11072, doi:10.1021/es402164f, 2013.
- Jia, L. W., Vecchi, G. A., Yang, X. S., Gudgel, R. G., Delworth, T. L., Stern, W. F., Paffendorf, K., Underwood, S. D., and Zeng, F. R.: The Roles of Radiative Forcing, Sea Surface Temperatures, and Atmospheric and Land Initial Conditions in US Summer Warming Episodes, *J. Climate*, 29, 4121–4135, doi:10.1175/Jcli-D-15-0471.1, 2016.
- John, J. G., Fiore, A. M., Naik, V., Horowitz, L. W., and Dunne, J. P.: Climate versus emission drivers of methane lifetime against loss by tropospheric OH from 1860–2100, *Atmos. Chem. Phys.*, 12, 12021–12036, doi:10.5194/acp-12-12021-2012, 2012.
- Koumoutsaris, S. and Bey, I.: Can a global model reproduce observed trends in summertime surface ozone levels?, *Atmos. Chem. Phys.*, 12, 6983–6998, doi:10.5194/acp-12-6983-2012, 2012.
- Krotkov, N. A., McLinden, C. A., Li, C., Lamsal, L. N., Celarier, E. A., Marchenko, S. V., Swartz, W. H., Bucsela, E. J., Joiner, J., Duncan, B. N., Boersma, K. F., Veefkind, J. P., Levelt, P. F., Fioletov, V. E., Dickerson, R. R., He, H., Lu, Z., and Streets, D. G.: Aura OMI observations of regional SO₂ and NO₂ pollution changes from 2005 to 2015, *Atmos. Chem. Phys.*, 16, 4605–4629, doi:10.5194/acp-16-4605-2016, 2016.
- Lamarque, J.-F., Bond, T. C., Eyring, V., Granier, C., Heil, A., Klimont, Z., Lee, D., Liousse, C., Mieville, A., Owen, B., Schultz, M. G., Shindell, D., Smith, S. J., Stehfest, E., Van Aardenne, J., Cooper, O. R., Kainuma, M., Mahowald, N., McConnell, J. R., Naik, V., Riahi, K., and van Vuuren, D. P.: Historical (1850–2000) gridded anthropogenic and biomass burning emissions of reactive gases and aerosols: methodology and application, *Atmos. Chem. Phys.*, 10, 7017–7039, doi:10.5194/acp-10-7017-2010, 2010.
- Lamarque, J. F., Kyle, G. P., Meinshausen, M., Riahi, K., Smith, S. J., van Vuuren, D. P., Conley, A. J., and Vitt, F.: Global and regional evolution of short-lived radiatively-active gases and aerosols in the Representative Concentration Pathways, *Climatic Change* 109, 191–212, doi:10.1007/s10584-011-0155-0, 2012.
- Langford, A. O., Aikin, K. C., Eubank, C. S., and Williams, E. J.: Stratospheric contribution to high surface ozone in Colorado during springtime, *Geophys. Res. Lett.*, 36, L12801, doi:10.1029/2009gl038367, 2009.
- Langford, A. O., Senff, C. J., Alvarez II, R. J., Banta, R. M., and Hardesty, R. M.: Long-range transport of ozone from the Los Angeles Basin: A case study, *Geophys. Res. Lett.*, 37, L06807, doi:10.1029/2010gl042507, 2010.
- Langford, A. O., Senff, C., Alvarez II, R., Brioude, J., Cooper, O., Holloway, J., Lin, M., Marchbanks, R., Pierce, R., Sandberg, S., Weickmann, A., and Williams, E.: An overview of the 2013 Las Vegas Ozone Study (LVOS): Impact of stratospheric intrusions and long-range transport on surface air quality, *Atmos. Environ.*, 109, 305–322, doi:10.1016/j.atmosenv.2014.08.040, 2014.
- Lee, H.-J., Kim, S.-W., Brioude, J., Cooper, O. R., Frost, G. J., Kim, C.-H., Park, R. J., Trainer, M., and Woo, J.-H.: Transport of NO_x in East Asia identified by satellite and in situ measurements and Lagrangian particle dispersion model simulations, *J. Geophys. Res.-Atmos.*, 119, 2574–2596, doi:10.1002/2013JD021185, 2014.
- Leibensperger, E. M., Mickley, L. J., and Jacob, D. J.: Sensitivity of US air quality to mid-latitude cyclone frequency and implications of 1980–2006 climate change, *Atmos. Chem. Phys.*, 8, 7075–7086, doi:10.5194/acp-8-7075-2008, 2008.
- Li, G., Bei, N., Cao, J., Wu, J., Long, X., Feng, T., Dai, W., Liu, S., Zhang, Q., and Tie, X.: Widespread and Persistent Ozone Pollution in Eastern China, *Atmos. Chem. Phys. Discuss.*, doi:10.5194/acp-2016-864, in review, 2016.

- Lin, M., Holloway, T., Oki, T., Streets, D. G., and Richter, A.: Multi-scale model analysis of boundary layer ozone over East Asia, *Atmos. Chem. Phys.*, 9, 3277–3301, doi:10.5194/acp-9-3277-2009, 2009.
- Lin, M., Holloway, T., Carmichael, G. R., and Fiore, A. M.: Quantifying pollution inflow and outflow over East Asia in spring with regional and global models, *Atmos. Chem. Phys.*, 10, 4221–4239, doi:10.5194/acp-10-4221-2010, 2010.
- Lin, M., Fiore, A. M., Cooper, O. R., Horowitz, L. W., Langford, A. O., Levy, H., Johnson, B. J., Naik, V., Oltmans, S. J., and Senff, C. J.: Springtime high surface ozone events over the western United States: Quantifying the role of stratospheric intrusions, *J. Geophys. Res.*, 117, D00V22, doi:10.1029/2012jd018151, 2012a.
- Lin, M., Fiore, A. M., Horowitz, L. W., Cooper, O. R., Naik, V., Holloway, J., Johnson, B. J., Middlebrook, A. M., Oltmans, S. J., Pollack, I. B., Ryerson, T. B., Warner, J. X., Wiedinmyer, C., Wilson, J., and Wyman, B.: Transport of Asian ozone pollution into surface air over the western United States in spring, *J. Geophys. Res.*, 117, D00V07, doi:10.1029/2011jd016961, 2012b.
- Lin, M., Horowitz, L. W., Oltmans, S. J., Fiore, A. M., and Fan, S.: Tropospheric ozone trends at Mauna Loa Observatory tied to decadal climate variability, *Nat. Geosci.*, 7, 136–143, doi:10.1038/ngeo2066, 2014.
- Lin, M., Fiore, A. M., Horowitz, L. W., Langford, A. O., Oltmans, S. J., Tarasick, D., and Rieder, H. E.: Climate variability modulates western U.S. ozone air quality in spring via deep stratospheric intrusions, *Nat. Commun.*, 6, 7105, doi:10.1038/ncomms8105, 2015a.
- Lin, M., Horowitz, L. W., Cooper, O. R., Tarasick, D., Conley, S., Iraci, L. T., Johnson, B., Leblanc, T., Petropavlovskikh, I., and Yates, E. L.: Revisiting the evidence of increasing springtime ozone mixing ratios in the free troposphere over western North America, *Geophys. Res. Lett.*, 42, 8719–8728, doi:10.1002/2015GL065311, 2015b.
- Lin, Y.-K., Lin, T.-H., and Chang, S.-C.: The changes in different ozone metrics and their implications following precursor reductions over northern Taiwan from 1994 to 2007, *Environ. Monit. Assess.*, 169, 143–157, doi:10.1007/s10661-009-1158-4, 2010.
- Liu, F., Zhang, Q., Ronald, J. V., Zheng, B., Tong, D., Yan, L., Zheng, Y. X., and He, K. B.: Recent reduction in NO_x emissions over China: synthesis of satellite observations and emission inventories, *Environ. Res. Lett.*, 11, 114002, doi:10.1088/1748-9326/11/11/114002, 2016.
- Liu, H. Y., Jacob, D. J., Chan, L. Y., Oltmans, S. J., Bey, I., Yantosca, R. M., Harris, J. M., Duncan, B. N., and Martin, R. V.: Sources of tropospheric ozone along the Asian Pacific Rim: An analysis of ozonesonde observations, *J. Geophys. Res.*, 107, 4573, doi:10.1029/2001jd002005, 2002.
- Loughner, C. P., Duncan, B. N., and Hains, J.: The benefit of historical air pollution emissions reductions during extreme heat, *Environ. Manage.*, 9, 34–38, 2014.
- Ma, Z., Xu, J., Quan, W., Zhang, Z., Lin, W., and Xu, X.: Significant increase of surface ozone at a rural site, north of eastern China, *Atmos. Chem. Phys.*, 16, 3969–3977, doi:10.5194/acp-16-3969-2016, 2016.
- McDonald, B. C., Dallmann, T. R., Martin, E. W., and Harley, R. A.: Long-term trends in nitrogen oxide emissions from motor vehicles at national, state, and air basin scales, *J. Geophys. Res.*, 117, D00V18, doi:10.1029/2012jd018304, 2012.
- McDuffie, E. E., Edwards, P. M., Gilman, J. B., Lerner, B. M., Dube, W. P., Trainer, M., Wolfe, D. E., Angevine, W. M., de-Gouw, J., Williams, E. J., Tevlin, A. G., Murphy, J. G., Fischer, E. V., McKeen, S., Ryerson, T. B., Peischl, J., Holloway, J. S., Aikin, K., Langford, A. O., Senff, C. J., Alvarez, R. J., Hall, S. R., Ullmann, K., Lantz, K. O., and Brown, S. S.: Influence of oil and gas emissions on summertime ozone in the Colorado Northern Front Range, *J. Geophys. Res.-Atmos.*, 121, 8712–8729, doi:10.1002/2016jd025265, 2016.
- Monks, P. S., Archibald, A. T., Colette, A., Cooper, O., Coyle, M., Derwent, R., Fowler, D., Granier, C., Law, K. S., Mills, G. E., Stevenson, D. S., Tarasova, O., Thouret, V., von Schneidmesser, E., Sommariva, R., Wild, O., and Williams, M. L.: Tropospheric ozone and its precursors from the urban to the global scale from air quality to short-lived climate forcer, *Atmos. Chem. Phys.*, 15, 8889–8973, doi:10.5194/acp-15-8889-2015, 2015.
- Morgenstern, O., Hegglin, M. I., Rozanov, E., O'Connor, F. M., Abraham, N. L., Akiyoshi, H., Archibald, A. T., Bekki, S., Butchart, N., Chipperfield, M. P., Deushi, M., Dhomse, S. S., Garcia, R. R., Hardiman, S. C., Horowitz, L. W., Jöckel, P., Josse, B., Kinnison, D., Lin, M., Mancini, E., Manyin, M. E., Marchand, M., Maréchal, V., Michou, M., Oman, L. D., Pitari, G., Plummer, D. A., Revell, L. E., Saint-Martin, D., Schofield, R., Stenke, A., Stone, K., Sudo, K., Tanaka, T. Y., Tilmes, S., Yamashita, Y., Yoshida, K., and Zeng, G.: Review of the global models used within phase 1 of the Chemistry-Climate Model Initiative (CCMI), *Geosci. Model Dev.*, 10, 639–671, doi:10.5194/gmd-10-639-2017, 2017.
- Naik, V., Horowitz, L. W., Fiore, A. M., Ginoux, P., Mao, J. Q., Aghedo, A. M., and Levy, H.: Impact of preindustrial to present-day changes in short-lived pollutant emissions on atmospheric composition and climate forcing, *J. Geophys. Res.*, 118, 8086–8110, doi:10.1002/jgrd.50608, 2013.
- Parrish, D. D., Lamarque, J.-F., Naik, V., Horowitz, L., Shindell, D. T., Staehelin, J., Derwent, R., Cooper, O. R., Tanimoto, H., Volz-Thomas, A., Gilge, S., Scheel, H.-E., Steinbacher, M., and Fröhlich, M.: Long-term changes in lower tropospheric baseline ozone concentrations: Comparing chemistry-climate models and observations at northern midlatitudes, *J. Geophys. Res.*, 119, 5719–5736, doi:10.1002/2013JD021435, 2014.
- Pfister, G. G., Walters, S., Emmons, L. K., Edwards, D. P., and Avise, J.: Quantifying the contribution of inflow on surface ozone over California during summer 2008, *J. Geophys. Res.*, 118, 12282–12299, doi:10.1002/2013jd020336, 2013.
- Pfister, G. G., Walters, S., Lamarque, J. F., Fast, J., Barth, M. C., Wong, J., Done, J., Holland, G., and Bruyere, C. L.: Projections of future summertime ozone over the US, *J. Geophys. Res.*, 119, 5559–5582, doi:10.1002/2013jd020932, 2014.
- Porter, W. C., Heald, C. L., Cooley, D., and Russell, B.: Investigating the observed sensitivities of air-quality extremes to meteorological drivers via quantile regression, *Atmos. Chem. Phys.*, 15, 10349–10366, doi:10.5194/acp-15-10349-2015, 2015.
- Pusede, S. E., Steiner, A. L., and Cohen, R. C.: Temperature and Recent Trends in the Chemistry of Continental Surface Ozone, *Chem. Rev.*, 115, 3898–3918, doi:10.1021/cr5006815, 2015.
- Rasmussen, D. J., Fiore, A. M., Naik, V., Horowitz, L. W., McGinnis, S. J., and Schultz, M. G.: Surface ozone-temperature rela-

- tionships in the eastern US: A monthly climatology for evaluating chemistry-climate models, *Atmos. Environ.*, 47, 142–153, doi:10.1016/j.atmosenv.2011.11.021, 2012.
- Reidmiller, D. R., Fiore, A. M., Jaffe, D. A., Bergmann, D., Cuvelier, C., Dentener, F. J., Duncan, B. N., Folberth, G., Gauss, M., Gong, S., Hess, P., Jonson, J. E., Keating, T., Lupu, A., Marmer, E., Park, R., Schultz, M. G., Shindell, D. T., Szopa, S., Vivanco, M. G., Wild, O., and Zuber, A.: The influence of foreign vs. North American emissions on surface ozone in the US, *Atmos. Chem. Phys.*, 9, 5027–5042, doi:10.5194/acp-9-5027-2009, 2009.
- Rieder, H. E., Fiore, A. M., Horowitz, L. W., and Naik, V.: Projecting policy-relevant metrics for high summertime ozone pollution events over the eastern United States due to climate and emission changes during the 21st century, *J. Geophys. Res.*, 120, 784–800, doi:10.1002/2014jd022303, 2015.
- Russell, A. R., Valin, L. C., and Cohen, R. C.: Trends in OMI NO₂ observations over the United States: effects of emission control technology and the economic recession, *Atmos. Chem. Phys.*, 12, 12197–12209, doi:10.5194/acp-12-12197-2012, 2012.
- Schnell, J. L., Prather, M. J., Josse, B., Naik, V., Horowitz, L. W., Zeng, G., Shindell, D. T., and Faluvegi, G.: Effect of climate change on surface ozone over North America, Europe, and East Asia, *Geophys. Res. Lett.*, 43, 3509–3518, doi:10.1002/2016GL068060, 2016.
- Schultz, M. G., Heil, A., Hoelzemann, J. J., Spessa, A., Thonicke, K., Goldammer, J. G., Held, A. C., Pereira, J. M. C., and van het Bolscher, M.: Global wildland fire emissions from 1960 to 2000, *Global Biogeochem. Cy.*, 22, Gb2002, doi:10.1029/2007gb003031, 2008.
- Schwietzke, S., Sherwood, O. A., Ruhwiler, L. M. P. B., Miller, J. B., Etiope, G., Dlugokencky, E. J., Michel, S. E., Arling, V. A., Vaughn, B. H., White, J. W. C., and Tans, P. P.: Upward revision of global fossil fuel methane emissions based on isotope database, *Nature*, 538, 88–91, doi:10.1038/nature19797, 2016.
- Seager, R. and Hoerling, M.: Atmosphere and Ocean Origins of North American Droughts, *J. Climate*, 27, 4581–4606, doi:10.1175/Jcli-D-13-00329.1, 2014.
- Shen, L., Mickley, L. J., and Gilleland, E.: Impact of increasing heat waves on US ozone episodes in the 2050s: Results from a multimodel analysis using extreme value theory, *Geophys. Res. Lett.*, 43, 4017–4025, doi:10.1002/2016gl068432, 2016.
- Shepherd, T. G.: CLIMATE SCIENCE: The dynamics of temperature extremes, *Nature*, 522, 422–424, 2015.
- Simon, H., Reff, A., Wells, B., Xing, J., and Frank, N.: Ozone Trends Across the United States over a Period of Decreasing NO_x and VOC Emissions, *Environ. Sci. Technol.*, 49, 186–195, doi:10.1021/es504514z, 2015.
- Solberg, S., Hov, O., Sovde, A., Isaksen, I. S. A., Coddeville, P., De Backer, H., Forster, C., Orsolini, Y., and Uhse, K.: European surface ozone in the extreme summer 2003, *J. Geophys. Res.*, 113, D07307, doi:10.1029/2007jd009098, 2008.
- Strode, S. A., Rodriguez, J. M., Logan, J. A., Cooper, O. R., Witte, J. C., Lamsal, L. N., Damon, M., Van Aartsen, B., Steenrod, S. D., and Strahan, S. E.: Trends and variability in surface ozone over the United States, *J. Geophys. Res.-Atmos.*, 120, 9020–9042, doi:10.1002/2014JD022784, 2015.
- Sun, L., Xue, L., Wang, T., Gao, J., Ding, A., Cooper, O. R., Lin, M., Xu, P., Wang, Z., Wang, X., Wen, L., Zhu, Y., Chen, T., Yang, L., Wang, Y., Chen, J., and Wang, W.: Significant increase of summertime ozone at Mount Tai in Central Eastern China, *Atmos. Chem. Phys.*, 16, 10637–10650, doi:10.5194/acp-16-10637-2016, 2016.
- Tanimoto, H.: Increase in springtime tropospheric ozone at a mountainous site in Japan for the period 1998–2006, *Atmos. Environ.*, 43, 1358–1363, doi:10.1016/j.atmosenv.2008.12.006, 2009.
- Tanimoto, H., Zbinden, R. M., Thouret, V., and Nedelec, P.: Consistency of tropospheric ozone observations made by different platforms and techniques in the global databases, *Tellus B*, 67, 27073, doi:10.3402/tellusb.v67.27073, 2016.
- Thompson, A. M., Witte, J. C., Smit, H. G. J., Oltmans, S. J., Johnson, B. J., Kirchhoff, V. W. J. H., and Schmidlin, F. J.: Southern Hemisphere Additional Ozoneondes (SHADOZ) 1998–2004 tropical ozone climatology: 3. Instrumentation, station-to-station variability, and evaluation with simulated flight profiles, *J. Geophys. Res.*, 112, D03304, doi:10.1029/2005jd007042, 2007.
- Travis, K. R., Jacob, D. J., Fisher, J. A., Kim, P. S., Marais, E. A., Zhu, L., Yu, K., Miller, C. C., Yantosca, R. M., Sulprizio, M. P., Thompson, A. M., Wennberg, P. O., Crouse, J. D., St. Clair, J. M., Cohen, R. C., Laughner, J. L., Dibb, J. E., Hall, S. R., Ullmann, K., Wolfe, G. M., Pollack, I. B., Peischl, J., Neuman, J. A., and Zhou, X.: Why do models overestimate surface ozone in the Southeast United States?, *Atmos. Chem. Phys.*, 16, 13561–13577, doi:10.5194/acp-16-13561-2016, 2016.
- van der Werf, G. R., Randerson, J. T., Giglio, L., Collatz, G. J., Mu, M., Kasibhatla, P. S., Morton, D. C., DeFries, R. S., Jin, Y., and van Leeuwen, T. T.: Global fire emissions and the contribution of deforestation, savanna, forest, agricultural, and peat fires (1997–2009), *Atmos. Chem. Phys.*, 10, 11707–11735, doi:10.5194/acp-10-11707-2010, 2010.
- VanCuren, R. and Gustin, M. S.: Identification of sources contributing to PM_{2.5} and ozone at elevated sites in the western US by receptor analysis: Lassen Volcanic National Park, California, and Great Basin National Park, Nevada, *Sci. Total Environ.*, 530, 505–518, doi:10.1016/j.scitotenv.2015.03.091, 2015.
- Verstraeten, W. W., Neu, J. L., Williams, J. E., Bowman, K. W., Worden, J. R., and Boersma, K. F.: Rapid increases in tropospheric ozone production and export from China, *Nat. Geosci.*, 8, 690–695, doi:10.1038/Ngeo2493, 2015.
- Wang, T., Ding, A. J., Gao, J., and Wu, W. S.: Strong ozone production in urban plumes from Beijing, China, *Geophys. Res. Lett.*, 33, L21806, doi:10.1029/2006gl027689, 2006.
- Wang, T., Wei, X. L., Ding, A. J., Poon, C. N., Lam, K. S., Li, Y. S., Chan, L. Y., and Anson, M.: Increasing surface ozone concentrations in the background atmosphere of Southern China, 1994–2007, *Atmos. Chem. Phys.*, 9, 6217–6227, doi:10.5194/acp-9-6217-2009, 2009.
- Wang, Y., McElroy, M. B., Munger, J. W., Hao, J., Ma, H., Nielsen, C. P., and Chen, Y.: Variations of O₃ and CO in summertime at a rural site near Beijing, *Atmos. Chem. Phys.*, 8, 6355–6363, doi:10.5194/acp-8-6355-2008, 2008.
- Wang, Y., Xie, Y., Cai, L., Dong, W., Zhang, Q., and Zhang, L.: Impact of the 2011 Southern US Drought on Ground-Level Fine Aerosol Concentration in Summertime, *J. Atmos. Sci.*, 72, 1075–1093, doi:10.1175/jas-d-14-0197.1, 2015.
- Warneke, C., de Gouw, J. A., Holloway, J. S., Peischl, J., Ryerson, T. B., Atlas, E., Blake, D., Trainer, M., and Parrish, D. D.: Multiyear trends in volatile organic compounds in Los Angeles, Cal-

- ifornia: Five decades of decreasing emissions, *J. Geophys. Res.*, 117, D00v17, doi:10.1029/2012jd017899, 2012.
- Xu, W., Lin, W., Xu, X., Tang, J., Huang, J., Wu, H., and Zhang, X.: Long-term trends of surface ozone and its influencing factors at the Mt Waliguan GAW station, China – Part 1: Overall trends and characteristics, *Atmos. Chem. Phys.*, 16, 6191–6205, doi:10.5194/acp-16-6191-2016, 2016.
- Yang, J., Tian, H. Q., Tao, B., Ren, W., Pan, S. F., Liu, Y. Q., and Wang, Y. H.: A growing importance of large fires in conterminous United States during 1984–2012, *J. Geophys. Res.-Biogeo.*, 120, 2625–2640, doi:10.1002/2015jg002965, 2015.
- Yurganov, L. N., Duchatelet, P., Dzhola, A. V., Edwards, D. P., Hase, F., Kramer, I., Mahieu, E., Mellqvist, J., Notholt, J., Novelli, P. C., Rockmann, A., Scheel, H. E., Schneider, M., Schulz, A., Strandberg, A., Sussmann, R., Tanimoto, H., Velazco, V., Drummond, J. R., and Gille, J. C.: Increased Northern Hemispheric carbon monoxide burden in the troposphere in 2002 and 2003 detected from the ground and from space, *Atmos. Chem. Phys.*, 5, 563–573, doi:10.5194/acp-5-563-2005, 2005.
- Zhang, L., Jacob, D. J., Boersma, K. F., Jaffe, D. A., Olson, J. R., Bowman, K. W., Worden, J. R., Thompson, A. M., Avery, M. A., Cohen, R. C., Dibb, J. E., Flock, F. M., Fuelberg, H. E., Huey, L. G., McMillan, W. W., Singh, H. B., and Weinheimer, A. J.: Transpacific transport of ozone pollution and the effect of recent Asian emission increases on air quality in North America: an integrated analysis using satellite, aircraft, ozonesonde, and surface observations, *Atmos. Chem. Phys.*, 8, 6117–6136, doi:10.5194/acp-8-6117-2008, 2008.
- Zhang, L., Jacob, D. J., Yue, X., Downey, N. V., Wood, D. A., and Blewitt, D.: Sources contributing to background surface ozone in the US Intermountain West, *Atmos. Chem. Phys.*, 14, 5295–5309, doi:10.5194/acp-14-5295-2014, 2014.
- Zhang, Y. Q., Cooper, O. R., Gaudel, A., Thompson, A. M., Nedelec, P., Ogino, S. Y., and West, J. J.: Tropospheric ozone change from 1980 to 2010 dominated by equatorward redistribution of emissions, *Nat. Geosci.*, 9, 875–879, doi:10.1038/Ngeo2827, 2016.

Attachment

C



Date: June 13, 2018
To: Timothy S. Franquist, Director, Air Quality Division
From: Yi Li, Environmental Engineering Specialist III
Subject: Investigation of intrastate, interstate and international contributions to high concentrations of ozone in Yuma, Arizona

Executive Summary

Air quality monitoring in Yuma, Arizona has shown the area is violating the 2015 National Ambient Air Quality Standard (NAAQS) for ozone. However, in comparison to many other ozone nonattainment areas (such as the Phoenix-Mesa Nonattainment Area), the Yuma area emits much less ozone precursors (nitrogen oxides and volatile organic compounds). This indicates that high concentrations of ozone in the Yuma area are the result of transport into the area and not due to local emissions. This memorandum summarizes two analyses of ozone concentrations in the Yuma Area: (1) a comparison of ground-based meteorological and ozone monitors in Yuma, Arizona, United States, and San Luis Rio Colorado, Sonora, Mexico; and (2) an analysis of data from the NASA Ozone Monitoring Instrument on the Aura satellite.

Ground-Based Monitor Data

The ground based monitors straddle the international border and are 18 miles (29 km) apart. Data collected by the monitors shows that the ambient ozone concentration is highly correlated at both sites ($r^2=0.72$), and that higher ozone concentrations at the Yuma site are associated with wind coming from the south and southwest.

NASA Ozone Monitoring Instrument Data

Given the location of Yuma at the nexus of Arizona, California, and Mexico, we thought it most appropriate to look at relative change concentrations in Arizona, northwestern Mexico and southern California from 2005 to 2017. Due to interference from the ozone layer of the stratosphere, we are not able to obtain direct ozone concentration data. Therefore, the ozone precursor Nitrogen Dioxide (NO_2) was investigated. Our analysis found: (1) NO_2 concentrations are highest in southern California and steadily decreasing, (2) NO_2 concentrations are lower in Arizona and also decreasing, and (3) NO_2 concentrations in northeastern Mexico are low but increasing. We also found that the area directly around the monitor was decreasing in concentrations for the 2005 to 2017 period, with most of the decrease from Arizona and California.

June 13, 2018

Background

Yuma, Arizona is the county seat of Yuma County, which shares a border with California and the Mexican states of Sonora and Baja California. The 2017 Yuma design value for ambient ozone concentrations (the design value covers the years 2015-17) was near the levels measured in the Phoenix-Mesa nonattainment area for the same period (Figure 1). The design value was 72 ppb in Yuma and 76 ppb in Phoenix-Mesa.

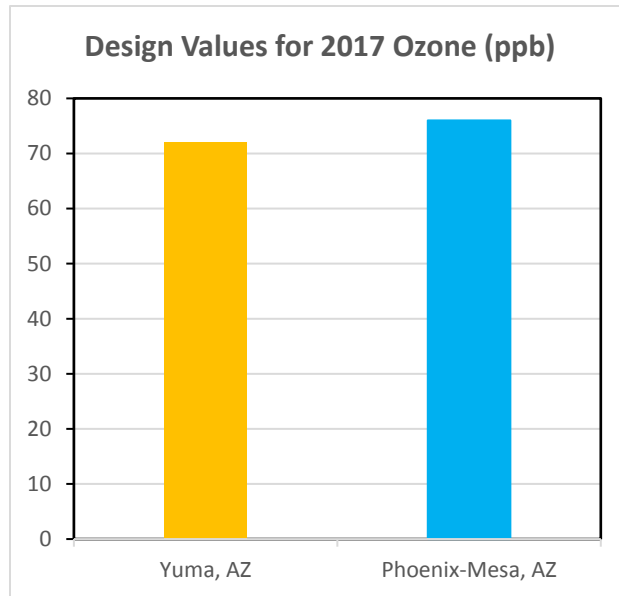


Figure 1 2017 Ozone Design Values

Elevated ozone concentrations are understood to be generated by high emissions of ozone precursors (mainly NO₂ and volatile organic compounds), which is in turn associated with human activity. However, when looking at levels of emissions and human activity, the Yuma area is much less than the Phoenix-Mesa area (Figure 2).

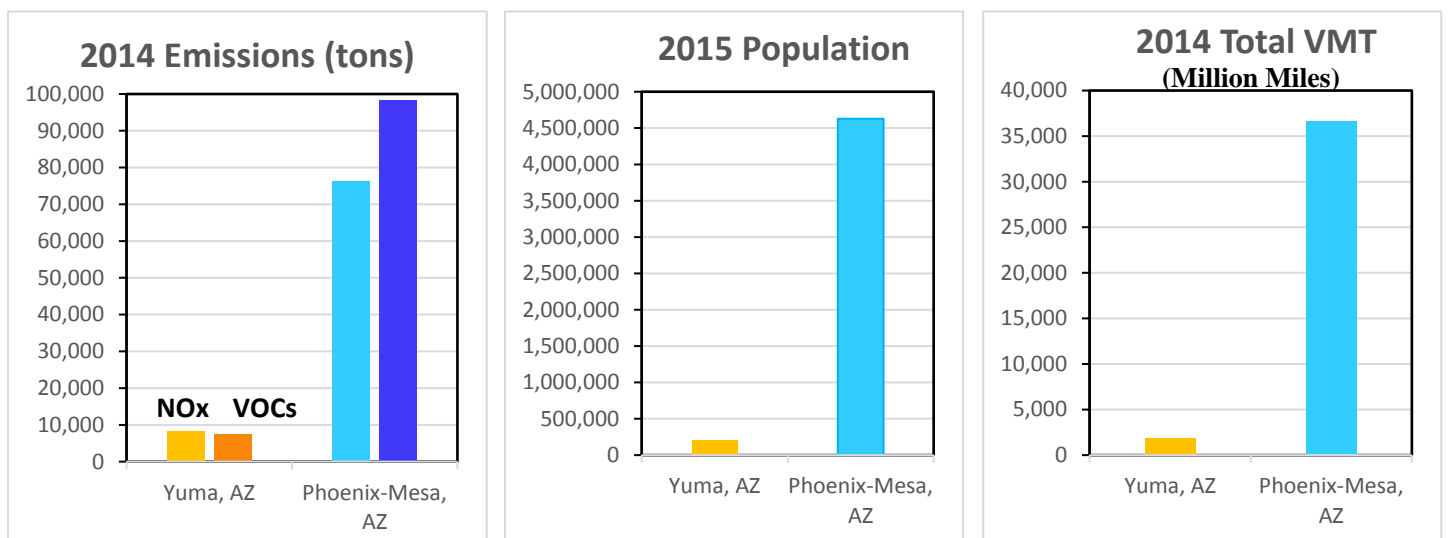
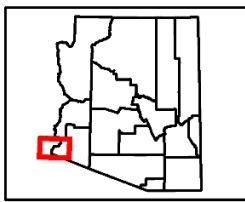
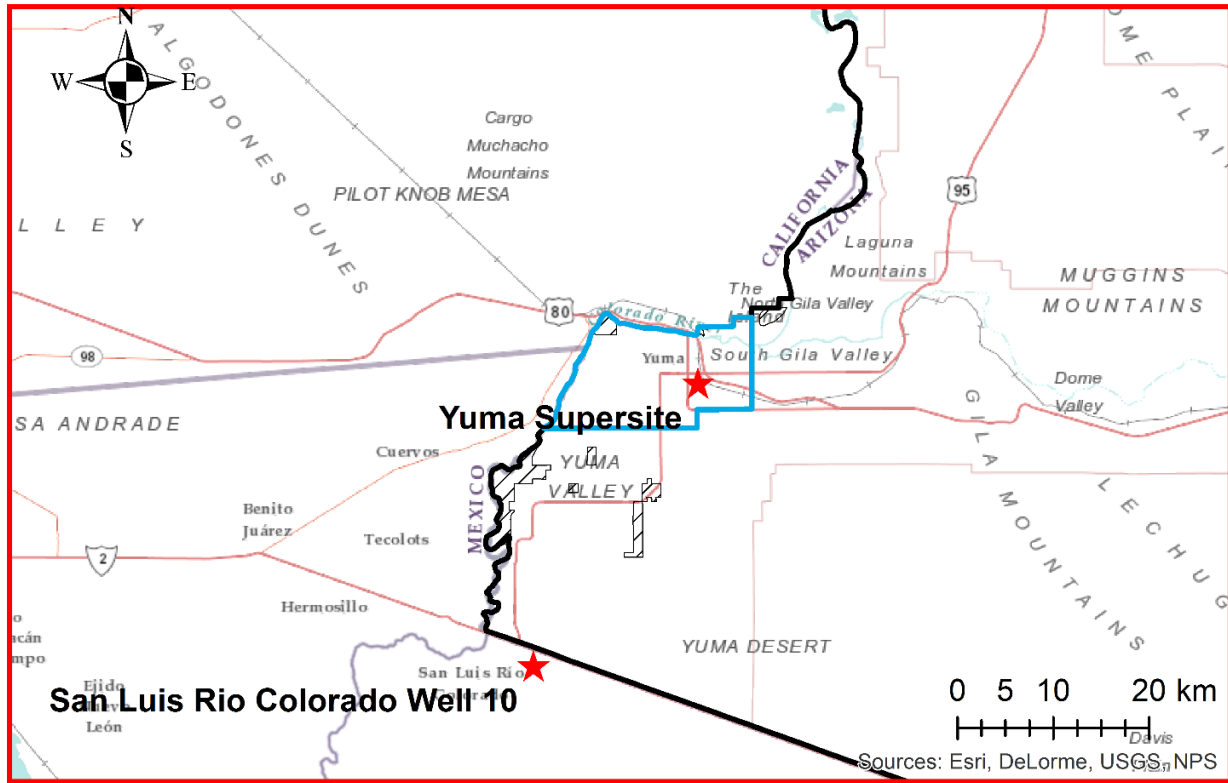


Figure 2 Emissions and Human Activity in Yuma and Phoenix-Mesa Areas

June 13, 2018

Ground-Based Monitoring Data

In addition to the ozone monitor in Yuma, ADEQ placed a monitor in San Luis Rio Colorado, Sonora Mexico. The monitors are 18 miles apart and on opposite sides of the international border. The location of the monitors is in Figure 3.



Legend

- ★ Monitors
- 2015 Proposed Yuma NAA
- ▨ Tribal Land
- ▭ County/Nation Boundary

Figure 3 Ozone Monitoring Locations

Data collected by the monitors for the 2017 ozone season is in Figures 4 and 5. In Figure 4, the data is shown with the Yuma measurements on top. In Figure 5, the data is shown with both stations superimposed. The ozone concentrations at both sites are correlated with an r-squared value of 0.72.

June 13, 2018

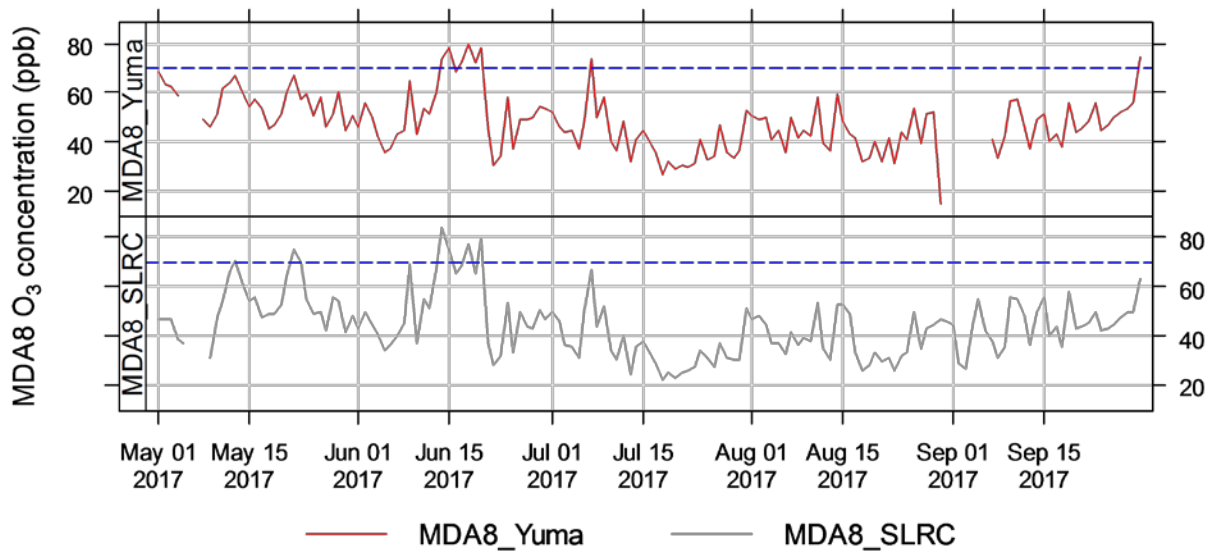


Figure 4 Ozone concentrations side-by-side

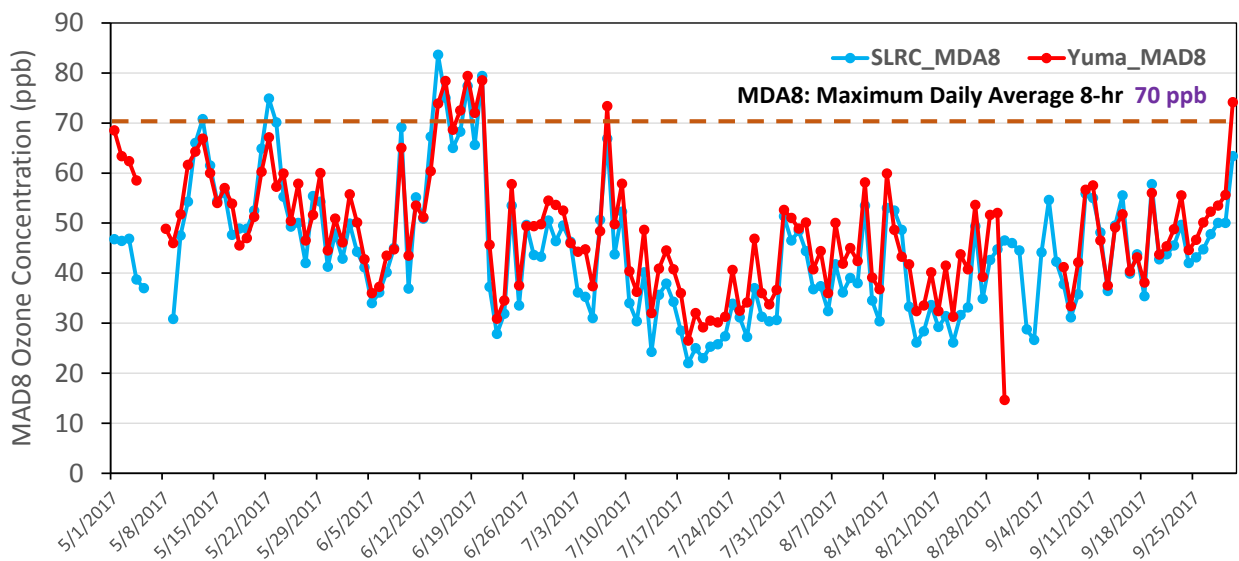


Figure 5 Ozone concentrations superimposed

Figure 6 presents the ozone concentration contribution from each wind direction on most days at both sites. Due south contributions are shaded orange and southwest contributions are shaded yellow. The wind direction on days when ozone concentrations exceeded the federal standard was from the south 80% of the time (31% due south, 43% from the southwest, and 6% from the southeast).

June 13, 2018

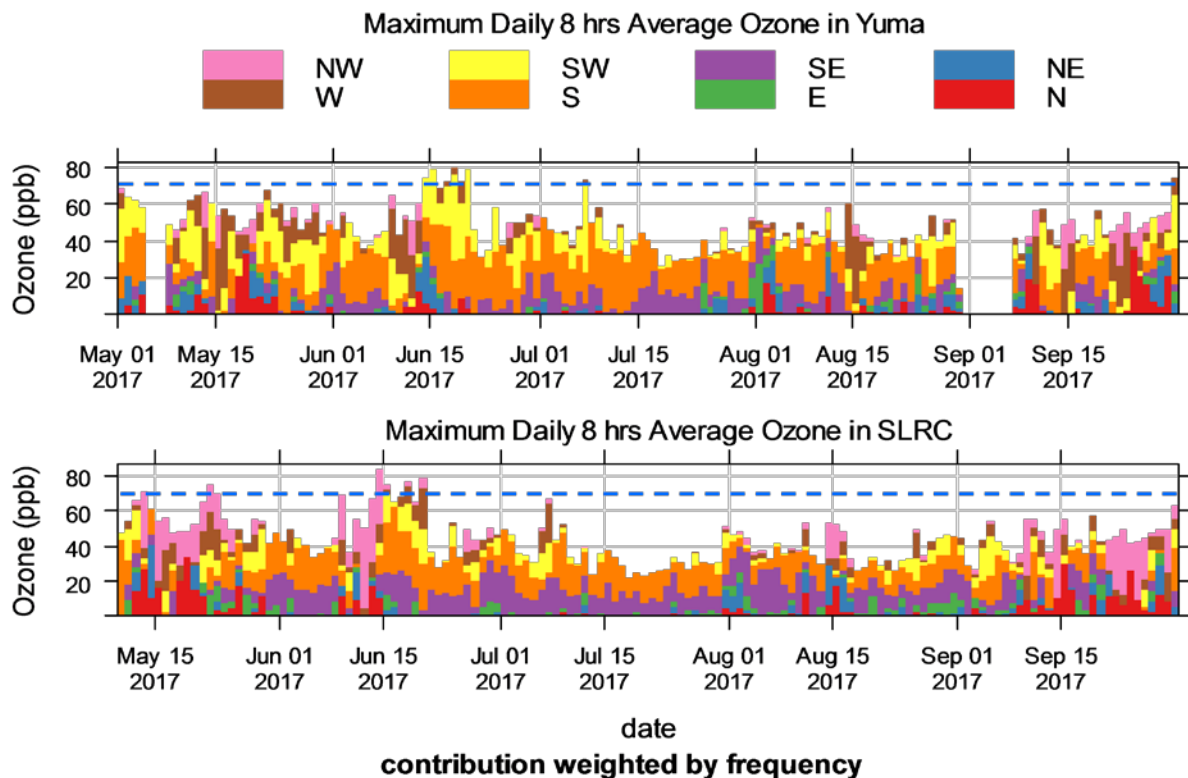


Figure 6 Ozone contribution by wind direction in Yuma and San Luis Rio Colorado

NASA Ozone Monitoring Instrument Data

Instrumentation

The Ozone Monitoring Instrument (OMI) is a spectrometer on NASA's Aura satellite (launched on July 15, 2004). The OMI instrument is a nadir viewing (downward facing) imaging spectrograph that measures the solar radiation backscattered by the Earth's atmosphere and surface over the entire wavelength range from 270 to 500 nm with a spectral resolution of about 0.5 nm. OMI combines the advantages of previous satellites (e.g., GOME, SCHIMACHY, OMPS etc), measuring the complete spectrum in the ultraviolet/visible wavelength range with a very high spatial resolution (13 km × 24 km) and daily global coverage (~ local time 1:45 pm).

Due to interference from the ozone layer of the stratosphere, we are not able to obtain direct ozone concentration. As an ozone precursor, nitrogen oxides (NO₂) play an important role in formation of ground-level ozone through several series of reactions with volatile organic compounds (VOCs) catalyzed by sunlight (Figure 7).

June 13, 2018

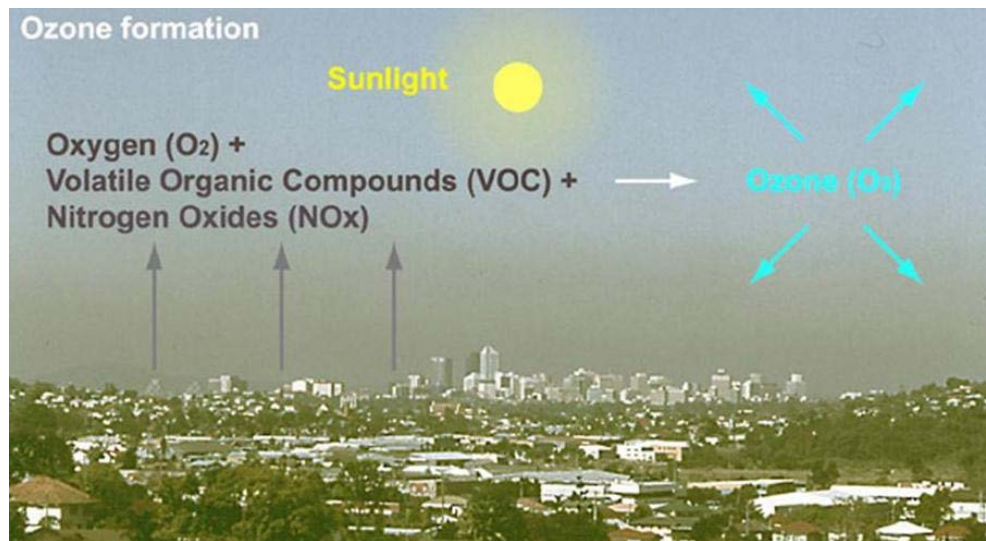


Figure 7 Diagram of Ground-level Ozone Formation

Methods

The OMI observes visible and ultraviolet (270-504 nm) solar backscatter radiation, which can be used to retrieve tropospheric NO₂ column densities with the Differential Optical Absorption Spectroscopy (DOAS) method. Since October 2004, OMI has provided NO₂ column densities retrieved by a spectral fitting algorithm. OMI observations have been widely used to study the trend of NO₂ column densities (Lamsal et al., 2015; Liu et al., 2016; Duncan et al., 2016, Majid et al., 2017). Over ten years of NO₂ data from OMI highlights air quality improvement throughout the U.S. (<https://www.nasa.gov/content/goddard/new-nasa-images-highlight-us-air-quality-improvement/>).

Since there is no NO₂ monitor near Yuma, AZ, in order to determine the regional emissions contributing to the Yuma ozone problem, we applied a hybrid inversion method to reveal the NO₂ spatial distributions and most importantly characterize the trends of NO₂ in Arizona, southern California, and northern Mexico. There are three operational OMI NO₂ products and their available information is listed in the table below:

Table 1. Information of OMI NO₂ operational products

Product Name	Acronym	Data Period	Reference
BErkeley High Resolution	BEHR	2005 – 2015	Russell et al.(2011); Laughner et al.(2016)
NASA standard product	NASA SP	2005 – 2017	Krotkov et al.(2017); Bucsela et al.(2013)
Dutch OMI NO₂	DOMINO	2005 – 2017	Boersma et al.(2007)

Note: More information on these three products can be found at Russell et al. (2011)

June 13, 2018

OMI NO₂ vertical column densities from Level 2 products are gridded to 0.5°x0.667° grid cells using quality flags and filtering criteria following the methods used in Jiang et al. (2018) and Qu et al. (2017). We processed the NO₂ retrieval data obtained from those three products for Yuma and its downwind areas including southern California, Arizona and Northern Mexico from 2005 to 2015. The whole region is within the area defined by latitude 25°N to 40°N and longitude 100°W to 125°W. The unit of retrieval NO₂ concentrations is molecules cm⁻², which is different from the parts per billion (ppb) we normally use. In order to clearly show the changes of retrieval NO₂ concentrations in the last ten years, the percentage difference is calculated using the equation below:

$$\frac{(2014 - 2015 \text{ Average}) - (2005 - 2006 \text{ Average})}{(2005 - 2006 \text{ Average})} \times 100\%$$

Results

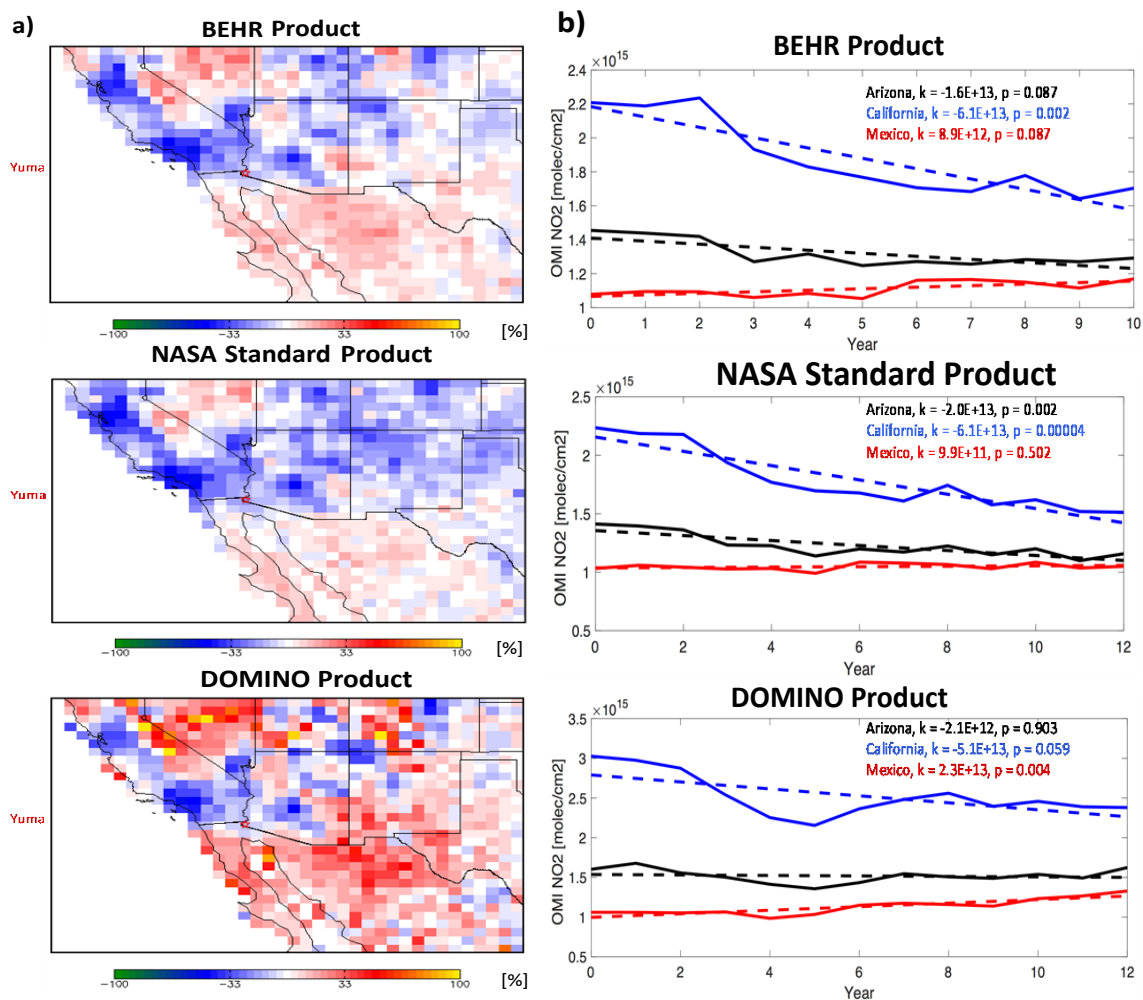


Figure 8 Percentage changes (%) of retrieval NO₂ concentrations (a) and trend analysis (b) from three OMI NO₂ products

June 13, 2018

Figure 8a shows a decreasing trend in southern California and Arizona. Especially, we notice a significant NO₂ decrease in metropolitan areas such as Los Angeles, San Francisco, and Phoenix; however, an increasing trend of NO₂ is spotted in northern Mexico.

In order to qualify the trends in each area, we averaged the annual NO₂ concentration(s) (only the area shown in the Figure 8a) and grouped them as California, Arizona and Mexico, respectively. Trend analysis was conducted for each area using Theil regression (Theil, 1992) and the Mann–Kendall test (Gilbert, 1987; Marchetto et al., 2013). We defined an increasing (decreasing) trend as a positive (negative) slope of the Theil regression, while the statistical significance of a trend was determined by the Mann–Kendall test (p value). A 90th percentile significance level (p <0.10) was assumed as in a previous study (Hand et al., 2012). The results of trend analysis are presented in the Figure 8b. The trends from the three products show the same patterns, that NO₂ is decreasing in Southern California and Arizona, while increasing in Mexico (except NASA SP, which showed no significant trend for Mexico). The results from another NO₂ study recently conducted by Majid et al. (2017) also showed a similar trend for California and Arizona (Figure 8).

Future Work

Volatile Organic Compounds (VOCs), as another important ozone precursor, should also be investigated. Unfortunately, OMI only has one product available for formaldehyde (HCHO) for the period from 2005 to 2015. This data is currently being reviewed with a summary available in the near future.

References

- Lamsal, L.N., Duncan, B.N., Yoshida, Y., Krotkov, N.A., Pickering, K.E., Streets, D.G. and Lu, Z., 2015. US NO₂ trends (2005–2013): EPA Air Quality System (AQS) data versus improved observations from the Ozone Monitoring Instrument (OMI). *Atmospheric Environment*, 110, pp.130-143.
- Liu, F., Zhang, Q., Zheng, B., Tong, D., Yan, L., Zheng, Y. and He, K., 2016. Recent reduction in NO_x emissions over China: synthesis of satellite observations and emission inventories. *Environmental Research Letters*, 11(11), p.114002.
- Duncan, B.N., Lamsal, L.N., Thompson, A.M., Yoshida, Y., Lu, Z., Streets, D.G., Hurwitz, M.M. and Pickering, K.E., 2016. A space-based, high-resolution view of notable changes in urban NO_x pollution around the world (2005–2014). *Journal of Geophysical Research: Atmospheres*, 121(2), pp.976-996.
- Majid, A., Martin, M.V., Lamsal, L.N. and Duncan, B.N., 2017. A decade of changes in nitrogen oxides over regions of oil and natural gas activity in the United States. *Elem Sci Anth*, 5.
- Russell, A.R., Perring, A.E., Valin, L.C., Bucsela, E.J., Browne, E.C., Wooldridge, P.J. and Cohen, R.C., 2011. A high spatial resolution retrieval of NO₂ column densities from OMI: method and evaluation. *Atmospheric Chemistry and Physics*, 11(16), pp.8543-8554.

June 13, 2018

Krotkov, N.A., Lamsal, L.N., Celarier, E.A., Swartz, W.H., Marchenko, S.V., Bucsela, E.J., Chan, K.L., Wenig, M. and Zara, M., 2017. The version 3 OMI NO₂ standard product. *Atmospheric Measurement Techniques*, 10(9), p.3133.

Bucsela, E.J., Krotkov, N.A., Celarier, E.A., Lamsal, L.N., Swartz, W.H., Bhartia, P.K., Boersma, K.F., Veefkind, J.P., Gleason, J.F. and Pickering, K.E., 2013. A new stratospheric and tropospheric NO₂ retrieval algorithm for nadir-viewing satellite instruments: applications to OMI. *Atmospheric Measurement Techniques*, 6(10), p.2607.

Boersma, K.F., Eskes, H.J., Veefkind, J.P., Brinksma, E.J., Van Der A, R.J., Sneep, M., Van Den Oord, G.H.J., Levelt, P.F., Stammes, P., Gleason, J.F. and Bucsela, E.J., 2007. Near-real time retrieval of tropospheric NO₂ from OMI. *Atmospheric Chemistry and Physics*, 7(8), pp.2103-2118.

Jiang, Z., McDonald, B.C., Worden, H., Worden, J.R., Miyazaki, K., Qu, Z., Henze, D.K., Jones, D.B., Arellano, A.F., Fischer, E.V. and Zhu, L., 2018. Unexpected slowdown of US pollutant emission reduction in the past decade. *Proceedings of the National Academy of Sciences*, p.201801191.

Qu, Z., Henze, D.K., Capps, S.L., Wang, Y., Xu, X., Wang, J. and Keller, M., 2017. Monthly top-down NO_x emissions for China (2005–2012): A hybrid inversion method and trend analysis. *Journal of Geophysical Research: Atmospheres*, 122(8), pp.4600-4625.

Theil, H., 1950. A rank-invariant method of linear and polynomial regression analysis, 3; confidence regions for the parameters of polynomial regression equations. *Indagationes Mathematicae*, 1(2), pp.467-482.

Gilbert, R.O., 1987. *Statistical methods for environmental pollution monitoring*. John Wiley & Sons.

Marchetto, A., Rogora, M. and Arisci, S., 2013. Trend analysis of atmospheric deposition data: a comparison of statistical approaches. *Atmospheric environment*, 64, pp.95-102.

Hand, J.L., Schichtel, B.A., Malm, W.C. and Pitchford, M.L., 2012. Particulate sulfate ion concentration and SO₂ emission trends in the United States from the early 1990s through 2010. *Atmospheric Chemistry and Physics*, 12(21), pp.10353-10365.

Attachment

D



(<http://www.worldbank.org/>)

Understanding Poverty (</en/understanding-poverty>) Health (</en/topic/health>)

BRIEF

Poverty and Health

August 25, 2014

[✉](mailto:?body=http%3A%2F%2Fwww.worldbank.org%2Fen%2Ftopic%2Fhealth%2Fbrief%2Fpoverty-health%3Fcid%3DEXT_WBEmailShare%26amp%3Fsubject=poverty%20&) (mailto:?body=http%3A%2F%2Fwww.worldbank.org%2Fen%2Ftopic%2Fhealth%2Fbrief%2Fpoverty-health%3Fcid%3DEXT_WBEmailShare%26amp%3Fsubject=poverty%20&)



Context

Poverty is a major cause of ill health and a barrier to accessing health care when needed. This relationship is financial: the poor cannot afford to purchase those things that are needed for good health, including sufficient quantities of quality food and health care. But, the relationship is also related to other factors related to poverty, such as lack of information on appropriate health-promoting practices or lack of voice needed to make social services work for them.

Ill health, in turn, is a major cause of poverty. This is partly due to the costs of seeking health care, which include not only out-of-pocket spending on care (such as consultations, tests and medicine), but also transportation costs and any informal payments to providers. It is also due to the considerable loss of income associated with illness in developing countries, both of the breadwinner, but also of family members who may be obliged to stop working or attending school to take care of an ill relative. In addition, poor families coping with illness might be forced to sell assets to cover medical expenses, borrow at high interest rates or become indebted to the community.

Strong health systems (<http://www.worldbank.org/en/topic/health/x/healthsystems>) improve the health status of the whole population, but especially of the poor among whom ill health and poor access to health care tends to be concentrated, as well as protect households from the potentially catastrophic effects of out-of-pocket health care costs. In general, poor health is disproportionately concentrated among the poor.

Strategy

The World Bank's work in the area of health equity and financial protection is defined by the 2007 Health, Nutrition and Population Strategy (<http://go.worldbank.org/QY4FTNVJR1>). The strategy identifies "preventing poverty due to illness (by improving financial protection)" as one of its four strategic objectives and commits the Bank's health team, both through its analytical work and its regional operations, to addressing vulnerability that arises from health shocks.

The strategy also stresses the importance of equity in health outcomes in a second strategic objective to "improve the level and distribution of key health, nutrition and population outcomes... particularly for the poor and the vulnerable".

The Bank supports governments to implement a variety of policies and programs to reduce inequalities in health outcomes and enhance financial protection. Generally, this involves mechanisms that help overcome geographic, social and psychological barriers to accessing care and reducing out-of-pocket cost of treatment. Examples include:

1. Reducing the direct cost of care at the point of service, e.g. through reducing/abolishing user fees for the poor or expanding health insurance to the poor (including coverage, depth and breadth).
2. Increasing efficiency of care to reduce total consumption of care, e.g. by limiting "irrational drug prescribing," strengthening the referral system, or improving the quality of providers (especially at the lower level).
3. Reducing inequalities in determinants of health status or health care utilization, such as reducing distance (through providing services closer to the poor), subsidizing travel costs, targeted health promotion, conditional cash transfers.
4. Expanding access to care by using the private sector or public-private partnerships.

The Bank's health team also promotes the monitoring of equity and financial protection by publishing global statistics on inequalities in health status, access to care and financial protection, as well as training government officials, policymakers and researchers in how to measure and monitor the same.

Results

Examples of how World Bank projects have improved health coverage for the poor and reduced financial vulnerability include:

The **Rajasthan Health Systems Development Project** (<http://www.worldbank.org/projects/P050655/rajasthan-health-systems-development-project?lang=en>) resulted in improved access to care for vulnerable Indians. The share of below-poverty line Indians in the overall inpatient and outpatient load at secondary facilities more than doubled between 2006 and 2011, well exceeding targets. In the same period, the share of the vulnerable tribal populations in the overall patient composition tripled.

The **Georgia Health Sector Development Project** (<http://www.worldbank.org/projects/P040555/health-sector-development-project?lang=en>) supported the government of Georgia in implementing the Medical Insurance Program for the Poor, effectively increasing the share of the government health expenditure earmarked for the poor from 4% in 2006 to 38% in 2011. It also increased the number of health care visits of both the general population and the poor, but by more for the poor (from 2 per capita per year to 2.6) than for the general population (from 2 to 2.3) over the same time period.

The **Mekong Regional Health Support Project** (<http://www.worldbank.org/projects/P079663/mekong-regional-health-support-project?lang=en>) helped the government of Vietnam to increase access to (government) health insurance from 29% to 94% among the poor, as well as from 7% to 68% among the near-poor. Hospitalization and consultation rates, at government facilities, also increased among both the poor and near-poor.

RELATED

Analyzing Health Equity Using Household Survey Data (<http://www.worldbank.org/en/topic/health/publication/analyzing-health-equity-using-household-survey-data>)

AdePT Software

(<http://econ.worldbank.org/WBSITE/EXTERNAL/EXTDEC/EXTRESEARCH/EXTPROGRAMS/EXTADEPT/0,,menuPK:7108381~pagePK:64168176~piPK:64168140~theSitePK:7108360,00.html>)

RELATED

PUBLICATION

Health Equity and Financial Protection Datasheets (<http://www.worldbank.org/en/topic/health/publication/health-equity-and-financial-protection-datasheets>)

PUBLICATION

Health Equity and Financial Protection Country Reports (2012) (<http://www.worldbank.org/en/topic/health/publication/health-equity-financial-protection-country-reports>)

ADEPT TRAINING

ADePT Training Resource Center (</en/topic/health/brief/adept-resource-center>)

About (<http://www.worldbank.org/en/about>)

Data (<http://data.worldbank.org>)

Research and Publications (<http://www.worldbank.org/en/research>)

Learning (<https://olc.worldbank.org>)

News (<http://www.worldbank.org/en/news>)

Projects and Operations (<http://projects.worldbank.org/?lang=en>)

Countries (<http://www.worldbank.org/en/country>)

Topics (<http://www.worldbank.org/en/topic>)

FOLLOW US



(<http://www.facebook.com/worldbank>)



(<http://www.twitter.com/worldbank>)



(<http://www.linkedin.com/company/the-world-bank>)



(<https://instagram.com/worldbank/>)



(<https://www.youtube.com/user/WorldBank>)



(<https://www.flickr.com/photos/worldbank>)

NEWSLETTER

Enter email to subscribe...

This Site in: [ENGLISH](#) ([HTTP://WWW.WORLDBANK.ORG](http://www.worldbank.org))

[Legal](http://www.worldbank.org/en/about/legal) (<http://www.worldbank.org/en/about/legal>) [Access to Information](http://www.worldbank.org/en/access-to-information) (<http://www.worldbank.org/en/access-to-information>) [Jobs](http://www.worldbank.org/en/about/careers) (<http://www.worldbank.org/en/about/careers>)
[Contact](http://www.worldbank.org/en/about/contacts) (<http://www.worldbank.org/en/about/contacts>)

[REPORT FRAUD OR CORRUPTION](https://intlbankforreconanddev.ethicspointvp.com/custom/IBRD/_CRF/ENGLISH/FORM_DATA.ASP) ([HTTPS://INTLBANKFORRECONANDDEV.ETHICSPPOINTVP.COM/CUSTOM/IBRD/_CRF/ENGLISH/FORM_DATA.ASP](https://intlbankforreconanddev.ethicspointvp.com/custom/IBRD/_CRF/ENGLISH/FORM_DATA.ASP))

(<http://www.worldbank.org/>)

[IBRD](http://www.worldbank.org/en/who-we-are/IBRD) ([HTTP://WWW.WORLDBANK.ORG/EN/WHO-WE-ARE/IBRD](http://www.worldbank.org/en/who-we-are/IBRD)) [IDA](http://www.worldbank.org/IDA) ([HTTP://WWW.WORLDBANK.ORG/IDA](http://www.worldbank.org/IDA)) [IFC](http://www.ifc.org/) ([HTTP://WWW.IFC.ORG/](http://www.ifc.org/)) [MIGA](http://www.miga.org/) ([HTTP://WWW.MIGA.ORG/](http://www.miga.org/))
[ICSID](http://ICSID.WORLDBANK.ORG/) ([HTTP://ICSID.WORLDBANK.ORG/](http://ICSID.WORLDBANK.ORG/))

© 2018 The World Bank Group, All Rights Reserved.

Attachment

E

Poverty and Ill Health: Physicians Can, and Should, Make a Difference

Michael McCally, MD, PhD; Andrew Haines, MD; Oliver Fein, MD; Whitney Addington, MD; Robert S. Lawrence, MD; and Christine K. Cassel, MD

A growing body of research confirms the existence of a powerful connection between socioeconomic status and health. This research has implications for both clinical practice and public policy and deserves to be more widely understood by physicians. Absolute poverty, which implies a lack of resources deemed necessary for survival, is self-evidently associated with poor health, particularly in less developed countries. Over the past two decades, economic decline or stagnation has reduced the incomes of 1.6 billion people. Strong evidence now indicates that relative poverty, which is defined in relation to the average resources available in a society, is also a major determinant of health in industrialized countries. For example, persons in U.S. states with income distributions that are more equitable have longer life expectancies than persons in less egalitarian states.

There are numerous possible approaches to improving the health of poor populations. The most essential task is to ensure the satisfaction of basic human needs: shelter, clean air, safe drinking water, and adequate nutrition. Other approaches include reducing barriers to the adoption of healthier modes of living and improving access to appropriate and effective health and social services. Physicians as clinicians, educators, research scientists, and advocates for policy change can contribute to all of these approaches. Physicians and other health professionals should understand poverty and its effects on health and should endeavor to influence policymakers nationally and internationally to reduce the burden of ill health that is a consequence of poverty.

Ann Intern Med. 1998;129:726-733.

From Mount Sinai School of Medicine and Cornell University Medical College, New York, New York; Royal Free and University College Schools of Medicine, London, United Kingdom; Rush School of Medicine, Chicago, Illinois; and Johns Hopkins School of Public Health, Baltimore, Maryland. For current author addresses, see end of text.

Poverty and social inequalities may be the most important determinants of poor health worldwide. Socioeconomic differences in health status exist even in industrialized countries where access to modern health care is widespread (1). In this paper, we make a formal argument for physician concern and action about poverty based on the following assertions. Physicians have a professional and a moral responsibility to care for the sick and to prevent suffering. Poverty is a significant threat to the health of both individual persons and populations; thus, physicians have a social responsibility to take action against poverty and its consequences for health. Physicians can help improve population health by addressing poverty in their roles as clinicians, educators, research scientists, and participants in policymaking.

Concepts of Poverty and Health

Poverty is a multidimensional phenomenon that can be defined in both economic and social terms. An economic measure of poverty identifies an income sufficient to provide a minimum level of consumption of goods and services. A sociologic measure of poverty is concerned not with consumption but with social participation (2). Poverty leads to a person's exclusion from the mainstream way of life and activities in a society (3). There is a difference between absolute poverty, which implies a lack of resources deemed necessary for survival in a given society, and relative poverty, which is defined in relation to the average resources available in a society. Economic measures are easy to obtain, but social measures may provide a better understanding of the causes and consequences of poverty. Steps have been taken toward the development of indices of deprivation, which have promising uses in health services and public health research (4).

In 1978, the World Health Organization (WHO), in the Alma-Ata Declaration, spelled out the dependence of human health (defined broadly) on social and economic development and noted that adequate living conditions are necessary for health (5). Despite their knowledge of this, governments and major development organizations have largely con-

tinued to view health narrowly as a responsibility of the medical sector, outside the scope of economic development efforts. Consequently, governments have encouraged many large-scale but narrowly focused economic development efforts, ignoring the connection between poverty and health (6). In developed countries, governments promote various practices, such as heavy pesticide applications, that are designed to increase economic development and competitiveness but that are environmentally unsound and personally unhealthy.

Poverty Causes Death and Illness on a Massive Scale

During the second half of the 1980s, the number of persons in the world who were living in extreme poverty increased. Currently, extreme poverty afflicts more than 20% of the world's population. A recent report from WHO points out that up to 43% of children in the developing world—230 million children—have low height for their age and that about 50 million children have low weight for their height (7). Micronutrient malnutrition (deficiencies of vitamin A, iodine, and iron) affects about 2 billion persons worldwide.

It has been estimated that if developing countries enjoyed the same health and social conditions as the most developed nations, the current annual toll of more than 12 million deaths in children younger than 5 years of age could be reduced to less than 400 000. An average person in one of the least developed countries has a life expectancy of 43 years; the life expectancy of an average person in one of the most developed countries is 78 years (7). This is not to deny that real gains in health have occurred in recent decades. For example, since 1950, life expectancy at birth in several developing countries has increased from 40 to more than 60 years. Similarly, worldwide, mortality rates for children younger than 5 years of age decreased from 280 to 106 per 1000, on average. Some countries show much sharper declines (7), but indices of health in these countries still fall far short of those in wealthier nations.

Poverty and Sustainable Development

The relation between poverty and health is complex, and we believe that it is best understood in the framework of a new notion of "ecosystem health," which places poverty and health in the nexus of environment, development, and population growth (8). Ecosystems provide the fundamental underpinning for public health in both developed and less developed countries, not only through food produc-

tion, for example, but also through their roles in economic development. For instance, they supply forest resources and biomass fuels and serve as habitats for the vectors of disease (9). Sustainability is produced by using resources in ways that meet the needs of current populations without compromising the ability of future generations to meet their own needs (10) and is predicated on the need to ensure a more equitable sharing of today's resources. Meeting the needs of the world's poor implies limitation of the current use of resources by industrialized nations.

Barriers to the benefits of development include rapid population growth, environmental degradation, and the unequal distribution of resources. At one extreme, traditional, preindustrial societies are characterized by relatively high birth rates coupled with high death rates attributable to acute infectious diseases and the hazards of childbearing; this leads to slow population growth. At the other extreme, in the most developed countries, population stability has occurred. In the intermediate situation, in less developed countries, population stability has not been reached, and the global population thus continues to increase. In some less developed countries, a "demographic trap" exists in which the development of resources cannot keep pace with the requirements of the growing population and poverty is worsened (11). The most developed countries escape the trap by buying additional essential resources in the global marketplace to make up the difference.

Environmental degradation exaggerates the imbalance between population and resources, increases the costs of development, and increases the extent and severity of poverty. For example, the need for fuel wood, timber for export, and farmland results in deforestation, which increases soil erosion, flooding, and mud slides and reduces agricultural productivity. As a result, biological diversity is lost, production becomes increasingly reliant on pesticides and fertilizers, and use of expensive fossil fuels increases. Water is a critical resource. In Punjab, the breadbasket of India, the major aquifer is decreasing at a rate of 20 cm per year, threatening health by reducing agricultural productivity and the supply of clean water (12). Economic development without regard to long-term environmental and social consequences also threatens sustainability by damaging the systems that sustain healthy communities.

Inequalities in Health Are Socially Determined

The strong and pervasive relation between an individual person's place in the structure of a soci-

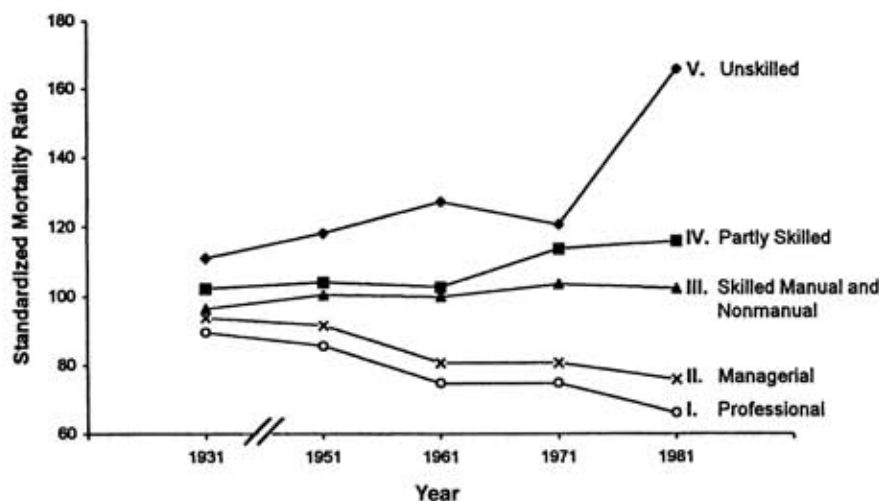


Figure 1. Comparison of standardized mortality ratios for men 15 to 64 years of age by social class over five decades in England and Wales. Figures have been adjusted to the classification of occupations used in 1951. Information on men 20 to 64 years of age in Great Britain was obtained from Black and colleagues (18).

ety and his or her health status has been clearly shown in research conducted over the past 30 years (13–16). In 1973, Kitagawa and Hauser (17) published convincing evidence of an increase in the differential mortality rates according to socioeconomic level in the United States between 1930 and 1960. They found that rates of death from most major causes was higher for persons in lower social classes. In Britain, research into health inequalities was summarized in 1980 in *The Black Report* (18), which was updated in 1992 (19) and is currently under review by an official working group. The report was prepared by a labor government–appointed research working group chaired by Sir Douglas Black, formerly Chief Scientist at the Department of Health and, at the time, President of the Royal College of Physicians. The *Black Report* concluded that “there are marked inequalities in health between the social classes in Britain” (Figure 1). Marmot and colleagues, in the well-known Whitehall studies of British civil servants begun in 1967, showed that mortality rates are three times greater for the lowest employment grades (porters) than for the highest grades (administrators) and that no improvement occurred between 1968 and 1988 (20–22).

Such findings could, in theory, be due to differences in age, smoking, nutrition, types of employment, accident rates, or living conditions, but the Whitehall study participants were from a relatively homogeneous population of office-based civil servants in London. They had largely stable, sedentary jobs and access to comprehensive health care. A second observation of the Whitehall investigations, confirmed by the Multiple Risk Factor Intervention Trial (MRFIT) studies in the United States, is that conventional risk factors (smoking, obesity, low levels of physical activity, high blood pressure, and high

plasma cholesterol levels) explain only about 25% to 35% of the differences in mortality rates among persons of different incomes (Figure 2) (23, 24).

An equally striking finding is Wilkinson’s observations of the relation between income distribution and mortality (25, 26). Wilkinson assembled two sets of observations. First, he found no clear relation between income or wealth and health when comparisons were drawn between countries (for example, there is no relation between per capita gross domestic product and life expectancy at birth in comparisons between developed countries at similar levels of industrialization). But Wilkinson also showed a strong relation between income inequality and mortality within countries, a relation that has been confirmed more recently (27, 28). The countries with the longest life expectancy are not necessarily the wealthiest but rather are those with the smallest spread of incomes and the smallest proportion of the population living in relative poverty. These countries (such as Sweden) generally have a longer life expectancy at a given level of economic development than less equitable nations (such as the United States).

Recent analysis of U.S. data supports earlier observations that the distribution of wealth within societies is associated with all-cause mortality and suggests that the relative socioeconomic position of the individual in U.S. society may be associated with health. Populations in U.S. states with income distributions that are more equitable have longer life expectancies than do those in less egalitarian states, even when average per capita income is taken into account (27, 28). Authors of the studies that revealed these findings recently introduced the notion of “social capital,” which is defined as civic engagement and levels of mutual trust among community

members, as an important variable intervening between income inequality and health status (29). Evans and associates (15) suggest that one's control of the work environment is an important connection between social and occupational class and mortality.

The Robin Hood index, also known as the Pietra ratio, is used to estimate the percentage of total income that would have to be transferred from groups above the mean to groups below the mean to equalize income distribution. A higher Robin Hood index value represents greater disparity in incomes. The strong correlation between income distribution and mortality rates shows that income disparity, in addition to absolute income level, is a powerful indicator of overall mortality (Figure 3) (27).

Inequalities in Income and Health Are Worsening

Many of the improvements in life expectancy and infant mortality rates that have occurred around the world are overshadowed by the countervailing influence of increasing disparities between rich and poor. Since 1980, economic decline or stagnation has af-

ected 100 countries, reducing the incomes of 1.6 billion persons (19). Between 1990 and 1993, the average income decreased by 20% or more in 21 countries, particularly countries in eastern Europe and the countries of the former Soviet Union (30). The net worth of the world's 358 richest persons is equal to the combined income of the poorest 45% of the world's population: 2.3 billion persons. Between 1960 and 1991, the ratio of the global income of the richest 20% of the world's population relative to the poorest 20% increased from 30:1 to 61:1 (30, 31).

Many recent improvements in population health have been threatened and, in some cases, reversed at the same time that income differentials have widened. For example, the proportion of underweight children in Africa may decrease from 26% in 1990 to 25% in 2005, but the total number of underweight children is projected to increase from 31.6 million to 39.2 million because of population growth.

In the United States and the United Kingdom, income distribution has become more unequal. According to the United Nations Development Programme, income distributions within each of these countries are now among the most unequal distri-

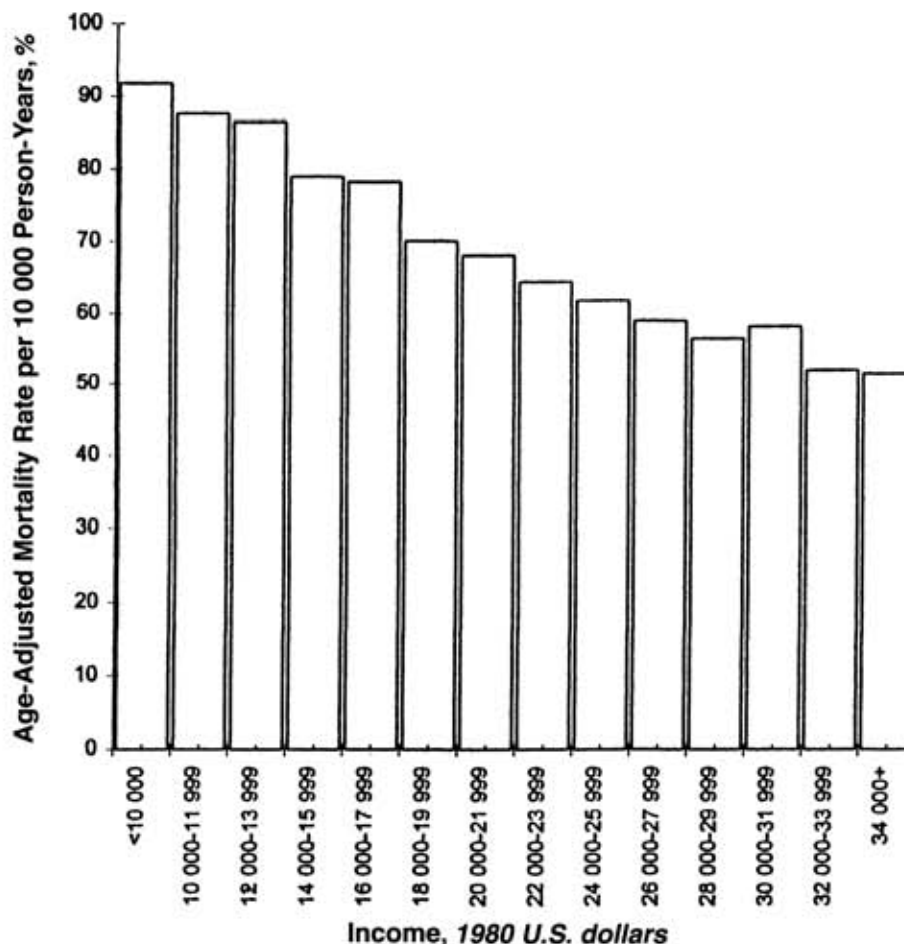


Figure 2. Income and age-adjusted mortality rates among 300 000 white men in the United States. Data obtained from Smith and colleagues (23).

butions in the world's industrialized countries (31, 32). For example, in the United Kingdom, the proportion of persons with an income less than half of the national average increased from less than 10% in 1982 to more than 20% in 1993, and unskilled men in Scotland now have a mortality rate three times that of professional men (33). This represents a widening from a twofold differential in the early 1970s. In the United Kingdom, the difference in mortality rates between rich and poor has increased because mortality rates have decreased faster among the rich than among the poor (34), and the proportion of children below the official poverty line has tripled in the past 10 years (35, 36). In the United States, inequality in income increased in all states except Alaska between 1980 and 1990 (37).

Effective Interventions Reduce Ill Health Due to Poverty

Some evidence suggests that improving the income of the poorest persons improves health in both developed and less developed countries. International data have been used to show that the doubling of per capita income (adjusted for purchasing power parity) from \$1000, using 1990 figures, corresponds to an increase of 11 years in life expectancy. The relation flattens off above an average per capita income of approximately \$5000 (Figure 4) (30). The distribution of income within households also influences health. It has been suggested, for example, that it takes 10 times more spending to achieve a given improvement in child nutrition in

Guatemala when income is earned by the father than when it is earned by the mother because the mother is more likely to spend the money on essentials for the family (30).

An important, possibly unique, randomized trial in Gary, Indiana, suggests that increasing the income of poor expectant mothers receiving welfare increased the birthweight of their babies (38). Education, particularly for mothers, has dramatically affected health. In Peru, for instance, the children of mothers with 7 or more years of education have a reduction in child mortality of nearly 75% compared with the children of mothers with no schooling. Studies in several countries have shown that mothers who have completed secondary or higher education are much more likely to treat childhood diarrhea appropriately with oral rehydration therapy. Families are also likely to be smaller when women are more educated (30).

A recent systematic review of the effectiveness of health service interventions, predominantly in industrialized countries, to reduce poverty-related inequalities in health suggests several characteristics of interventions that may be successful, although they do not directly affect income (39). These include programs that target high-risk groups; outreach programs that include home visits; and programs that overcome barriers to the use of services by providing transportation or convenient access and by using prompts and reminders. Large-scale multidisciplinary interventions involving a range of agencies and programs may be cost-effective. The Special Supplemental Food Program for Women, Infants and Chil-

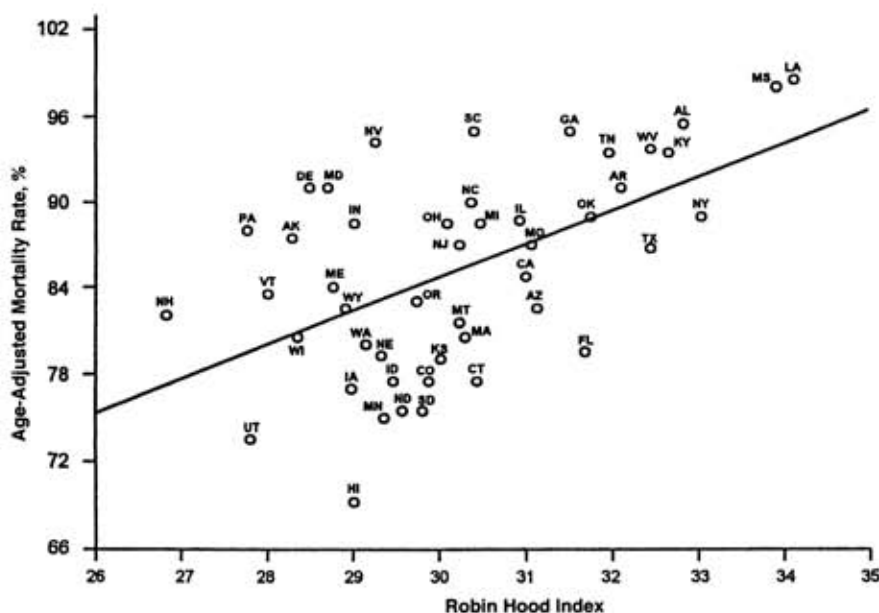


Figure 3. Age-adjusted mortality in the United States in 1990 and the Robin Hood index of income inequality. Circles represent the states of the United States. Data were not available for New Mexico, Rhode Island, and Virginia. Adapted from Kennedy and colleagues [27] with permission.

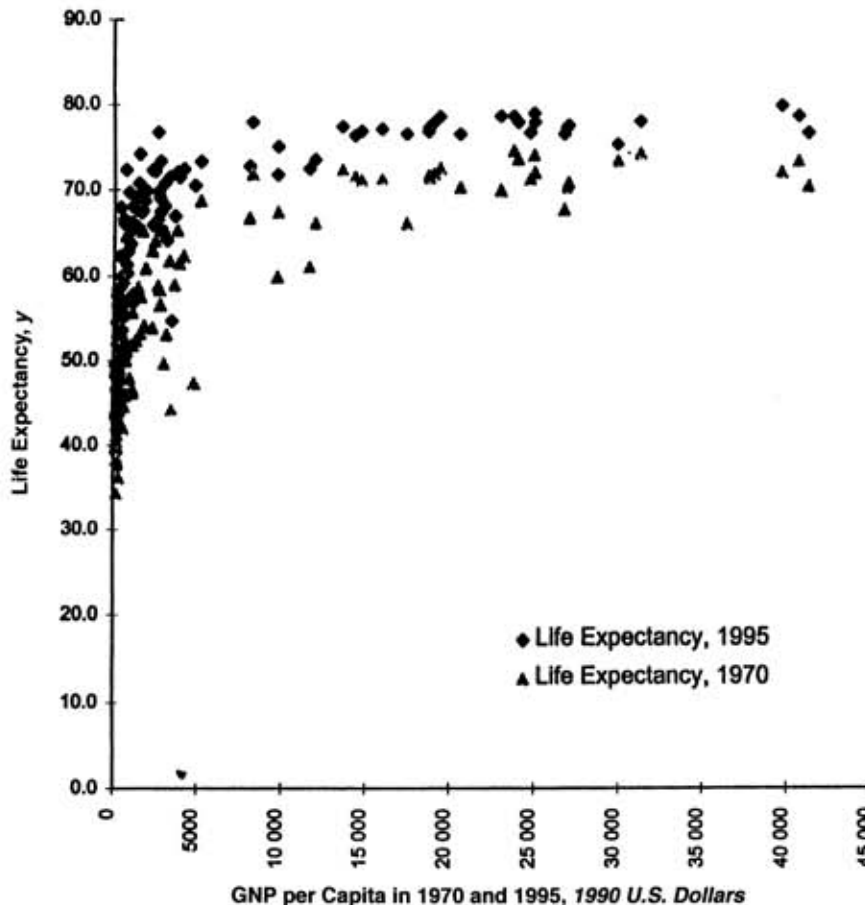


Figure 4. Life expectancy at birth and gross national product (GNP) in 1970 and 1995 in rich and poor countries in 1990 U.S. dollars. Triangles represent life expectancy in 1970; diamonds represent life expectancy in 1995. Data obtained from World Development Indicators, World Bank, 1995.

dren (WIC) was initiated in 1972 in the United States and provides healthy food, education about nutrition, and health services to low-income women and their children. Data analysis suggests substantial reductions in the number of babies with low and very low birth weights as a result (40). The project paid for itself through equivalent savings in medical care. Project Head Start provides preschool children and their families with education, health care, and social services. Short- and long-term benefits have been shown in health, developmental, and social outcomes (41).

Economic analysis confirms that primary care interventions, including measures designed to reduce childhood malnutrition, improve immunization against childhood diseases, provide chemotherapy against tuberculosis, provide condoms and education to combat the spread of HIV, and reduce smoking (including consumer taxes on tobacco) are cost-effective (42).

Physicians Have Special Responsibilities

It is widely accepted that physicians have a special and central professional responsibility to treat

disease and reduce mortality rates, a responsibility that arises from their knowledge of medicine and medical practice (43). The physician-patient relationship is a fiduciary one, based on the inherent responsibility of physicians to deserve the trust of patients. Professionalism also extends this relationship to society, which confers on the profession respect and certain kinds of autonomy and authority. In the context of the physician-society relationship, the physician's fiduciary responsibility takes the form of concern for the public health. Most major traditions of medical ethics suggest that physicians have a special responsibility for the care of poor persons, defined as those who cannot afford to pay for treatment (44).

In addition, physician responsibilities in patient care extend to the social context of health and disease. Physicians regularly attempt to influence both patients' lifestyles and their environments to help prevent illness. They do so because illness is often precipitated by behavioral and social factors. Physicians in practice have an obligation to act on behalf of the general public welfare (for example, by reporting infectious diseases to the proper authorities). Recently, it has become widely accepted

that physicians should work to promote smoking cessation, encourage use of seatbelts, and prevent firearm injury. Health hazards should not be ruled out as medical concerns because their remedy requires social or political action. Although the proper form and extent of political involvement for physicians may at times be controversial, concern for the health of the public has been an important responsibility of the medical profession at least since the Industrial Revolution (45).

It may be argued that although physicians have a responsibility to care for persons who are ill even though they are poor and cannot pay, medicine has no particular responsibility with respect to the general condition of poverty. Physicians' efforts to mitigate poverty may be seen as going beyond the bounds of the patient-physician relationship. However, efforts against poverty may have parallels in widely accepted attempts by physicians to prevent child abuse or health hazards in the workplace. Although patients may not ask to be protected from toxins or abuse, physicians have agreed that they have a responsibility to assist patients who may be in danger and, when possible, to prevent harm. If poverty is connected to ill health in a direct and powerful way, it can be argued that physicians have some degree of responsibility for addressing poverty itself to the best of their ability.

Physicians Can Help Mitigate the Health Inequalities Caused by Poverty

A panel convened by the King's Fund of London recently proposed four types of interventions to correct health inequalities related to poverty: addressing social and economic factors; reducing barriers to the adoption of healthier ways of living; improving the physical environment; and improving access to appropriate, effective health and social services (46). Physicians have clear roles to play in each of these efforts.

Physicians can address social and economic factors both on the level of the individual patient and on the level of the community. By being aware of socioeconomic factors, such as insurance status, educational background, occupational history, housing conditions, and social isolation, physicians can make more comprehensive diagnoses and tailor therapies to patients' needs. Unfortunately, in residency training, the social history (if it is taken at all) is often labeled "noncontributory." Raik and colleagues (47) examined the content of resident case presentations on inpatient rounds and found remarkably low rates of mention of socioeconomic factors. Physicians as teachers can address these factors on rounds and in

describing their own patients to trainees and colleagues.

On the community level, physicians can advocate for public policies to improve the health of the disadvantaged. Jarman (48) showed that physicians know that it is more complicated and takes more time to care for poor patients than for patients who are not poor. With this evidence, he was able to persuade the National Health Service in the United Kingdom to take patient economic status into account in rewarding general practitioners who work in deprived areas. Given the growth of managed care in the United States, physicians should be at the forefront of those calling for poverty-based risk adjustments to capitated payments.

As research scientists, physicians can advance the understanding of the mechanisms by which deprivation leads to ill health and the development of more effective interventions to reduce inequality in health (49). Similarly, physicians who are aware of the adverse effects of international debt on health can urge debt relief for the poorest countries (50).

Physicians may also be able to assist in removing barriers to healthy lifestyles—for example, campaigning against the promotion of tobacco, which is increasingly being targeted to adolescents in less developed countries and in minority communities in the United States (51).

Physicians can affect environmental factors associated with poverty by advocating for legislation to maintain and improve the quality of air, drinking water, and food. Physician-led public health efforts in the United States have been instrumental in reducing the incidence of lead poisoning, which is strongly associated with poverty. Internationally, physicians are participating in local initiatives surrounding Agenda 21, developed at the 1992 Earth Summit in Rio de Janeiro, Brazil. More than 1300 local communities in 31 countries have developed their own action plans, many of which feature health issues. Through the WHO Healthy Cities Project, cities have addressed such issues as smoking, sanitation, air pollution, and socioeconomic differences in health (52).

Approaches to improving access to effective health and social services in the United States and elsewhere have been extensively reviewed (39, 53). However, more than 800 million persons lack access to health services worldwide, and the increasing imposition of user fees (copayments and deductibles) in many countries has exacerbated inequities in care (54). Physicians and their associations should lead the movement for universal access to health care (55).

An international meeting on health and poverty hosted by WHO and Action in International Medicine (which has approximately 100 affiliated organizations in more than 30 countries) urged associa-

tions of health professionals to engage in activities to reduce health inequalities due to poverty (56). Dr. Gro Harlem Brundtland, the newly appointed Director General of WHO, has indicated that she intends to make the reduction of ill health due to poverty a priority for her term of office (57). The United Nations Declaration of Human Rights includes access to the basic necessities of life, such as food and water, as well as health care. However, 50 years after the Declaration was written, we are still far from providing this access to everyone. Physicians have an important role to play in helping to transform the rhetoric of the Declaration into reality.

Requests for Reprints: Michael McCally, MD, PhD, Department of Community and Preventive Medicine, Box 1043, Mount Sinai School of Medicine, New York, NY 10029; e-mail, mm6@doc.mssm.edu.

Current Author Addresses: Dr. McCally: Department of Community and Preventive Medicine, Box 1043, Mount Sinai School of Medicine, New York, NY 10029.

Dr. Haines: Department of Primary Care and Population Sciences, Royal Free and University College Schools of Medicine, Rowland Hill Street, London, NW3 2PF, United Kingdom.

Dr. Fein: Cornell University Medical College, 1300 York Avenue, Box 577, New York, NY 10021.

Dr. Addington: Primary Care Institute, Rush School of Medicine, 1653 West Congress Parkway, Suite 807 Kidston, Chicago, IL 60612.

Dr. Lawrence: Professional Education and Programs, Johns Hopkins School of Public Health, 615 North Wolfe Street, Room 205, Baltimore, MD 21218.

Dr. Cassel: Department of Geriatrics and Adult Development, Mount Sinai School of Medicine, New York, NY 10029.

References

1. **Graubard SR, ed.** Health and wealth. *Daedalus*. 1994;123:1-216.
2. **Rainwater L.** What Money Buys: Inequality and the Social Meaning of Income. New York: Basic Books; 1974.
3. **Ringen S.** The Possibility of Politics: A Study in the Political Economy of the Welfare State. New York: Oxford Univ Pr; 1987.
4. **Townsend P.** The International Analysis of Poverty. London: Harvester-Wheatsheaf; 1993.
5. Primary Health Care: Report of the International Conference on Primary Health Care, Alma-Ata, USSR, 6-12 September 1978. Geneva: World Health Organization; 1978.
6. **Cooper Weil DE, Alicibusan AP, Wilson JF, Reich MR, Bradley DJ.** The Impact of Development Policies on Health: A Review of the Literature. Geneva: World Health Organization; 1990.
7. The World Health Report 1995: Bridging the Gaps. Report of the Director-General. Geneva: World Health Organization; 1995.
8. **Shahi GS, Levy BS, Louis GE, Binger A, Kjellstrom T, Lawrence RS.** The environment-development-health interface. In: Shahi GS, Levy BS, Binger A, Kjellstrom T, Lawrence RS, eds. International Perspectives on Environment, Development, and Health: Toward a Sustainable World. A Collaborative Initiative of the World Health Organization, the United Nations Development Programme, and the Rockefeller Foundation. New York: Springer; 1997.
9. **Ewert AW, Kessler WB.** Human health and natural ecosystems: impacts and linkages. *Ecosystem Health*. 1996;2:271-8.
10. **Brundtland GH.** Our Common Future: The World Commission on Environment and Development. New York: Oxford Univ Pr; 1987.
11. **McCally M.** Human health and population growth. In: Chivian E, McCally M, Haines A, Hu H, eds. Critical Condition: Human Health and the Environment. Cambridge, MA: MIT Pr; 1995.
12. **Brown LR.** Dividing the Waters. State of the World 1996. New York: WW Norton; 1996.
13. **Frank JW, Mustard JF.** The determinants of health from a historical perspective. *Daedalus*. 1994;123:1-19.
14. **Feinstein JS.** The relationship between socioeconomic status and health: a review of the literature. *Milbank Q*. 1993;71:279-322.
15. **Evans RG, Barer ML, Marmor TR.** Why Are Some People Healthy and Others Not? The Determinants of Health of Populations. New York: Aldine de Gruyter; 1994.
16. **Fein O.** The influence of social class on health status: American and British research on health inequalities. *J Gen Intern Med*. 1995;10:577-86.

17. **Kitagawa EM, Hauser PM.** Differential Mortality in the United States: A Study in Socioeconomic Epidemiology. Cambridge, MA: Harvard Univ Pr; 1973.
18. **Black D, Morris JN, Smith C, Townsend P.** Inequalities in Health Care: The Black Report. New York: Penguin; 1982.
19. **Townsend P, Davidson N, Whitehead M.** Inequalities in Health. London: Penguin; 1992.
20. **Marmot MG.** Social differentials in health within and between populations. *Daedalus*. 1994; 123:197-216.
21. **Marmot MG, Shipley MJ, Rose G.** Inequalities in death—specific explanations of a general pattern? *Lancet*. 1984;1:1003-6.
22. **Marmot MG, Smith GD, Stansfeld S, Patel C, North F, Head J, et al.** Health inequalities among British civil servants: the Whitehall II study. *Lancet*. 1991;337:1387-93.
23. **Smith GD, Wentworth D, Neaton JD, Stamler R, Stamler J.** Socioeconomic differentials in mortality risk among men screened for the Multiple Risk Factor Intervention Trial: I: White men. *Am J Public Health*. 1996;86:486-96.
24. **Smith GD, Wentworth D, Neaton JD, Stamler R, Stamler J.** Socioeconomic differentials in mortality risk among men screened for the Multiple Risk Factor Intervention Trial: II: Black men. *Am J Public Health*. 1996;86:497-504.
25. **Wilkinson RG.** National mortality rates: the impact of inequality? *Am J Public Health*. 1992;82:1082-8.
26. **Wilkinson RG.** Divided we fall [Editorial]. *BMJ*. 1994;308:1113-4.
27. **Kennedy BP, Kawachi I, Prothrow-Stith D.** Income distribution and mortality: cross sectional ecological study of the Robin Hood index in the United States. *BMJ*. 1996;312:1004-7.
28. **Kaplan GA, Pamuk ER, Lynch JW, Cohen RD, Balfour JL.** Inequality in income and mortality in the United States: analysis of mortality and potential pathways. *BMJ*. 1996;312:999-1003.
29. **Kawachi I, Kennedy BP, Lochner K, Prothrow-Stith D.** Social capital, income inequality, and mortality. *Am J Public Health*. 1997;87:1491-8.
30. **World Bank.** World Development Report 1993: Investing in Health. New York: Oxford Univ Pr; 1993.
31. United Nations Development Programme. Human Development Report 1996. New York: Oxford Univ Pr; 1996.
32. United Nations Development Programme. Human Development Report 1994. New York: Oxford Univ Pr; 1994.
33. **Smith T.** The changing pattern of mortality in young adults aged 15 to 34 in Scotland between 1972 and 1992. *Scott Med J*. 1994;39:144-5.
34. **Watt GC.** All together now: why social deprivation matters to everyone. *BMJ*. 1996;312:1026-9.
35. **McKee M.** Poor children in rich countries [Editorial]. *BMJ*. 1993;307:1575-6.
36. **Judge K, Benzeval M.** Health inequalities: new concerns about the children of single mothers. *BMJ*. 1993;306:677-80.
37. **Income and Poverty.** Washington, DC: US Bureau of the Census; 1993.
38. **Kehrer BH, Wolin CM.** Impact of income maintenance on low birth weight: evidence from the Gary Experiment. *J Hum Resour*. 1979;14:434-62.
39. **Arblaster L, Lambert M, Entwistle V, Forster M, Fullerton D, Sheldon T, et al.** A systematic review of the effectiveness of health service interventions aimed at reducing inequalities in health. *J Health Serv Res Policy*. 1996; 1:93-103.
40. **Rush D, Horvitz DG, Seaver WB, Alvir JM, Garbowski GC, Leighton J, et al.** The National WIC Evaluation: evaluation of the Special Supplemental Food Program for Women, Infants, and Children. I. Background and introduction. *Am J Clin Nutr*. 1988;48:389-93.
41. **Schorr EB, Schorr D.** Within Our Reach: Breaking the Cycle of Disadvantage. New York: Anchor Books; 1988.
42. **Jamison DT, Mosely WN, Meashom AR, Bobadilla J, eds.** Disease Control Priorities in Developing Countries: A Summary. Washington, DC: World Bank; 1993.
43. **Jonsen AR, Jameton AJ.** Social and political responsibilities of physicians. *J Med Philos*. 1977;2:376-400.
44. **Amundsen DW.** History of medical ethics. In: *Encyclopedia of Bioethics*. New York: MacMillan; 1995:1522-36.
45. **Rosen G.** From Medical Police to Social Medicine: Essays on the History of Health Care. New York: Science History Publications; 1974.
46. **Benzeval M, Judge K, Whitehead M, eds.** Tackling Inequalities in Health: An Agenda for Action. London: King's Fund; 1995.
47. **Raik B, Fein O, Wachspres S.** Measuring the use of population perspective on internal medicine attending rounds. *Acad Med*. 1995;70:1047-9.
48. **Jarman B.** Identification of underprivileged areas. *Br Med J (Clin Res Ed)*. 1983;286:1705-9.
49. **Townsend P, Phillimore P, Beattie A.** Health and Deprivation: Inequality and the North. London: Croom Helm; 1988.
50. **Logie DE, Benatar SR.** Africa in the 21st century: can despair be turned to hope? *BMJ*. 1997;315:1444-6.
51. **Aguirre-Molina M, Gorman DM.** Community-based approaches for the prevention of alcohol, tobacco, and other drug use. *Annu Rev Public Health*. 1996;17:337-58.
52. **von Schirmding Y.** Intersectoral Action for Health: Addressing Health and Environmental Concerns in Sustainable Development. Geneva: World Health Organization; 1997.
53. **Gepkens A, Gunning-Schleppers LJ.** Interventions to reduce socioeconomic health differences: a review of the international literature. *European Journal of Public Health*. 1996;6:218-26.
54. **Creese A.** User fees [Editorial]. *BMJ*. 1997;315:202-3.
55. **American College of Physicians.** Universal Coverage: Renewing the Call to Action. Philadelphia: American Coll Physicians; 1996.
56. **Haines A, Smith R.** Working together to reduce poverty's damage [Editorial]. *BMJ*. 1997;314:529-30.
57. **Brundtland GH.** Interview. *BMJ*. 1998;316:13.